Zircon fingerprint of the Neoproterozoic North Atlantic: perspectives from East Greenland

Hugo K.H. Olierook, Milo Barham, Christopher L. Kirkland, Julie Hollis, Anna Vass

PII: S0301-9268(19)30695-3
DOI: https://doi.org/10.1016/j.precamres.2020.105653
Reference: PRECAM 105653

To appear in: *Precambrian Research*

Received Date: 2 December 2019
Revised Date: 7 February 2020
Accepted Date: 7 February 2020

Please cite this article as: H.K.H. Olierook, M. Barham, C.L. Kirkland, J. Hollis, A. Vass, Zircon fingerprint of the Neoproterozoic North Atlantic: perspectives from East Greenland, *Precambrian Research* (2020), doi: https://doi.org/10.1016/j.precamres.2020.105653

Zircon fingerprint of the Neoproterozoic North Atlantic: perspectives from East Greenland

Hugo K. H. Olierook[1,2]*, Milo Barham[1,2], Christopher L. Kirkland[1,2], Julie Hollis[3], Anna Vass[3]

[1]Centre for Exploration Targeting – Curtin Node, School of Earth and Planetary Sciences, Curtin University, GPO Box U1987, Perth, WA 6845, Australia

[2]John de Laeter Centre, Curtin University, GPO Box U1987, Perth, WA 6845, Australia

[3]Geology Department, Ministry of Mineral Resources, Government of Greenland, P.O. Box 930, 3900 Nuuk, Greenland

*Corresponding author: hugo.olierook@curtin.edu.au; +61 8 9266 7827

Keywords: Eleonore Bay; U-Pb; detrital; Caledonian; provenance; Hf

Abstract

Correlations across the once-contiguous North Atlantic region remain challenging, particularly for pre-Caledonian packages. Here, we present new zircon U-Pb and Hf isotope data from five metasedimentary samples and three granites from East Greenland to assess the age and provenance of Meso- to Neoproterozoic successions in this area, and to evaluate their correlatives across the North Atlantic region. Detrital zircon U-Pb data yield maximum depositional ages of 936 ± 15 Ma (2σ) that indicate the metasedimentary rocks are probably a component of the Neoproterozoic Nathorst Land Group (lower Eleonore Bay Supergroup). Intruding granites are exclusively of Caledonian age at 426 ± 1 Ma (2σ) and contain a significant xenocrystic cargo with comparable ages to detrital zircon in the host metasedimentary sequences. Detrital zircon age components are concentrated between ca. 1850 and 920 Ma, with prominent peaks at ca. 1620 Ma, 1450 Ma and 1080 Ma, and additional subcomponents at 2900–2600 Ma (~4%) and 2030–1940 Ma (~2%). Provenance of this detritus is probably from the East Laurentian margin via axial drainage to East Greenland. Statistical analyses of a newly-compiled circum-Atlantic detrital zircon dataset corroborates a model in which sedimentation occurred in three distinct megasequences: (1) 1020–950 Ma, as a response to the opening of the Asgard Sea that followed Laurentia–Baltica collision, (2) 920–840 Ma, recording the onset of further rifting of the North Atlantic and attempted breakup of Rodinia, and (3) 740–635 Ma, concomitant with the breakup of Rodinia and ending with the Marinoan glaciation. The first two megasequences show strong U-Pb and εHf similarities in both space and time across the North Atlantic. However, there is a significant increase in detrital zircon disparity between the second and third megasequences, which we propose is associated with increased compartmentalization of depocentres with localized supply and distinct sediment routing pathways during continental breakup.

1 INTRODUCTION

The North Atlantic region records repeated continental breakup and amalgamation across at least two Wilson cycles from the Mesoproterozoic to Cenozoic (Buiter and Torsvik, 2014; Cawood et al., 2016; Gee et al., 2013; Holbrook et al., 2001). In spite of the importance of the North Atlantic region for an understanding of supercontinent tectonics and global geodynamics (Lancaster et al., 2011; Spencer et al., 2015), many areas and time periods remain poorly studied (Fig. 1). Adding to this challenge is the fact that many exposures across the now rifted eastern Laurentian and western Baltican continents are in remote locations, including East Greenland, the Canadian and Norwegian High Arctic, and Svalbard (Fig. 1, Table 1). Although more work has been undertaken in Scotland, Ireland and southern to central Scandinavia (Fig. 1, Table 1), insufficient studies on the aforementioned remote locations hinder a comprehensive understanding of the geological history. Another obstacle to understanding the pre-Caledonian geological history of the North Atlantic region is the extensive tectono-magmatic modification of the earlier Precambrian lithotectonic sequences during post-depositional orogenesis (e.g., Cawood et al., 2004; Kirkland et al., 2008a; Pettersson et al., 2009a; Slama et al., 2011). One mechanism to address this potentially cryptic overprinting is to evaluate those sequences where this tectonic complexity can, at least, be well seen in the field. Hence, it is these remote Precambrian regions – which offer some of the best field exposures in the North Atlantic – that can offer some answers to Wilson cycle tectonics, sedimentary routing systems and plate configurations in the Meso- and Neoproterozoic.

Of the main Proterozoic regions exposed across the circum-North Atlantic region, the East Greenland sequence is perhaps one of the least well understood (Figs. 1, 2). The East Greenland Meso- to Neoproterozoic sedimentary rift basin sequence includes three first order successions: (i) the Krummedal Succession, (ii) the Nathorst Land Group (lower Eleonore Bay Supergroup), and (iii) the Lyell Land, Ymer Ø and Andrée Land Groups (upper Eleonore Bay Supergroup;Gilotti et al., 2008;

Higgins, 1988; Sønderholm and Tirsgaard, 1993). Only a handful of studies have attempted to constrain the depositional age and provenance of the Meso- to Neoproterozoic rift basin sequences that extend from 70 to 76° N (>~650 km) in East Greenland. These studies utilized zircon U-Pb data (Dhuime et al., 2007; Kalsbeek et al., 2000; Slama et al., 2011; Strachan et al., 1995; Watt et al., 2000) and, only in the case of Slama et al. (2011), were complementary zircon Hf isotopes used. Consequently, many questions remain as to the depositional age of the Meso- to Neoproterozoic sedimentary rocks in East Greenland, the provenance of these rift successions and their correlations to various units across the North Atlantic region.

In this study, we provide zircon U-Pb and Hf isotope data from metasedimentary rocks and intruding granites in Wollaston Forland, a prominent peninsula in East Greenland between 74 and 75°N (Fig. 3). The metasedimentary samples were tentatively assigned to the Nathorst Land Group from mapping at 1: 250,000 by the Geological Survey of Greenland (GEUS; Escher, 2007; Henriksen and Higgins, 2008). However, these metasedimentary rocks also share lithological similarities (Sønderholm and Tirsgaard, 1993) and high-grade metamorphic characteristics (Gilotti et al., 2008) with the Krummedal Succession (see section 2.2.1). Granites were dated to assess whether these were Silurian or Neoproterozoic in age. Neoproterozoic granites are restricted to the Krummedal Succession (Leslie and Nutman, 2003), aiding stratigraphic assignment of the metasedimentary rocks. Using these new data, complemented with detrital U-Pb and Hf data from other Neoproterozoic North Atlantic rift basin correlatives, we evaluate the stratigraphic position of the East Greenland sequence within the broader Meso- to Neoproterozoic successions of the North Atlantic region. This approach allows us to recognise provenance patterns in time and space, which we argue have geodynamic significance.

2 GEOLOGICAL BACKGROUND

2.1 Overview of the North Atlantic region

The North Atlantic region has experienced repeated extensional and compressional activity from the Mesoproterozoic to Cenozoic, exploiting approximately the same crustal discontinuities for breakup and amalgamation events (Cawood et al., 2016; Gee et al., 2013; Holbrook et al., 2001). Distinct rock packages of Laurentian, Baltican and Amazonian affinity first amalgamated during the end of the Mesoproterozoic along the Grenvillian and Sveconorwegian orogenies (Bingen et al., 2008; Cawood and Pisarevsky, 2017; Gower and Krogh, 2002; Slagstad et al., 2017). Protracted and episodic rifting occurred in the latest Mesoproterozoic to Neoproterozoic. The latest Mesoproterozoic to early Neoproterozoic (Tonian) events in the North Atlantic region are collectively referred to as the accretionary Valhalla Orogen to differentiate it from the more southerly and generally older Grenvillian, Sveconorwegian and Sunsas Orogens that were collisional in nature (Cawood et al., 2010; Slagstad et al., 2019). Continued crustal attenuation caused the breakup of Laurentia and Baltica towards the end of the Neoproterozoic and the opening of the Iapetus Ocean (Cawood et al., 2001; Cawood et al., 2007; Hartz and Torsvik, 2002). In the Ordovician–Silurian, ca. 200 Myr later, Laurentia and Baltica re-collided together with the Avalonian continent from the south during the Caledonian Orogeny (McKerrow et al., 2000; Woodcock and Strachan, 2009). The Laurentian and Baltican continents (with pieces of Avalonia) have since been rifted apart again in the Late Cretaceous and Paleogene to form the present day configuration of the North Atlantic Ocean (Storey et al., 2007; Torsvik et al., 2001). The timing of these rifting and amalgamation events also coincide with the building and breakup of Rodinia and Gondwana/Pangea (Merdith et al., 2019; Mitchell et al., 2019). This repeated history in a relatively narrow spatial location attests to the completion of two Wilson cycles across a billion year timescale (Buiter and Torsvik, 2014).

2.2 Geological setting of the Meso- to Neoproterozoic successions, East Greenland

Meso- to Neoproterozoic sedimentary sequences are exposed in eastern and northeastern Greenland from 70.0 to 81.5°N and provide a record of the protracted rifting history of the Rodinian supercontinent (Fig. 2; Kalsbeek et al., 2000; Sønderholm et al., 2008). The succession disconformably overlies Neoarchean to Paleoproterozoic crystalline basement and subordinate Paleoproterozoic supracrustal rocks (Higgins, 1988; Thrane, 2002). From oldest to youngest, the Meso- to Neoproterozoic sequences comprise the Krummedal Succession (Higgins, 1988), the Eleonore Bay Supergroup (Sønderholm and Tirsgaard, 1993) and the Tillite Group (Fig. 2; Hambrey and Spencer, 1987).

2.2.1 Krummedal Succession

In its present-day configuration, the Krummedal Succession is separated from the Archean to Paleoproterozoic basement by low-angle extensional detachments that are probably coeval with thrusting during the Caledonian Orogeny (Gilotti et al., 2008). In the north (~76°N), the Smallefjord Succession was correlated with the Krummedal Succession on the basis of lithological, metamorphic, structural and geochronological similarities (Strachan et al., 1995). The Krummedal Succession comprises at least 4 km of medium- to high-grade, migmatitic mica schists, paragneisses and impure quartzites (Higgins, 1988). Two series of granites are present within the Krummedal Succession. More rarely, an ‘older’ granite suite at ca. 950–920 Ma intruded the Krummedal Succession during extension associated with the Renlandian Orogeny (Kalsbeek et al., 2000; Leslie and Nutman, 2003; Watt et al., 2000)(Cawood et al., 2010). During Silurian extensional episodes, voluminous granites intrude the Krummedal Succession as subhorizontal sheets associated with the Caledonian Orogeny (Gilotti and McClelland, 2005).

The age of the Krummedal Succession is constrained by both detrital zircon geochronology and intrusion of granitoids. Geochronology of Krummedal Succession detrital zircon populations demonstrates a dominance of Paleoproterozoic to Mesoproterozoic grains (ca. 1700–1200 Ma) with

the youngest grains dated at ca. 1040 Ma (Kalsbeek et al., 2000; Leslie and Nutman, 2003; Strachan et al., 1995; Watt et al., 2000). Intrusion of the 'older' granite suite in the Krummedal Succession at ca. 950–920 Ma provides a firm minimum age for the succession (Kalsbeek et al., 2000; Leslie and Nutman, 2003; Watt et al., 2000). Thus, the detrital zircon and intruding granite ages bracket sedimentation of the Krummedal Succession to between ca. 1040 and 920 Ma.

The provenance of the Krummedal Succession still remains enigmatic, although correlations have been made across the North Atlantic as far east as the Arctic Norwegian Caledonides (Kirkland et al., 2008a). The inferred underlying orthogneisses in East Greenland typically have ages of ca. 2800–2700 Ma and ca. 2000–1900 Ma (Thrane, 2002), which are rarely found in the zircon cargo of the Krummedal Succession (Kalsbeek et al., 2000; Leslie and Nutman, 2003; Strachan et al., 1995). Known Paleo- to Mesoproterozoic crust is rare in East Greenland, probably indicating that grains of this age in the Krummedal Succession were derived from more distal or currently unrecognized sub-ice sources. Potential source terranes include Grenvillian orogens in Laurentia (Gower, 1996; Rivers, 1997) or the Sveconorwegian Orogen in Baltica (Åhäll and Connelly, 1998), both of which are compatible with axial drainage from the south (in present-day coordinates) and similar detrital spectra in the rest of the North Atlantic region (e.g., Kirkland et al., 2008a; Pettersson et al., 2009a). However, distinguishing Laurentian from Baltican crust on U-Pb and Hf isotopes remains problematic (Slagstad and Kirkland, 2017).

2.2.2 Eleonore Bay Supergroup (Nathorst Land, Lyell Land, Ymer Ø and Andrée Land Groups)

Structurally overlying the Krummedal Succession is the Eleonore Bay Supergroup, which has an estimated total thickness of >14 km (Sønderholm et al., 2008; Sønderholm and Tirsgaard, 1993). The contact between the Krummedal Succession and Eleonore Bay Supergroup is now structural across an extensional detachment (Hartz and Andresen, 1995) but, originally, the younger supergroup was thrust westwards over the older succession (Smith and Robertson, 1999).

The lower ~12 km of the Eleonore Bay Supergroup comprises primarily paralic to shallow marine siliciclastic sedimentary rocks of the Nathorst Land (~9 km) and Lyell Land Groups (~ 3 km), whereas the upper ~2 km are dominantly carbonate platform deposits of the Ymer Ø and Andrée Land Groups (Sønderholm and Tirsgaard, 1993). The Nathorst and Lyell Land Groups host lithologically similar successions, although the Nathorst Land Group does comprise minor carbonates and microbialites, which the Lyell Land Group lacks (Sønderholm et al., 2008; Sønderholm and Tirsgaard, 1993). In Andrée Land, ~2.5–3.0 km of the Nathorst Land Group were eroded away prior to the deposition of the Lyell Land Group, indicating at least one significant stratigraphic break (Smith and Robertson, 1999). It is not known whether this unconformity is present away from Andrée Land (Sønderholm et al., 2008) but it is probable that the Eleonore Bay Supergroup can be divided into a lower (Nathorst Land Group) and upper component (Lyell Land, Ymer Ø and Andrée Land Groups). The Eleonore Bay Supergroup has been intruded by Silurian granites during the Caledonian Orogeny (Gilotti and McClelland, 2005; Slama et al., 2011). However, unlike the Krummedal Succession, there is no evidence for the 'older' granite suite (ca. 950–920 Ma) intruding the Eleonore Bay Supergroup (Kalsbeek et al., 2000).

Accurate depositional ages for the various groups in the Eleonore Bay Supergroup are still lacking. Only a few samples have been analyzed for detrital zircon geochronology from the siliciclastic sequences, including five samples from two areas from the Nathorst Land Group (Dhuime et al., 2007; Watt et al., 2000), and four samples from two areas within the Lyell Land Group (Slama et al., 2011; Watt et al., 2000). The maximum depositional age inferred from the youngest zircon grains from the Nathorst Land Group is ca. 990 Ma (Dhuime et al., 2007) and ca. 880 Ma for the Lyell Land Group (Slama et al., 2011). The upper age for the Eleonore Bay Supergroup is constrained by Marinoan-aged diamictites of the overlying Tillite Group (Fairchild and Hambrey, 1995; Halverson et al., 2005; Halverson et al., 2004), which corresponds to an age of ca. 650 Ma for the top of the Eleonore Bay Supergroup.

The provenance of the Nathorst and Lyell Land Groups is markedly different (Dhuime et al., 2007; Slama et al., 2011). Concordant detrital zircon cargo age populations from the Nathorst Land Group range predominantly from ca. 1800 to 1200 Ma (Dhuime et al., 2007; Watt et al., 2000), mimicking that of the Krummedal Succession (Kalsbeek et al., 2000; Strachan et al., 1995; Watt et al., 2000). The implication is that either the Nathorst Land Group was derived from the same source terranes as the Krummedal Succession or that the latter succession was exhumed and recycled. In contrast, the Lyell Land Group has a dominant detrital zircon population age peak from ca. 1100 to 1000 Ma, with only minor components of 1800–1200 Ma and rare (3–4%) Archean grains (Slama et al., 2011; Watt et al., 2000). Slama et al. (2011) proposed that the source of these grains was situated in the eastern part of the Canadian Shield on the basis of intrusions that were associated with the final stage of the Grenville Orogeny and dated at ca. 1095–980 Ma (Gower, 1996; Rivers, 1997). This is also compatible with large-scale detrital provenance studies that suggest that the bulk of material was axially-derived from more southerly domains (Spencer and Kirkland, 2016).

2.2.3 Tillite Group

The Tillite Group conformably overlies the Eleonore Bay Supergroup (Moncrieff and Hambrey, 1988; Sønderholm and Tirsgaard, 1993). The lower sequence is Cryogenian in age and comprises diamictites and marine deposits (Hambrey and Spencer, 1987) that were deposited during the Marinoan glaciation as part of "Snowball" Earth (Fairchild and Kennedy, 2007; Hoffman et al., 1998; Li et al., 2013). The upper part of the Tillite Group is probably Ediacaran in age and consists of dolomitic mudstone and shallow marine to supratidal sandstone (Hambrey and Spencer, 1987). The Tillite Group is unconformably overlain by the Cambrian–Ordovician Kong Oscar Fjord Group, which represents early passive margin sedimentation after the opening of the Iapetus Ocean (Smith and Rasmussen, 2008).

The basal age of the Tillite Group is constrained by the age of the Marinoan glaciation (ca. 660 Ma, see above and Halverson et al., 2005). The minimum age at the top of the Tillite Group is ca. 540 Ma, constrained by the presence of distinctive early Cambrian fauna in the overlying succession (Smith et al., 2004b). No detrital zircon work has been conducted on the Tillite Group to further constrain its maximum depositional age, provenance or correlations across the North Atlantic region.

3 SAMPLE SELECTION

Eight samples, including five metasedimentary samples from the Nathorst Land Group and three intruding granites, were collected from four localities in Wollaston Forland during an expedition in East Greenland in 2018 (Fig. 3, Table 1)

One granite (590201; 19.32606 °W, 74.58298 °N) and one metasedimentary (590204; 19.33057 °W, 74.57573 °N) sample were collected from the northeastern part of Wollaston Forland, on the Kap Berlin peninsula (Fig. 3, Table 1). The granite is inferred into the basement, based on observations of enclaves of metasedimentary rocks within the granite. Sample 590201 was collected from an undeformed biotite granite. Sample 590204 was gathered from an enclave of isoclinally-folded, biotite-plagioclase-quartz ± garnet psammitic gneiss with a strong gneissosity within the undeformed granite.

One granite (547408; 19.78191 °W, 74.40077 °N) and one metasedimentary (590210; 19.78527 °W, 74.39987 °N) sample were collected from the centre of Wollaston Forland (Fig. 3, Table 1). Like the northeast part of Wollaston Forland, the metasedimentary rocks are enclaves within the granite. Sample 547408 was collected from a sulphide-mineralized granite. Sample 590210 was extracted from a decametre-scale quartzite enclave within the mineralized granite. The outcrop area of

Proterozoic basement is tens of meters wide and long, and so is below the resolution of the map area in Fig. 3.

Two banded metasedimentary samples (590207; 20.08284 °W, 74.62391 °N and 590214; 20.11136 °W, 74.63862 °N) were taken from the northwest of Wollaston Forland, near Kap Schumacher (Fig. 3, Table 1). Sample 590207 represents a foliated quartzite that has been intruded by granite. Sample 590214 was collected from a garnet-sillimanite-biotite metapelite.

One granite (590239; 20.19881 °W, 74.37070 °N) and one metasedimentary (590232; 20.20857 °W, 74.30931 °N) sample were collected from the southwestern part of Wollaston Forland, on either side of the Lille Sødal ravine (Fig. 3, Table 1). Here, the granite occurs as several m-wide sheets that steeply cross-cut the metasedimentary succession. Granite sample 590239 was taken from a pink granite with stretched quartz crystals. The pink granite cross-cuts quartzite, similar in lithology to where samples 590207 and 590210 were sampled. Sample 590232 was selected from a garnet-bearing, foliated, isoclinally-folded and melted psammite.

4 METHODS

4.1 Sample preparation and grain imaging

All eight samples were disaggregated by jaw crushing to liberate constituent minerals. Heavy mineral fractions were separated using heavy liquid and magnetic susceptibility techniques. All zircon grains were mounted in 25 mm diameter epoxy stubs and polished to half-grain thickness to expose their interiors. Mounted grains were imaged with transmitted and reflected light on an optical microscope and, subsequently, with back-scattered electron (BSE) and cathodoluminescence (CL) imaging using a Tescan Mira3 variable pressure field emission gun scanning electron microscope (VP-FEG-SEM) at the John de Laeter Centre (JdLC) at Curtin University. Transmitted and reflected light images were

used to assess grain shape and transparency as a means to assess zircon growth and modification processes. BSE and CL images were used to document internal zonation patterns (e.g. oscillatory, sector) and identify growth and recrystallization textures as an aid to targeting in situ analysis (Corfu et al., 2003).

4.2 Zircon U-Pb and Lu-Hf isotopic data

Zircon U-Pb and Lu-Hf isotopic measurements were collected simultaneously using the laser ablation split stream system housed in the GeoHistory Facility, JdLC, Curtin University, in four sessions across one week. Where possible, multiple spots were collected from both grain cores and rims. Analyses were conducted targeting >100 grains to capture minor subpopulations without preselecting grains, in order to minimise sample bias and yield an objective detrital zircon distribution (Vermeesch, 2004). An overview of operating conditions is given here but more detail can be found in Spencer et al. (2017) and Gardiner et al. (2019). An excimer laser (Resonetics S-155-LR 193 nm) was used with a laser fluence of 3 J cm^{-2} and repetition rate of 10 Hz for ~30–35 s of total analysis time and 60 s of background capture. All analyses were preceded by three cleaning pulses. The sample cell was flushed by ultrahigh purity He (0.68 L min^{-1}) and N_2 (2.8 mL min^{-1}). As a result of zircon grain size variation between samples, analytical spot diameters varied between 50 µm (session 1) and 38 µm (sessions 2–4). Any systematic difference between these approaches was excluded by repeated analysis of grains from session 1 (50 µm) in session 2 (38 µm), targeting similar growth domains.(see supplementary Fig. A).

U-Pb data were collected on an Agilent 7700s quadrupole (session 1) or Agilent 8900 triple quadrupole (sessions 2–4) mass spectrometers with high purity Ar as the carrier gas (flow rate 0.98 L min^{-1}). Analyses of unknowns were bracketed with analyses of the primary zircon reference material GJ-1 (601.86 ± 0.37 Ma; Horstwood et al., 2016; Jackson et al., 2004) to monitor and correct for mass fractionation and instrumental drift. A range of secondary zircon reference materials spanning

Archean to Phanerozoic ages – R33 (419.26 ± 0.39 Ma; Black et al., 2004), 91500 (1062.4 ± 0.4 Ma; Wiedenbeck et al., 1995) and OG1 (3465.4 ± 0.6 Ma; Stern et al., 2009) – were used to monitor data accuracy and precision, and were corrected for mass bias and fractionation based on measured isotopic ratios of the primary reference material. During the analytical sessions, R33, 91500 and OG1 yielded statistically-reliable weighted mean ages of 417.3 ± 1.7 to 420.3 ± 1.3, 1059.1 ± 2.9 to 1063.8 ± 2.4, and 3464 ± 10 to 3477 ± 17, respectively, all of which are within 2σ of the published age (see supplementary Table A for full U-Pb standard compilation). Zircon data are considered concordant where the $^{207}Pb/^{206}Pb$ and $^{238}U/^{206}Pb$ systems overlap with the concordia curve (Ludwig, 1998). All zircon dates are presented as the most precise date between $^{206}Pb/^{238}U$ and $^{207}Pb/^{206}Pb$ ages (Supplementary Table B). This includes those recalculated in the compilation in Supplementary Table C.

Lu–Hf isotopic data were collected from the same analytical volume as U–Th–Pb data on a Nu Instruments Plasma II MC-ICPMS. Measurements of ^{172}Yb, ^{173}Yb, ^{175}Lu, $^{176}Hf+Yb+Lu$, ^{177}Hf, ^{178}Hf, ^{179}Hf and ^{180}Hf were made simultaneously. Mud Tank zircon was used as the primary reference material for Hf isotope ratios, with a $^{176}Hf/^{177}Hf$ ratio of 0.282505 ± 0.000044 (Woodhead and Hergt, 2005). Corrected $^{176}Lu/^{177}Hf$ ratios were determined through processing against the R33 zircon standard (0.001989 ± 0.000869; Black et al., 2004). 91500 (0.282306 ± 0.000008; Woodhead and Hergt, 2005), FC1 (0.282172 ± 0.000042; Salters and Hart, 1991) and GJ-1 (0.282000 ± 0.000005; Morel et al., 2008) were used as secondary standards to monitor accuracy of data processing. During the analytical sessions, secondary standards across the four sessions yielded statistically reliable corrected $^{176}Hf/^{177}Hf$ weighted average ratios: 91500 yielded 0.282274 ± 0.000028 to 0.282314 ± 0.000018; FC1 yielded 0.282159 ± 0.000033 to 0.282217 ± 0.000034, and; GJ-1 yielded 0.281985 ± 0.000026 to 0.282009 ± 0.000016, all of which overlap within 2σ of the published values (see supplementary Table B for full Hf isotope standard compilation). The stable $^{178}Hf/^{177}Hf$ and $^{180}Hf/^{177}Hf$ ratios for Mud Tank yielded values of 1.46712 ± 0.00004 to 1.46718 ± 0.00004 and

1.88668 ± 0.00009 to 1.88688 ± 0.00008, respectively, across the four sessions (Supplementary Table A), overlapping with expected terrestrial and Mud Tank $^{178}Hf/^{177}Hf$ and $^{180}Hf/^{177}Hf$ values (Gain et al., In Press; Patchett and Tatsumoto, 1981). Decay constants, chondritic uniform reservoir (CHUR) and depleted mantle values are taken from Söderlund et al. (2004), Bouvier et al. (2008) and Griffin et al. (2002), respectively.

Data were reduced in Iolite (Paton et al., 2011) and in-house Excel macros. Detrital zircon population ages were assessed using Isoplot 4.15 software (Ludwig, 2012), with Excel macros used to produce detrital zircon age probability density plots and cumulative density plots (Gehrels et al., 2008). Kernel density plots of detrital zircon age populations, were performed in the R statistical "provenance" analysis package (Vermeesch et al., 2016). Full isotopic data for the samples are given in supplementary Table B. Epsilon notation Hf isotopic data relative to CHUR at the time of crystallization [$\varepsilon Hf_{(t)}$] were computed for concordant zircon grains using the age of the crystal, and the measured (present-day) $^{176}Lu/^{177}Hf$ and $^{176}Hf/^{177}Hf$ values.

4.3 Compilation and evaluation of previously published detrital zircon data

In order to work towards resolving some of the stratigraphic correlations across the North Atlantic region (see discussion), we have compiled detrital zircon U-Pb and Hf isotopic data from latest Mesoproterozoic to Cryogenian successions in the North Atlantic region. We only use concordant U-Pb data that have analyzed a single crystal domain (i.e., core or rim, but not across zones). We define concordant analyses as those where the 2σ error ellipse overlaps with the concordia curve (Spencer et al., 2016). We exclude any grains or grain rims that have been interpreted to be of metamorphic genesis in the original publications.

We use statistical analyses to scrutinize U-Pb data using the K–S test (Massey, 1951), coupled U-Pb and Hf isotopic data using the Detzrcr code (Detrital Zircon in R; Kristoffersen et al., 2016) and

zircon disparity tests (Barham et al., 2019a). The K–S test returns a distance value that defines the maximum vertical separation from between the age curves of any two of detrital zircon samples on a cumulative probability diagram. Thus a distance of 1.0 indicates a 100% difference, i.e. that all grains in one sample are older than all the grains in another sample, while a distance of 0 indicates a perfect match of ages between samples. Each distance metric is associated with a corresponding p-value that describes the probability that random sampling could account for any differences between samples, and thus that two samples could have been drawn from the same population ($p > 0.05$). The similarity of detrital zircon populations was also assessed through a modified 'likeness' metric of Satkoski et al. (2013), which considers both the temporal consistency and magnitude of age peaks between probability density plots of any two detrital zircon samples. This likeness metric can be applied to both U-Pb and Hf model ages and incorporate 95% confidence intervals to assess likelihood of sample relatedness (Andersen et al., 2016; Kristoffersen et al., 2016). While these similarity tests inform relationships between any two samples, associations within sample groups are more difficult to assess through traditional similarity matrices. For this reason, similarity values across sample groups are commonly visualised via multi-dimensional scaling (MDS; Vermeesch, 2013), whereby the distances (taken from a K–S test, or equivalent) between multiple detrital zircon sample pairs within any group of samples are rationalised into a 2D plot. The closer proximity of samples on an MDS plot equates to greater similarity of their detrital age signatures. Thus, an MDS plot visually displays relative sample differences based on a mathematical approach to rationalise a matrix of sample pair comparisons. Tracking how detrital zircon similarity metrics change through time may be further facilitated via disparity metrics (Barham et al., 2019a; Barham et al., 2019b). This technique assesses the magnitudes of 'distances' (typically from a K–S test) of different detrital zircon age populations within distinct spatial or temporal sample sets (in this case, megasequences, see discussion). Rather than using distance values between pairs of samples within a sample group to produce an MDS plot, they can be used to quantify how closely related the overall group is (Barham et al., 2019b). Both the

average nearest neighbour distance (mean of the distance measure between the most similar sample pairs for all samples within a group) and average inter-sample distances (mean distance measure across all sample pairs within a group) provide insight into the nature of differences between detrital zircon sample populations (visualised spatially from MDS space in Fig. 4). Tracking both disparity metrics allows identification of any sub-grouping within a larger set of samples, while comparing the average values that define any chosen sample grouping can inform larger scale changes in basin and/or crustal evolution controlling zircon generation, dispersion and mixing (Barham et al., 2019a).

5 RESULTS

5.1 Zircon morphology and textures

Zircon grains are 60–150 μm in length and have low to moderate aspect ratios of 1:1 to 4:1 (Fig. 5, Supplementary Fig. B). In all metasedimentary samples, internal zircon textures are dominantly (sub-)rounded oscillatory- and sector-zoned cores with most grains displaying thin, weakly- oscillatory-zoned overgrowths with a dark or bright CL response (Fig. 5a–c, grains with purple spots). Grains with rounded terminations tend to have limited development of grain rims (Fig. 5, most purple spots), whereas rare idiomorphic zircon shows clear overgrowths (Fig. 5e, green spot). Grain cores also occasionally exhibit homogeneous CL response (Fig. 5b), particularly bright CL response (Fig. 5a–c) or chaotic zoning (Fig. 5c), all of which have yielded concordant dates. Rarely, overgrowths with homogeneous CL responses approach thicknesses >40 μm, especially in sample 590232 (Fig. 5e).

In granitic samples, internal zircon textures can be similar to those found in metasedimentary samples (Fig. 5, red spots), but oscillatory- and sector-zoned zircon grains without core–rim distinctions are also present (Fig. 5e). In sample 590239, a lack of core–rim domains is especially notable (Fig. 5e).

This same sample also includes a significant portion of grains with a dark, homogeneous CL response (Supplementary Fig. B).

5.2 Zircon U-Pb data

5.2.1 Metasedimentary samples

The five metasedimentary samples yielded a mixture of concordant and discordant analyses (Fig. 6). Concordant grain ages are concentrated between ca. 2900 and 920 Ma, with only two analyses younger than 920 Ma that were not collected across core–rim domains (Fig. 6). The concordant population older than 920 Ma were exclusively collected from (predominantly rounded) grain cores that are interpreted to be detrital. The internal textures of these grains are predominantly oscillatory-or sector zoned but a subordinate portion are more homogeneous (Fig. 5). Each of the metasedimentary samples show broadly equivalent age subpopulations (Fig. 6–7). Dating of grain cores reveal that ~94% of the concordant population is part of a continuous spread of ages between ca. 1850 and 910 Ma with distinct age peaks at ca. 1620 Ma, 1450 Ma and 1080 Ma. Additional age subpopulations include minor clusters at ca. 2900–2600 Ma (~4%) and ca. 2030–1940 Ma (~2%). There is no clear distinction in CL response between the different subpopulations (Fig. 5a–c), with the exception that the youngest subpopulation tends to be low in U (Fig. 5d).

The youngest detrital zircon grains in samples 590204, 590207 and 590210 are broadly equivalent in age (950–910 Ma; Fig. 6–7). Weighted mean $^{206}Pb/^{238}U$ ages of the youngest grain(s) for samples 590204, 590207 and 590210 were calculated at 950 ± 23 Ma (n = 1), 925 ± 18 Ma (n = 2, MSWD = 0.02, p = 0.88) and 933 ± 49 Ma (n = 1), respectively. These dates yield a combined weighted mean $^{206}Pb/^{238}U$ age of 936 ± 15 Ma (n = 6, MSWD = 0.59, p = 0.71). The youngest grains in sample 590214 and 590232 were older than ca. 1000 Ma (Fig. 6).

The two analyses younger than 910 Ma are both from sample 590232 (Fig. 6e). These two analyses targeted grain rims with homogeneous CL response (e.g., 590232-15 in Fig. 5e) and yielded U–Pb dates of 417 ± 11 and 419 ± 10 Ma (green squares, Fig. 6e), overlapping with the granite ages (see section 5.2.2 and Fig. 6g–h). The homogeneous CL response and overgrowth nature of these analyses implies they represent metamorphic rims.

5.2.2 Granitic samples

Two granite samples (547408 and 590201) yielded similar zircon age subpopulations to the metasedimentary samples, with sample 590201 having additional ca. 510 (n = 3) and ca. 430 Ma (n = 13) subpopulations, and a single concordant ca. 800 Ma analysis (Fig. 6f–g). Given that the granite samples show emplacement relationships with metasedimentary units in the field (Fig. 3), grains older than ca. 1000 Ma are considered to be inherited zircon. The four concordant ca. 800 and ca. 510 Ma dates reflect core–rim sampling mixtures. The Silurian subpopulation was analyzed on idiomorphic oscillatory-zoned grains without core–rim textural distinctions (Fig. 5e). This subpopulation yielded a $^{206}Pb/^{238}U$ weighted mean age of 427 ± 5 Ma (n = 13, MSWD = 1.05, p = 0.32), which is interpreted as the magmatic crystallization of granite sample 590201.

One of the granite samples (590239) yielded only a single age population on oscillatory- and sector-zoned crystals (Fig. 5e, Fig. 6h). Of the 212 total spots, 145 were concordant and yielded a $^{206}Pb/^{238}U$ weighted mean age of 426 ± 1 Ma (MSWD = 1.05, p = 0.32), considered as the crystallization age of the granite. This age overlaps with the crystallization age of granite sample 590201.

5.3 Zircon Hf isotope data

The Hf isotopic data can be broadly subdivided into two categories: (i) detrital and inherited grains older than 920 Ma with $\varepsilon Hf_{(t)}$ = –12 to +8 (two outliers at –17 and –21), and (ii) ca. 425 Ma magmatic and metamorphic zircon analyses with $\varepsilon Hf_{(t)}$ = –15 to +2 (Fig. 8).

The detrital cores in metasedimentary samples and the inherited cores in granitic samples overlap in age–Hf isotopic space (Fig. 8). Two other notable observations are that that the ca. 1450–1350 Ma subpopulation lacks any points with $\varepsilon Hf_{(t)}$ below –5 and the Archean subpopulation is exclusively <+4 $\varepsilon Hf_{(t)}$ (Fig. 8).

The large range in zircon Hf isotopic compositions for the Caledonian granites needs to be assessed for validity. There is no correlation between $^{176}Yb/^{177}Hf$ and $^{176}Hf/^{177}Hf$ or $^{176}Lu/^{177}Hf$ and $^{176}Hf/^{177}Hf$ for the Caledonian magmatic zircon grains (Supplementary Table B). This lack of correlation indicates that the large range of Hf isotopic compositions for the Caledonian granites are not a function of isobaric interference of ^{176}Yb or ^{176}Lu on ^{176}Hf. Additionally, there is no indication from CL images that these analyses reflect physical mixtures of magmatic cores and metamorphic rims (Supplementary Fig. B). Thus, the large range in εHf units for the Caledonian granites is interpreted as a function of disequilibrium of magma composition (e.g., Tang et al., 2014) or magma mixing (e.g., Griffin et al., 2002).

6 DISCUSSION

6.1 Ages and stratigraphic position of metasedimentary rocks in Wollaston Forland

The presented U-Pb age data help resolve whether the metasedimentary rocks sampled in Wollaston Forland belong to the Meso- to Neoproterozoic Krummedal Succession or the Neoproterozoic Nathorst Land Group (lower Eleonore Bay Supergroup). The presence of ca. 930 ma detrital zircon grains implies that the Nathorst Land Group crops out in Wollaston Forland (Figs. 5d, 6).

The simplest explanation for the ca. 930 Ma detrital grains in our metasedimentary samples is that they were derived from the ca. 930 Ma ‘older’ granite suite. It is worth emphasizing that these grains appear magmatic, with Th/U = 0.2–0.9 (Supplementary Table B) and oscillatory- to sector-zoning

(Fig. 5d), unlike metamorphic grains of this age previously found in the Krummedal (Smallefjord) Succession (Strachan et al., 1995). Although the onset of deposition of the Nathorst Land Group remains poorly constrained (<800 Ma?; Sønderholm and Tirsgaard, 1993), mapping has revealed that the ca. 930 Ma 'older' granite suite does not intrude into it (Kalsbeek et al., 2000). Thus, the most plausible explanation is that the ca. 930 Ma detrital grains were eroded from the 'older' granite suite. The presence of what is highly likely ca. 930 Ma grains derived from the 'older' granite suite indicates that the Wollaston Forland metasedimentary rocks belong to the Nathorst Land Group.

6.2 Provenance of the Eleonore Bay Supergroup

The detrital zircon and Hf isotopic data reported here from the Nathorst Land Group poorly match the most proximal terranes in East Greenland that dominantly comprise Archean- (ca. 3610, 3070–2980 Ma, 2800–2680 Ma) and Paleoproterozoic-aged (ca. 2000–1900 Ma, 1750 Ma) zircon grains (Johnston and Kylander-Clark, 2013; Kalsbeek et al., 1993b; McClelland et al., 2016; Thrane, 2002). The implication is that either the Greenland basement was not exposed, blocked from shedding detritus into the Eleonore Bay Supergroup basin, or that the supergroup was allochthonous to Greenland. It is difficult to constrain which of these models is correct, particularly given the similarity of U-Pb and Hf isotopic signatures across the potential North Atlantic source regions (Slagstad and Kirkland, 2017).

The East Greenland basement may still have been a minor proximal source. First, there is a minor but significant presence of ca. 950–930 Ma detritus with εHf values between –8 and –2 (Fig. 8a), which are known from Renlandian-aged magmatism and metamorphism throughout the western North Atlantic region (Bird et al., 2018; Cawood et al., 2010), including East Greenland (Kalsbeek et al., 2000; Leslie and Nutman, 2003; Watt et al., 2000). Components with ages of ca. 950–900 Ma are present in Baltica (Bingen and Solli, 2009) but with relatively high εHf values (Fig. 8a), implying that

at least some of the source material was derived from the western side of the North Atlantic region (i.e., Laurentia). Second, the minor Archean to Paleoproterozoic population present in the samples may have also been derived locally, but these could also have been derived from more distal Laurentian terranes to the south (in present-day coordinates) along the Grenville Orogen (Krabbendam et al., 2017). Thus, East Greenland may have been a proximal source to the Nathorst Land Group but this is not a requirement as other source terranes may also account for the Archean, Paleoproterozoic and earliest Neoproterozoic subpopulations (Fig. 7–8).

The detrital zircon cargo of our samples is well matched by known Laurentian and Baltican source terranes, although the age and Hf isotopic signal of both these source regions are very similar (Fig. 8; Slagstad and Kirkland, 2017). Given current paleogeographic reconstructions, Amazonia may also have been a source of detrital zircon grains (Cawood and Pisarevsky, 2017). One subpopulation at ca. 1350 found in sample 590207 is not well known in either Laurentia or Baltica (Fig. 7); it is uncertain where this subpopulation is derived from. Baltica notably lacks the Renlandian (ca. 970–920 Ma) and Shawinigan/Elzevirian-aged (ca. 1300–1130 Ma) orogenic events that are found in Laurentia, both of which are present in the detrital zircon record from East Greenland (Fig. 7). The implication is that a Laurentian source region is more likely than a Baltican source, which was previously suggested (Dhuime et al., 2007; Watt et al., 2000). It is thus likely that sediment was transported axially along the western margin (Laurentian) of the North Atlantic region (in present-day coordinates), having potentially limited influence from the opposing eastern, Baltican margin. Such a process is a common phenomenon in extensional basins (e.g., Olierook et al., 2019b).

6.3 Correlations across the Neoproterozoic North Atlantic region

Various workers have attempted to correlate the latest Mesoproterozoic to Neoproterozoic sedimentary basins across the North Atlantic region, with several authors proposing a first order

classification into three distinct “lithostratigraphic packages”, “lithotectonic groupings” or “megasequences” (Bingen et al., 2011; Cawood et al., 2007; Kirkland et al., 2008b). We follow the notion that these three sedimentary packages are related to principal sequence stratigraphic cycles (Williams, 1993) and therefore adopt the term “megasequence”. However, assigning absolute ages to the different megasequences, and correlating them across the North Atlantic region is complicated by a paucity of radiometrically-dateable material, particularly for megasequences 2 and 3, and an absence of fossils for megasequences 1 and 2 (Fig. 9).

6.3.1 Megasequence 1 (ca. 1020–950 Ma)

Megasequence 1 is latest Mesoproterozoic to early Neoproterozoic (ca. 1020–950 Ma) in age and can be found across almost the entire North Atlantic region, from the far west in the allochthonous Pearya Terrane to the allochthonous nappes now found on the western Baltican margin in Norway and Sweden (Fig. 9). Sedimentation at this time is thought to have occurred in extensional basins during the opening of the Asgard Sea between northern Laurentia and Baltica, and were probably sourced from the Grenville Orogen (*sensu stricto*) and possibly the Baltican margin (Bingen et al., 2011; Cawood et al., 2010; Kirkland et al., 2008b). Maximum depositional ages are constrained by the youngest detrital zircon grains, whilst minimum age constraints are provided by granitoid intrusions and associated metamorphic events during the Renlandian Orogeny (Fig. 9–10). Given that these sequences were deposited soon after the Grenvillian–Sveconorwegian orogenies, it is not surprising that the youngest detrital zircon grains are temporally close to the true depositional age (cf. Cawood et al., 2012).

The maximum depositional age for megasequence 1, defined by the youngest detrital zircon, varies from 1039 ± 27 Ma (Krummedal Succession, East Greenland) to 955 ± 24 Ma (Smerenburgfjorden Complex, Svalbard; Fig. 8). The Sleat Group has a slightly older maximum depositional age (1056 ± 17 Ma, Fig. 9), and it is still uncertain whether it is truly part of megasequence 1 (cf. Krabbendam et

al., 2017; Rainbird et al., 2001; Spencer et al., 2015). It is unclear whether the onset of sedimentation is diachronous across the North Atlantic region, or whether the difference in youngest detrital zircon ages is a consequence of differences in available zircon-bearing source terranes. Additionally, there is some component of younger age resetting (i.e., minor Pb-loss) on the $^{206}Pb/^{238}U$ ages. For example, the youngest detrital zircon grain of 955 ± 24 Ma from the Smerenburgfjorden Complex in Svalbard is nearly 5% discordant (Pettersson et al., 2009a), with potentially some Pb-loss caused by later Caledonian intrusions (Pettersson et al., 2009b). With this in mind, most youngest zircon analyses with <1% discordance yielded ages that are between ca. 1030 Ma and ca. 1000 Ma (Fig. 9–10, Table 1, Supplementary Table C).

The minimum age of megasequence 1 is supported by the numerous granitoid intrusion ages and associated metamorphic events across most of the North Atlantic region associated with the Renlandian Orogeny between ca. 970 and 920 Ma (Fig. 9; Bird et al., 2018; Cawood et al., 2010; Leslie and Nutman, 2003). An additional older intrusion occurs in the middle of the stratigraphic package in the Pearya Terrane at 993 ± 3 Ma (Estrada et al., 2018). The northwest of Scotland notably lacks Renlandian-aged granitoids (Fig. 10) in both the Hebridean Foreland (Torridon Group) and Moine, Naver and Sgurr Beag Nappes (Morar Group). The implication is that the zone of Renlandian deformation and magmatism was isolated to the northern part of the North Atlantic region (in present-day coordinates) and was not active further south towards Laurentia (Cawood et al., 2010). In Scotland, the timing of cessation may be informed by sequence stratigraphic interpretations that indicate that the Torridon and Morar Groups were deposited in approximately one supersequence each (Krabbendam et al., 2017), which would last ~50 Myr (Williams, 1993). Considering that deposition in NW Scotland started at or soon after ca. 1000–990 Ma, and with a depositional timeframe of ~50 Myr, it is plausible that deposition of the Torridon and Morar Groups also ceased between ca. 970 and 920 Ma.

The detrital zircon cargo is relatively similar across the North Atlantic region for megasequence 1, both in U-Pb ages (Fig. 10–11) and coupled U-Pb and Hf isotopic data (Fig. 8b, Fig. 12). The sequences in East Greenland (Krummedal Succession), Svalbard (Isbjørnhamna Group, Krossfjorden Group and Smerenburgfjorden Complex) and Scotland (Torridon and Morar ± Sleat Groups) are all relatively similar, dominated by ca. 1.7–1.6 Ga zircon grains with subordinate 1.4–1.3 Ga grains and, in some cases, significant contributions of ca. 1.0 Ga grains (Fig. 10–11). Meso- to Neoarchean grains are also present in small but significant quantities in East Greenland and Scotland (Fig. 8b, Fig. 12), and these are probably locally derived from the North Atlantic Craton (southern Greenland) and Lewisian Complex (Scotland), respectively (Cawood et al., 2010; Kalsbeek et al., 1993a; Kinny and Friend, 1997; Kolb et al., 2013). The coupled Hf isotopic record tells a similar story, albeit missing a portion of the 1.7–1.6 Ga subpopulation that is a dominant component in studies focussed solely on U-Pb dating (cf. Fig. 8b, Fig. 10).

On the other side of the North Atlantic, the Norwegian Caledonides have similar age populations (Fig. 10) and εHf values (Fig. 8b) to the western North Atlantic but also significant ca. 1.2–1.1 Ga and ca. 1.8 Ga age populations that are not found in such significant quantities in East Greenland, Svalbard and Scotland. Nevertheless, the Norwegian Caledonides cannot be statistically differentiated from the rest of the megasequence 1 units on U-Pb and Hf isotopic data (Slagstad and Kirkland, 2017), showing particular similarities to groups in Scotland (Fig. 12).

The only units with significantly different detrital zircon cargo in megasequence 1 are: (i) from Shetland (Westing and Yell Sound Groups), which have a primary ca. 1.0 Ga subpopulation and a Mesoarchean peak that is more significant than other units from megasequence 1, and, (ii) the Sleat Group, which has a dominant 1.8 Ga subpopulation (Fig. 10–11) and may precede megasequence 1 altogether (Kinnaird et al., 2007; Krabbendam et al., 2017). Other regions such as dredged samples from the Lomonosov Ridge (Knudsen et al., 2018) and in drill holes in the Norwegian Sea (Slagstad

et al., 2011) may also be part of megasequence 1 but have poorly constrained stratigraphic context, and are only included in Table 1 but excluded from Fig. 10–11.

6.3.2 Megasequence 2 (ca. 920–840 Ma)

The second megasequence is thought to be a consequence of rifting of the supercontinent Rodinia (Li et al., 2008; Lyu et al., 2017; Merdith et al., 2019). Although this extensional episode did not lead to continental breakup (Olierook et al., 2019a; Preiss, 2000), it facilitated thinning of the lithosphere for its eventual breakup towards the late Tonian and into the Cryogenian. The maximum depositional age of megasequence 2 is moderately-well defined by the youngest detrital zircon grains, which were probably sourced from granitoid intrusions associated with the ca. 970–920 Ma Renlandian Orogeny (Cawood et al., 2010). The minimum depositional age of megasequence 2 is poorly constrained in most locations (Fig. 9), except for the presence of 870–840 Ma granitoid intrusions in Scotland (Friend et al., 1997; Kirkland et al., 2008b; Rogers et al., 1998; Rogers et al., 2001), ca. 840 Ma intrusions in the Norwegian Caledonides (Kirkland et al., 2006) and potential ca. 900–850 Ma acritarchs in the Northeast Terrane of Svalbard (Knoll, 1982). Cessation of sedimentation was probably caused by regional uplift (Dalziel and Soper, 2001; Paulsson and Andréasson, 2002).

Depositional time spans for megasequence 2 are relatively similar across most of the North Atlantic region, commencing primarily after 920 Ma and probably ceasing by ca. 840 Ma, but perhaps even as early as ca. 870 Ma (Fig. 9). A cessation of sedimentation by ca. 870 Ma (upper Moine Supergroup) is indicated in the Moine, Naver and Sgurr Beag Nappes in NW Scotland (Fig. 9; Friend et al., 1997; Millar, 1999; Rogers et al., 2001). It is possible that deposition started and ceased ~20–30 Myr earlier in Scotland than in other regions. Such a process would attest to diachronous extension, propagating from the interior of Rodinia towards outboard peri-Rodinian subduction zones (Li et al., 2008; Merdith et al., 2017). However, this claim is difficult to substantiate given the poorly-constrained maximum depositional age of other sequences (Fig. 9).

Statistical comparison of the provenance signatures in megasequence 2 shows that most of the units (with the exception of the para-autochthonous Vadsø Group) have relatively minor age variation but systematic differences in εHf data (Fig. 8c, 10, 11). Minor variation in the proportion of late Paleoproterozoic (1800–1600 Ma) and mid- to late Mesoproterozoic detrital cargo exists, well highlighted in the MDS plot (Fig. 11). In the Hf isotopic data, the allochthonous nappe samples from the Särv and Sørøy Successions in Norway have consistently higher εHf (average, +3) than those samples from Scotland and East Greenland (average, –2), resembling the averages of Baltican and Laurentian magmatic sources, respectively (Fig. 8c). This is also reflected in Fig. 12, where the Särv and Sørøy Successions are markedly different in terms of Hf isotopic signature from the East Greenland and Scottish sequences (Nathorst Land and Loch Eil Groups). However, the underlying successions from Megasequence 1 (Svaerholt Succession, Morar Group, Torridon ± Sleat Groups) also need to be considered; if these are equally different in terms of Hf isotopic signature, then it may be possible to suggest that there is a dichotomy of sediment sources, with the allochthonous nappe samples coming from Baltica and the Scottish and Greenland samples originating from Laurentia. Statistical analysis implies that such a clear distinction is not possible, with the Svaerholt Succession sharing age and Hf isotope similarities not only with the Särv and Sørøy Successions but also with the Torridon and Krossfjorden Group from megasequence 1 and the Loch Eil Group from megasequence 2 (Svalbard, Fig. 12). The implication is that assigning clear Baltican or Laurentian sources to megasequence 2 is equivocal, echoing earlier interpretations (Slagstad and Kirkland, 2017).

6.3.3 Megasequence 3 (ca. 740–635 Ma)

The third megasequence is thought to have developed in response to further rifting of the North Atlantic region and eventual breakup and opening of the Iapetus Ocean in the Ediacaran (Cawood et al., 2001). It is also concomitant with the broader dismemberment of Rodinia from ca. 750 to ca. 635 Ma (Li et al., 2008; Merdith et al., 2019). The maximum depositional age is difficult to constrain due

to the paucity of post-840 Ma zircon-bearing crystalline sources (Fig. 9). A lack of contemporaneous zircon-generating events is typical of extensional environments because felsic rocks are rarely produced (Cawood et al., 2012). Instead, rift basins incorporate older detritus, either freshly sourced from terranes (older than 840 Ma in the North Atlantic situation) or recycled from previous depositional sequences (Barham and Kirkland, in press; Gawthorpe and Leeder, 2000; Olierook et al., 2019b). Acritarchs in the Lyell Land Group in East Greenland and upper Murchisonfjorden Supergroup in the Northeast Terrane in Svalbard indicate an early Cryogenian (ca. 720 Ma) onset to deposition here (Fig. 9) but placing an onset age is difficult for other regions. The minimum depositional age for megasequence 3 is relatively well-constrained due to the extensive presence of glacigenic rocks across the region associated with the ca. 650–635 Ma Marinoan glaciation (Bingen et al., 2005; Halverson et al., 2005; Li et al., 2013).

Megasequence 3 displays a far more varied provenance based on both age (Fig. 10–11) and Hf isotopic data (Fig. 8d, Fig. 12). Like megasequence 2, there are some geographic distinctions in Hf isotopic data between sedimentary rocks proximal to Baltica (i.e., Sparagmite Sequence) and those deposited closer to Laurentia (e.g., Pearya Succession II and Lyell Land Group, Fig. 8d, Fig. 12). However, this dichotomy is blurred when adding in all other geographic locations in the age spectra; for example, the Grampian Group in Ireland has a rather similar spectra to the Sparagmite Sequence (Fig. 10–11).

There is also significant local variation observed in both space and time, particularly notable in the Scottish and Irish Nappes. For example, the Grampian Groups in Scotland and Ireland have distinct ca. 1520 and 1680 Ma peaks (Banks et al., 2007; McAteer et al., 2010b), respectively, accounting for localized differences across relatively short distances (Fig. 10). There are also significant temporally-distinct differences in the U-Pb record between the Grampian, Appin and Argyll Groups in Scotland,

and between the Deilegga, Sofiebogen and Kapp Lyell Groups in SW Svalbard (Fig. 10–11), attesting to evolving sediment sources.

6.4 Implications for tectonic and basin evolution of the North Atlantic region

Megasequences 1 and 2 are characterized by greater homogeneity of detrital zircon age signatures than megasequence 3, particularly well highlighted on a zircon disparity plot (Fig. 13). This graph shows that both average distances between nearest neighbours (how close are the most similar samples to each other in a sample group) and average inter-sample distances (how similar are all the samples in a sample group to each other overall) are very similar for megasequences 1 and 2, but far more disparate for megasequence 3, and there are a few possible explanations for this observation.

The overall spatially- and temporally-similar zircon cargo between megasequences 1 and 2 indicates that their source regions are alike. We explain the low zircon disparity in megasequences 1 and 2 to be controlled principally by axial sedimentary transport pathways, which allows for the homogenization of detritus down-stream (Cawood et al., 2003a; Davis et al., 2010; Murphy and Hamilton, 2000). In megasequences 1 and 2, most sediment appears to be transported axially from south to north (in present-day coordinates) to deliver Laurentian and potentially Baltican detritus from the Rodinian interiors to the outer margin and into the Asgard Sea (Friend et al., 2003; Krabbendam et al., 2017). However, their specific source-to-sink mechanisms are probably significantly different, principally because megasequences 1 and 2 were deposited in distinct tectonic regimes, namely syn-collisional (foreland) to syn-extensional (rift) settings, respectively (Cawood et al., 2004; Krabbendam et al., 2017). In megasequence 1, the detrital zircon population was probably sourced directly from dominantly Mesoproterozoic crystalline basement in Laurentia (Krabbendam et al., 2017; Spencer et al., 2015). However, for megasequence 2, there was probably a significant degree of recycling of

sedimentary rocks deposited during the first megasequence. The evidence for this stems from the presence of Renlandian-aged material (ca. 950–920 Ma) in megasequence 2 (this study; Bird et al., 2018; Cawood et al., 2010; Leslie and Nutman, 2003), which implies that granite-intruded rocks of megasequence 1 were exhumed and recycled into successor, extensional basins of megasequence 2. In this scenario, megasequence 2 recycled some proportion from megasequence 1 as well as probably sourcing more primary Laurentian ± Baltican material via axial drainage. The paucity of Archean and Paleoproterozoic material implies that localized older sources (e.g., the Lewisian Gneiss Complex in Scotland) were not exposed, and that there was insufficient exhumation to erode down to the deep crystalline basement from the rift margin flanks. The implication of a lack of rift-shoulder detritus for megasequence 2 is that – despite occurring in an extensional regime – sedimentation kept track with the generation of accommodation space to minimize relative elevation differences with surrounding basement (Olierook et al., 2019b; Sircombe and Freeman, 1999).

Between megasequences 2 and 3, there is a significant increase in zircon disparity (Fig. 13). In detail, megasequence 3 shows: (i) an increased contribution of Archean detritus where Archean basement provinces are known to be proximal (e.g., Lewisian Complex, Scotland; Archean basement in northeast Greenland), (ii) a larger proportion of ca. 1.5 Ga material in Svalbard, and (iii) a significant portion of late Meso- to Neoproterozoic material in parts of the Pearya Terrane, East Greenland, Svalbard and Shetland (Fig. 11).

The influx of Archean material has previously been attributed to exhumation of proximal crystalline basement (Cawood et al., 2003b; Glover et al., 1995) or the removal of a distal orographic barrier between sequences 2 and 3 (i.e., a topographically-high Grenville Orogen; Spencer and Kirkland, 2016). The unroofing model is able to account for the Archean detritus influx in regions where Archean cratons are proximal. In particular, the proportion of Archean detrital zircon grains increases after deposition of the first sedimentary group in megasequence 3. For example, the Grampian Group

in Scotland still has minimal Archean detritus, but the Appin and Argyll Groups have dominant and significant proportions, respectively. Similarly, in East Greenland, the Lyell Land Group shows negligible Archean and Paleoproterozoic detritus, but the Morænesø Group in northeast Greenland shows abundant amounts of basement-derived zircon cargo (Fig. 10). This unroofing process could also be occurring in other portions of the North Atlantic (e.g., Svalbard, Norwegian Caledonides) but these simply lack the proximal Archean basement at the time of deposition. As an alternative model, the removal of a topographically-high Grenville Orogen (*sensu stricto*) has been attributed to preventing interior Laurentian detritus (including Archean material) from entering the axial drainage pathway from Rodinia interior towards the Asgard Sea (Spencer and Kirkland, 2016). Although removal of a Grenvillian (*sensu stricto*) orographic barrier could explain the source of Archean and Paleoproterozoic material, its transport via axial drainage would serve to homogenize the zircon cargo. Given the higher zircon disparity (Fig. 13), an orographic barrier model is less plausible.

The ca. 1.5 Ga material is thought to be derived from Baltican sources (Gasser and Andresen, 2013; Ziemniak et al., 2019), and the Neoproterozoic component is probably derived from local sources rather than via long-distance transport (Estrada et al., 2018; Malone et al., 2014; Slama et al., 2011; Strachan et al., 2013; Ziemniak et al., 2019). These components are not explained by an unroofing model, and a more holistic model is needed to explain the zircon disparity across the North Atlantic during megasequence 3.

To explain all the interbasinal differences in megasequence 3, we invoke a change from shared circum-Atlantic sediment transport mechanisms in megasequences 1 and 2 (i.e., axial transport) to more localized and compartmentalized basin formation in megasequence 3. This mechanism facilitates the localized exhumation of crystalline basement during rift-shoulder uplift (Daradich et al., 2003; Fitzgerald, 1992), which is able to account for the exposure of Archean and Paleoproterozoic basement found in Scotland and East Greenland, and the 1.5 Ga basement found in Baltica.

Compartmentalization also necessitates topographic barriers between (sub-)basins that can, in turn, be eroded and peneplaned (Sircombe and Freeman, 1999). If these topographic barriers comprise unroofed crystalline basement (together with recycled sedimentary rocks from Megasequences 1 and 2), then its erosion facilitates the delivery of that crystalline basement from the rift-shoulders to the basin (Olierook et al., 2019b). It also facilitates the contribution and delivery of uncommon Neoproterozoic detritus.

The question remains why such a significant change occurred between megasequences 2 and 3. During extension leading up to continental breakup, it is common for fault-bound sub-basins to develop (Olierook et al., 2015; Whipp et al., 2014), each of which may have unique transport mechanisms that disconnect broad-scale source-to-sink pathways and instead promote localized routing systems (Barham and Kirkland, in press; Gawthorpe and Leeder, 2000; Leeder and Gawthorpe, 1987; Olierook et al., 2019b). We suggest that much of the disparity observed in megasequence 3 occurred because Rodinia was disaggregating in the Cryogenian and Ediacaran (Li et al., 2008; Merdith et al., 2019), yielding distinct sediment transport pathways and compartmentalized basins.

7 CONCLUSIONS

New zircon U-Pb and Hf isotope data from five metasedimentary samples yield maximum depositional ages of 936 ± 15 Ma (2σ) that indicate that sampled metasedimentary rocks belong to the Neoproterozoic Nathorst Land Group (lower Eleonore Bay Supergroup). Intruding granites are exclusively of Caledonian age at 426 ± 1 Ma (2σ) and contain significant inherited zircon cargo comparable to the detritus in the host metasedimentary sequences. Detrital zircon age components are concentrated between ca. 1850 and 920 Ma, with prominent peaks at ca. 1620 Ma, 1450 Ma and 1080 Ma, and additional subpopulations at 2900–2600 Ma (~4%) and 2030–1940 Ma (~2%). Provenance of

this sedimentary detritus is probably from the East Laurentian margin via axial drainage to East Greenland. Statistical analyses of detrital zircon data and auxiliary temporal information from the North Atlantic region affirms the notion that sedimentation occurred in three distinct megasequences: (1) 1020–950 Ma, as a response to the final collisional phase of the Grenvillian Orogeny (*sensu lato*), (2) 920–840 Ma, recording the onset of initial rifting of the North Atlantic and Rodinia in general, and (3) 740–635 Ma, concomitant with the breakup of Rodinia and ending with the Marinoan glaciation. The first two megasequences show strong U-Pb and εHf similarities in both space and time across the North Atlantic. There is a significant increase in detrital zircon age population disparity between the second and third megasequences, which we propose is associated with regionally distinctive basement exhumation and depocentre development with independent sediment routing pathways during continental breakup.

Acknowledgements

This work was supported by the Ministry of Mineral Resources, Government of Greenland. The Tescan Mira3 at the JdLC was funded using ARC LIEF grant LE130100053. The LA-ICP-MS instrument in the JdLC, Curtin University, was funded via an Australian Geophysical Observing System grant provided to AuScope Pty Ltd. by the AQ44 Australian Education Investment Fund program. N. J. Evans and B. J. McDonald are thanked for aiding LA-ICP-MS analysis. W. McClelland, an anonymous reviewer and the editorial handling of V. Pease significantly improved this manuscript.

References

Agyei-Dwarko, N.Y., Augland, L.E., Andresen, A., 2012. The Heggmovatn supracrustals, North Norway—A late Mesoproterozoic to early Neoproterozoic (1050–930Ma) terrane of Laurentian origin in the Scandinavian Caledonides. Precambrian Research 212-213, 245-262.

Åhäll, K.-I., Connelly, J., 1998. Intermittent 1.53–1.13Ga magmatism in western Baltica; age constraints and correlations within a postulated supercontinent. Precambrian Research 92, 1-20.

Albrecht, L.G., 2000. Early structural and metamorphic evolution of the Scandinavian Caledonides: a study of the eclogite-bearing Seve Nappe Complex at the Arctic Circle, Sweden.

Andersen, T., Elburg, M., Cawthorn-Blazeby, A., 2016. U–Pb and Lu–Hf zircon data in young sediments reflect sedimentary recycling in eastern South Africa. Journal of the Geological Society 173, 337-351.

Banks, C.J., Smith, M., Winchester, J.A., Horstwood, M.S.A., Noble, S.R., Ottley, C.J., 2007. Provenance of intra-Rodinian basin-fills: The lower Dalradian Supergroup, Scotland. Precambrian Research 153, 46-64.

Barham, M., Kirkland, C.L., in press. Changing of the guards: Detrital zircon provenance tracking sedimentological reorganization of a post-Gondwanan rift margin. Basin Research https://doi.org/10.1111/bre.12403.

Barham, M., Kirkland, C.L., Hollis, J., 2019a. Spot the difference: Zircon disparity tracks crustal evolution. Geology 47, 435-439.

Barham, M., Kirkland, C.L., Hollis, J., 2019b. Spot the difference: Zircon disparity tracks crustal evolution: REPLY. Geology 47, e482-e482.

Bertrand-Sarfati, K., Caby, R., 1976. Carbonates et stromatolites du sommet du Groupe d'Eleonore Bay (Precambrien terminal) au Canning Land (Groenland oriental). Rapport Grønlands Geologiske Undersøgelse 119, 51.

Bingen, B., Belousova, E.A., Griffin, W.L., 2011. Neoproterozoic recycling of the Sveconorwegian orogenic belt: Detrital-zircon data from the Sparagmite basins in the Scandinavian Caledonides. Precambrian Research 189, 347-367.

Bingen, B., Griffin, W.L., Torsvik, T.H., Saeed, A., 2005. Timing of Late Neoproterozoic glaciation on Baltica constrained by detrital zircon geochronology in the Hedmark Group, south-east Norway. Terra Nova 17, 250-258.

Bingen, B., Nordgulen, Ø., Viola, G., 2008. A four-phase model for the Sveconorwegian orogeny, SW Scandinavia. Norwegian Journal of Geology/Norsk Geologisk Forening 88.

Bingen, B., Solli, A., 2009. Geochronology of magmatism in the Caledonian and Sveconorwegian belts of Baltica: synopsis for detrital zircon provenance studies. Norwegian Journal of Geology/Norsk Geologisk Forening 89.

Bird, A., Cutts, K., Strachan, R., Thirlwall, M.F., Hand, M., 2018. First evidence of Renlandian (c. 950–940 Ma) orogeny in mainland Scotland: Implications for the status of the Moine Supergroup and circum-North Atlantic correlations. Precambrian Research 305, 283-294.

Black, L.P., Kamo, S.L., Allen, C.M., Davis, D.W., Aleinikoff, J.N., Valley, J.W., Mundil, R., Campbell, I.H., Korsch, R.J., Williams, I.S., Foudoulis, C., 2004. Improved 206Pb/238U microprobe geochronology by the monitoring of a trace-element-related matrix effect; SHRIMP, ID–TIMS, ELA–ICP–MS and oxygen isotope documentation for a series of zircon standards. Chemical Geology 205, 115-140.

Bouvier, A., Vervoort, J.D., Patchett, P.J., 2008. The Lu–Hf and Sm–Nd isotopic composition of CHUR: Constraints from unequilibrated chondrites and implications for the bulk composition of terrestrial planets. Earth and Planetary Science Letters 273, 48-57.

Buiter, S.J.H., Torsvik, T.H., 2014. A review of Wilson Cycle plate margins: A role for mantle plumes in continental break-up along sutures? Gondwana Research 26, 627-653.

Cawood, P.A., Hawkesworth, C., Dhuime, B., 2012. Detrital zircon record and tectonic setting. Geology 40, 875-878.

Cawood, P.A., McCausland, P.J.A., Dunning, G.R., 2001. Opening Iapetus: Constraints from the Laurentian margin in Newfoundland. GSA Bulletin 113, 443-453.

Cawood, P.A., Nemchin, A.A., Freeman, M., Sircombe, K., 2003a. Linking source and sedimentary basin: Detrital zircon record of sediment flux along a modern river system and implications for provenance studies. Earth and Planetary Science Letters 210, 259-268.

Cawood, P.A., Nemchin, A.A., Smith, M., Loewy, S., 2003b. Source of the Dalradian Supergroup constrained by U–Pb dating of detrital zircon and implications for the East Laurentian margin. Journal of the Geological Society 160, 231-246.

Cawood, P.A., Nemchin, A.A., Strachan, R., Prave, T., Krabbendam, M., 2007. Sedimentary basin and detrital zircon record along East Laurentia and Baltica during assembly and breakup of Rodinia. Journal of the Geological Society 164, 257-275.

Cawood, P.A., Nemchin, A.A., Strachan, R.A., Kinny, P.D., Loewy, S., 2004. Laurentian provenance and an intracratonic tectonic setting for the Moine Supergroup, Scotland, constrained by detrital zircons from the Loch Eil and Glen Urquhart successions. Journal of the Geological Society 161, 861-874.

Cawood, P.A., Pisarevsky, S.A., 2017. Laurentia-Baltica-Amazonia relations during Rodinia assembly. Precambrian Research 292, 386-397.

Cawood, P.A., Strachan, R., Cutts, K., Kinny, P.D., Hand, M., Pisarevsky, S., 2010. Neoproterozoic orogeny along the margin of Rodinia: Valhalla orogen, North Atlantic. Geology 38, 99-102.

Cawood, P.A., Strachan, R.A., Merle, R.E., Millar, I.L., Loewy, S.L., Dalziel, I.W.D., Kinny, P.D., Jourdan, F., Nemchin, A.A., Connelly, J.N., 2015. Neoproterozoic to early Paleozoic extensional and compressional history of East Laurentian margin sequences: The Moine Supergroup, Scottish Caledonides. GSA Bulletin 127, 349-371.

Cawood, P.A., Strachan, R.A., Pisarevsky, S.A., Gladkochub, D.P., Murphy, J.B., 2016. Linking collisional and accretionary orogens during Rodinia assembly and breakup: Implications for models of supercontinent cycles. Earth and Planetary Science Letters 449, 118-126.

Chew, D.M., Flowerdew, M.J., Page, L.M., Crowley, Q.G., Daly, J.S., Cooper, M., Whitehouse, M.J., 2008. The tectonothermal evolution and provenance of the Tyrone Central Inlier, Ireland: Grampian imbrication of an outboard Laurentian microcontinent? Journal of the Geological Society 165, 675-685.

Claesson, S., Roddick, J.C., 1983. 40Ar/39Ar data on the age and metamorphism of the Ottfjället dolerites, Särv Nappe, Swedish Caledonides. Lithos 16, 61-73.

Corfu, F., Hanchar, J.M., Hoskin, P.W.O., Kinny, P., 2003. Atlas of Zircon Textures. Reviews in Mineralogy and Geochemistry 53, 469-500.

Cutts, K.A., Hand, M., Kelsey, D.E., Wade, B., Strachan, R.A., Clark, C., Netting, A., 2009. Evidence for 930 Ma metamorphism in the Shetland Islands, Scottish Caledonides: implications for Neoproterozoic tectonics in the Laurentia–Baltica sector of Rodinia. Journal of the Geological Society 166, 1033-1047.

Dallmann, W.K., Elvevold, S., Gerland, S., Hormes, A., Majka, J., Ottemöller, L., Pavlova, O., Sander, G., 2015. Geoscience atlas of Svalbard.

Dalziel, I.W.D., Soper, N.J., 2001. Neoproterozoic extension on the Scottish promontory of Laurentia: paleogeographic and tectonic implications. The Journal of Geology 109, 299-317.

Daradich, A., Mitrovica, J.X., Pysklywec, R.N., Willett, S.D., Forte, A.M., 2003. Mantle flow, dynamic topography, and rift-flank uplift of Arabia. Geology 31, 901-904.

Davis, S.J., Dickinson, W.R., Gehrels, G.E., Spencer, J.E., Lawton, T.F., Carroll, A.R., 2010. The Paleogene California River: evidence of Mojave-Uinta paleodrainage from U-Pb ages of detrital zircons. Geology 38, 931-934.

Dhuime, B., Bosch, D., Bruguier, O., Caby, R., Pourtales, S., 2007. Age, provenance and post-deposition metamorphic overprint of detrital zircons from the Nathorst Land group (NE Greenland)—A LA-ICP-MS and SIMS study. Precambrian Research 155, 24-46.

Emery, M.R.G., 2005. Poly-orogenic history of the Moine rocks of Glen Urquhart, eastern Inverness-shire.

Escher, J.C., 2007. Geological map of Greenland, 74 Ø. 1 Wollaston Forland, 1: 250 000. Geological Survey of Denmark and Greenland, https://data.geus.dk/maparchive/ViewMap.xhtml?mapMapId=3277, Copenhagen.

Estrada, S., Mende, K., Gerdes, A., Gärtner, A., Hofmann, M., Spiegel, C., Damaske, D., Koglin, N., 2018. Proterozoic to Cretaceous evolution of the western and central Pearya Terrane (Canadian High Arctic). Journal of Geodynamics 120, 45-76.

Fairchild, I.J., Hambrey, M.J., 1995. Vendian basin evolution in East Greenland and NE Svalbard. Precambrian Research 73, 217-233.

Fairchild, I.J., Kennedy, M.J., 2007. Neoproterozoic glaciation in the Earth System. Journal of the Geological Society 164, 895-921.

Fitzgerald, P.G., 1992. The Transantarctic Mountains of southern Victoria Land: The application of apatite fission track analysis to a rift shoulder uplift. Tectonics 11, 634-662.

Friend, C.R.L., Kinny, P.D., Rogers, G., Strachan, R.A., Paterson, B.A., 1997. U-Pb zircon geochronological evidence for Neoproterozoic events in the Glenfinnan Group (Moine Supergroup): the formation of the Ardgour granite gneiss, north-west Scotland. Contributions to Mineralogy and Petrology 128, 101-113.

Friend, C.R.L., Strachan, R.A., Kinny, P.D., Watt, G.R., 2003. Provenance of the Moine Supergroup of NW Scotland: evidence from geochronology of detrital and inherited zircons from (meta)sedimentary rocks, granites and migmatites. Journal of the Geological Society 160, 247-257.

Gain, S.E.M., Gréau, Y., Henry, H., Belousova, E., Dainis, I., Griffin, W.L., O'Reilly, S.Y., In Press. Mud Tank Zircon: Long-Term Evaluation of a Reference Material for U-Pb Dating, Hf-Isotope Analysis and Trace Element Analysis. Geostandards and Geoanalytical Research.

Gardiner, N.J., Kirkland, C.L., Hollis, J., Szilas, K., Steenfelt, A., Yakymchuk, C., Heide-Jørgensen, H., 2019. Building Mesoarchaean crust upon Eoarchaean roots: the Akia Terrane, West Greenland. Contributions to Mineralogy and Petrology 174, 20.

Gasser, D., Andresen, A., 2013. Caledonian terrane amalgamation of Svalbard: detrital zircon provenance of Mesoproterozoic to Carboniferous strata from Oscar II Land, western Spitsbergen. Geological Magazine 150, 1103-1126.

Gawthorpe, R., Leeder, M., 2000. Tectono-sedimentary evolution of active extensional basins. Basin Research 12, 195-218.

Gee, D.G., Andréasson, P.-G., Lorenz, H., Frei, D., Majka, J., 2015. Detrital zircon signatures of the Baltoscandian margin along the Arctic Circle Caledonides in Sweden: The Sveconorwegian connection. Precambrian Research 265, 40-56.

Gee, D.G., Janák, M., Majka, J., Robinson, P., van Roermund, H., 2013. Subduction along and within the Baltoscandian margin during closing of the Iapetus Ocean and Baltica-Laurentia collision. Lithosphere 5, 169-178.

Gee, D.G., Ladenberger, A., Dahlqvist, P., Majka, J., Be'eri-Shlevin, Y., Frei, D., Thomsen, T., 2014. The Baltoscandian margin detrital zircon signatures of the central Scandes. Geological Society, London, Special Publications 390, 131-155.

Gee, J., Nakanishi, M., 1995. Magnetic petrology and magnetic properties of western Pacific guyots: implications for seamount paleopoles, In: Haggerty, J.A., Premoli Silva, I., Rack, F., McNutt, M.K. (Eds.), Proceeding ODP, Scientific Results. Ocean Drilling Program, College Station, Texas, pp. 615-630.

Gehrels, G.E., Valencia, V.A., Ruiz, J., 2008. Enhanced precision, accuracy, efficiency, and spatial resolution of U-Pb ages by laser ablation–multicollector–inductively coupled plasma–mass spectrometry. Geochemistry, Geophysics, Geosystems 9, n/a-n/a.

Gilotti, Jane A., McClelland, William C., 2005. Leucogranites and the Time of Extension in the East Greenland Caledonides. The Journal of Geology 113, 399-417.

Gilotti, J.A., McClelland, W.C., Higgins, A.K., Gilotti, J.A., Smith, M.P., 2008. Geometry, kinematics, and timing of extensional faulting in the Greenland Caledonides—A synthesis, The Greenland Caledonides: Evolution of the Northeast Margin of Laurentia. Geological Society of America, p. 0.

Glover, B.W., Key, R.M., May, F., Clark, G.C., Phillips, E.R., Chacksfield, B.C., 1995. A Neoproterozoic multi-phase rift sequence: the Grampian and Appin groups of the southwestern Monadhliath Mountains of Scotland. Journal of the Geological Society 152, 391-406.

Gower, C.F., 1996. The evolution of the Grenville Province in eastern Labrador, Canada. Geological Society, London, Special Publications 112, 197-218.

Gower, C.F., Krogh, T.E., 2002. AU–Pb geochronological review of the Proterozoic history of the eastern Grenville Province. Canadian Journal of Earth Sciences 39, 795-829.

Griffin, W.L., Wang, X., Jackson, S.E., Pearson, N.J., O'Reilly, S.Y., Xu, X., Zhou, X., 2002. Zircon chemistry and magma mixing, SE China: In-situ analysis of Hf isotopes, Tonglu and Pingtan igneous complexes. Lithos 61, 237-269.

Halverson, G.P., Hoffman, P.F., Schrag, D.P., Maloof, A.C., Rice, A.H.N., 2005. Toward a Neoproterozoic composite carbon-isotope record. GSA Bulletin 117, 1181-1207.

Halverson, G.P., Maloof, A.C., Hoffman, P.F., 2004. The Marinoan glaciation (Neoproterozoic) in northeast Svalbard. Basin Research 16, 297-324.

Hambrey, M.J., Spencer, A.M., 1987. Late Precambrian glaciation of central east Greenland. Nyt Nordisk Forlag.

Hartz, E., Andresen, A., 1995. Caledonian sole thrust of central East Greenland: A crustal-scale Devonian extensional detachment? Geology 23, 637-640.

Hartz, E.H., Torsvik, T.H., 2002. Baltica upside down: A new plate tectonic model for Rodinia and the Iapetus Ocean. Geology 30, 255-258.

Henriksen, N., Higgins, A.K., 2008. Caledonian orogen of East Greenland 70°N–82°N: Geological map at 1:1,000,000—Concepts and principles of compilation, In: Higgins, A.K., Gilotti, J.A., Smith, M.P. (Eds.), The Greenland Caledonides: Evolution of the Northeast Margin of Laurentia. Geological Society of America, p. 0.

Higgins, A.K., 1988. The Krummedal supracrustal sequence in East Greenland, Later Proterozoic stratigraphy of the northern Atlantic regions. Springer, pp. 86-96.

Higgins, A.K., Soper, N.J., Smith, M.P., Rasmussen, J.A., 2004. The Caledonian thin-skinned thrust belt of Kronprins Christian Land, eastern North Greenland. Geological Survey of Denmark and Greenland Bulletin 6, 41-56.

Highton, A.J., Hyslop, E.K., Noble, S.R., 1999. U-Pb zircon geochronology of migmatization in the northern Central Highlands: evidence for pre-Caledonian (Neoproterozoic) tectonometamorphism in the Grampian block, Scotland. Journal of the Geological Society 156, 1195-1204.

Hoffman, P.F., Kaufman, A.J., Halverson, G.P., Schrag, D.P., 1998. A Neoproterozoic Snowball Earth. Science 281, 1342-1346.

Holbrook, W.S., Larsen, H.C., Korenaga, J., Dahl-Jensen, T., Reid, I.D., Kelemen, P.B., Hopper, J.R., Kent, G.M., Lizarralde, D., Bernstein, S., Detrick, R.S., 2001. Mantle thermal structure and active upwelling during continental breakup in the North Atlantic. Earth and Planetary Science Letters 190, 251-266.

Horstwood, M.S.A., Košler, J., Gehrels, G., Jackson, S.E., McLean, N.M., Paton, C., Pearson, N.J., Sircombe, K., Sylvester, P., Vermeesch, P., Bowring, J.F., Condon, D.J., Schoene, B., 2016. Community-Derived Standards for LA-ICP-MS U-(Th-)Pb Geochronology – Uncertainty Propagation, Age Interpretation and Data Reporting. Geostandards and Geoanalytical Research 40, 311-332.

Jackson, S.E., Pearson, N.J., Griffin, W.L., Belousova, E.A., 2004. The application of laser ablation-inductively coupled plasma-mass spectrometry to in situ U–Pb zircon geochronology. Chemical Geology 211, 47-69.

Jahn, I., Strachan, R.A., Fowler, M., Bruand, E., Kinny, P.D., Clark, C., Taylor, R.J.M., 2016. Evidence from U–Pb zircon geochronology for early Neoproterozoic (Tonian) reworking of an Archaean inlier in northeastern Shetland, Scottish Caledonides. Journal of the Geological Society 174, 217-232.

Johansson, Å., Gee, D.G., Larionov, A.N., Ohta, Y., Tebenkov, A.M., 2005. Grenvillian and Caledonian evolution of eastern Svalbard – a tale of two orogenies. Terra Nova 17, 317-325.

Johansson, Å., Larionov, A.N., Gee, D.G., Ohta, Y., Tebenkov, A.M., Sandelin, S., 2004. Grenvillian and Caledonian tectono-magmatic activity in northeasternmost Svalbard. Geological Society, London, Memoirs 30, 207-232.

Johansson, Å., Larionov, A.N., Tebenkov, A.M., Gee, D.G., Whitehouse, M.J., Vestin, J., 1999. Grenvillian magmatism of western and central Nordaustlandet, northeastern Svalbard. Earth and Environmental Science Transactions of the Royal Society of Edinburgh 90, 221-254.

Johnston, S.M., Kylander-Clark, A.R.C., 2013. Discovery of an Eo-Meso-Neoarchean terrane in the East Greenland Caledonides. Precambrian Research 235, 295-302.

Kalsbeek, F., Austrheim, H., Bridgwater, D., Hansen, B.T., Pedersen, S., Taylor, P.N., 1993a. Geochronology of Archaean and Proterozoic events in the Ammassalik area, South-East Greenland, and comparisons with the Lewisian of Scotland and the Nagssugtoqidian of West Greenland. Precambrian Research 62, 239-270.

Kalsbeek, F., Nutman, A.P., Taylor, P.N., 1993b. Palaeoproterozoic basement province in the Caledonian fold belt of North-East Greenland. Precambrian Research 63, 163-178.

Kalsbeek, F., Thrane, K., Higgins, A.K., Jepsen, H.F., Leslie, A.G., Nutman, A.P., Frei, R., 2008. Polyorogenic history of the East Greenland Caledonides. The Greenland Caledonides: evolution of the Northeast Margin of Laurentia. Edited by AK Higgins, JA Gilotti, and MP Smith. Geological Society of America Memoir 202, 55-72.

Kalsbeek, F., Thrane, K., Nutman, A.P., Jepsen, H.F., 2000. Late Mesoproterozoic to early Neoproterozoic history of the East Greenland Caledonides: evidence for Grenvillian orogenesis? Journal of the Geological Society 157, 1215-1225.

Kinnaird, T.C., Prave, A.R., Kirkland, C.L., Horstwood, M., Parrish, R., Batchelor, R.A., 2007. The late Mesoproterozoic–early Neoproterozoic tectonostratigraphic evolution of NW Scotland: the Torridonian revisited. Journal of the Geological Society 164, 541-551.

Kinny, P.D., Friend, C.R.L., 1997. U-Pb isotopic evidence for the accretion of different crustal blocks to form the Lewisian Complex of northwest Scotland. Contributions to Mineralogy and Petrology 129, 326-340.

Kinny, P.D., Friend, C.R.L., Strachan, R.A., Watt, G.R., Burns, I.M., 1999. U–Pb geochronology of regional migmatites in East Sutherland, Scotland: evidence for crustal melting during the Caledonian orogeny. Journal of the Geological Society 156, 1143-1152.

Kirkland, C.L., Daly, J.S., Whitehouse, M., 2007. Provenance and Terrane Evolution of the Kalak Nappe Complex, Norwegian Caledonides: Implications for Neoproterozoic Paleogeography and Tectonics. The Journal of Geology 115, 21-41.

Kirkland, C.L., Daly, J.S., Whitehouse, M.J., 2006. Granitic magmatism of Grenvillian and late Neoproterozoic age in Finnmark, Arctic Norway—Constraining pre-Scandian deformation in the Kalak Nappe Complex. Precambrian Research 145, 24-52.

Kirkland, C.L., Daly, J.S., Whitehouse, M.J., 2008a. Basement–cover relationships of the Kalak Nappe Complex, Arctic Norwegian Caledonides and constraints on Neoproterozoic terrane assembly in the North Atlantic region. Precambrian Research 160, 245-276.

Kirkland, C.L., Pease, V., Whitehouse, M.J., Ineson, J.R., 2009. Provenance record from Mesoproterozoic-Cambrian sediments of Peary Land, North Greenland: Implications for the ice-covered Greenland Shield and Laurentian palaeogeography. Precambrian Research 170, 43-60.

Kirkland, C.L., Strachan, R.A., Prave, A.R., 2008b. Detrital zircon signature of the Moine Supergroup, Scotland: Contrasts and comparisons with other Neoproterozoic successions within the circum-North Atlantic region. Precambrian Research 163, 332-350.

Knoll, A.H., 1982. Microfossil-based biostratigraphy of the Precambrian Hecla Hoek sequence, Nordaustlandet, Svalbard. Geological Magazine 119, 269-279.

Knudsen, C., Hopper, J.R., Bierman, P.R., Bjerager, M., Funck, T., Green, P.F., Ineson, J.R., Japsen, P., Marcussen, C., Sherlock, S.C., 2018. Samples from the Lomonosov Ridge place new constraints on the geological evolution of the Arctic Ocean. Geological Society, London, Special Publications 460, 397-418.

Kolb, J., Thrane, K., Bagas, L., 2013. Field relationship of high-grade Neo- to Mesoarchaean rocks of South-East Greenland: Tectonometamorphic and magmatic evolution. Gondwana Research 23, 471-492.

Korja, A., Lahtinen, R., Nironen, M., 2006. The Svecofennian orogen: a collage of microcontinents and island arcs. Geological Society, London, Memoirs 32, 561-578.

Kosteva, N., Tebenkov, A.M., Gsoltsin, N., Kapitonov, I., Provenance of Neoproterozoic sediments in Nordaustlandet, Svalbard: LA-ICP-MS dating of detrital zircons, pp. 89-90.

Krabbendam, M., Bonsor, H., Horstwood, M.S.A., Rivers, T., 2017. Tracking the evolution of the Grenvillian foreland basin: Constraints from sedimentology and detrital zircon and rutile in the Sleat and Torridon groups, Scotland. Precambrian Research 295, 67-89.

Kristoffersen, M., Andersen, T., Elburg, M.A., Watkeys, M.K., 2016. Detrital zircon in a supercontinental setting: locally derived and far-transported components in the Ordovician Natal Group, South Africa. Journal of the Geological Society 173, 203-215.

Lamminen, J., 2011. Provenance and correlation of sediments in Telemark, South Norway: status of the Lifjell Group and implications for early Sveconorwegian fault tectonics. Norwegian Journal of Geology/Norsk Geologisk Forening 91.

Lancaster, P.J., Storey, C.D., Hawkesworth, C.J., Dhuime, B., 2011. Understanding the roles of crustal growth and preservation in the detrital zircon record. Earth and Planetary Science Letters 305, 405-412.

Leeder, M., Gawthorpe, R., 1987. Sedimentary models for extensional tilt-block/half-graben basins. Geological Society, London, Special Publications 28, 139-152.

Leslie, A.G., Nutman, A.P., 2003. Evidence for Neoproterozoic orogenesis and early high temperature Scandian deformation events in the southern East Greenland Caledonides. Geological Magazine 140, 309-333.

Li, Z.-X., Bogdanova, S., Collins, A., Davidson, A., De Waele, B., Ernst, R., Fitzsimons, I., Fuck, R., Gladkochub, D., Jacobs, J., 2008. Assembly, configuration, and break-up history of Rodinia: a synthesis. Precambrian Research 160, 179-210.

Li, Z.-X., Evans, D.A.D., Halverson, G.P., 2013. Neoproterozoic glaciations in a revised global palaeogeography from the breakup of Rodinia to the assembly of Gondwanaland. Sedimentary Geology 294, 219-232.

Lorenz, H., Gee, D.G., Larionov, A.N., Majka, J., 2012. The Grenville–Sveconorwegian orogen in the high Arctic. Geological Magazine 149, 875-891.

Ludwig, K., 2012. User's manual for Isoplot version 3.75–4.15: a geochronological toolkit for Microsoft. Excel Berkley Geochronological Center Special Publication.

Ludwig, K.R., 1998. On the Treatment of Concordant Uranium-Lead Ages. Geochimica et Cosmochimica Acta 62, 665-676.

Lyu, P.-L., Li, W.-X., Wang, X.-C., Pang, C.-J., Cheng, J.-X., Li, X.-H., 2017. Initial breakup of supercontinent Rodinia as recorded by ca 860–840 Ma bimodal volcanism along the southeastern margin of the Yangtze Block, South China. Precambrian Research 296, 148-167.

Majka, J., Be'Eri-Shlevin, Y., Gee, D.G., Czerny, J., Frei, D., Ladenberger, A., 2014. Torellian (c. 640 Ma) metamorphic overprint of Tonian (c. 950 Ma) basement in the Caledonides of southwestern Svalbard. Geological Magazine 151, 732-748.

Majka, J., Mazur, S., Manecki, M., Czerny, J., Holm, D.K., 2008. Late Neoproterozoic amphibolite-facies metamorphism of a pre-Caledonian basement block in southwest Wedel Jarlsberg Land, Spitsbergen: New evidence from U–Th–Pb dating of monazite. Geological Magazine 145, 822-830.

Malone, S.J., McClelland, W.C., Gosen, W.v., Piepjohn, K., 2014. Proterozoic Evolution of the North Atlantic–Arctic Caledonides: Insights from Detrital Zircon Analysis of Metasedimentary Rocks from the Pearya Terrane, Canadian High Arctic. The Journal of Geology 122, 623-647.

Malone, S.J., McClelland, W.C., von Gosen, W., Piepjohn, K., 2017. The earliest Neoproterozoic magmatic record of the Pearya terrane, Canadian high Arctic: Implications for Caledonian terrane reconstructions. Precambrian Research 292, 323-349.

Massey, F.J.J., 1951. The Kolmogorov-Smirnov test for goodness of fit. Journal of the American Statistical Association 46, 68-78.

McAteer, C.A., Daly, J.S., Flowerdew, M.J., Whitehouse, M.J., 2010a. Dalradian Grampian Group affinity for the Bowmore Sandstone Group, Islay, SW Scotland. Scottish Journal of Geology 46, 97-111.

McAteer, C.A., Daly, J.S., Flowerdew, M.J., Whitehouse, M.J., Kirkland, C.L., 2010b. A Laurentian provenance for the Dalradian rocks of north Mayo, Ireland, and evidence for an original basement–cover contact with the underlying Annagh Gneiss Complex. Journal of the Geological Society 167, 1033-1048.

McAteer, C.A., Daly, J.S., Flowerdew, M.J., Whitehouse, M.J., Monaghan, N.M., 2014. Sedimentary provenance, age and possible correlation of the Iona Group SW Scotland. Scottish Journal of Geology 50, 143-158.

McAteer, C.A., Stephen Daly, J., Flowerdew, M.J., Connelly, J.N., Housh, T.B., Whitehouse, M.J., 2010c. Detrital zircon, detrital titanite and igneous clast U–Pb geochronology and basement–cover relationships of the Colonsay Group, SW Scotland: Laurentian provenance and correlation with the Neoproterozoic Dalradian Supergroup. Precambrian Research 181, 21-42.

McClelland, W.C., Gilotti, J.A., Ramarao, T., Stemmerik, L., Dalhoff, F., 2016. Carboniferous basin in Holm Land records local exhumation of the North-East Greenland Caledonides: Implications for the detrital zircon signature of a collisional orogen. Geosphere 12, 925-947.

McClelland, W.C., von Gosen, W., Piepjohn, K., 2019. Tonian and Silurian magmatism in Nordaustlandet: Svalbard's place in the Caledonian orogen. Circum-Arctic Structural Events: Tectonic Evolution of the Arctic Margins and Trans-Arctic Links with Adjacent Orogens 541, 63.

McKerrow, W.S., Mac Niocaill, C., Dewey, J.F., 2000. The Caledonian orogeny redefined. Journal of the Geological Society 157, 1149-1154.

Merdith, A.S., Collins, A.S., Williams, S.E., Pisarevsky, S., Foden, J.D., Archibald, D.B., Blades, M.L., Alessio, B.L., Armistead, S., Plavsa, D., Clark, C., Müller, R.D., 2017. A full-plate global reconstruction of the Neoproterozoic. Gondwana Research 50, 84-134.

Merdith, A.S., Williams, S.E., Brune, S., Collins, A.S., Müller, R.D., 2019. Rift and plate boundary evolution across two supercontinent cycles. Global and Planetary Change 173, 1-14.

Millar, I.L., 1999. Neoproterozoic extensional basic magmatism associated with the West Highland granite gneiss in the Moine Supergroup of NW Scotland. Journal of the Geological Society 156, 1153-1162.

Mitchell, R.N., Spencer, C.J., Kirscher, U., He, X.-F., Murphy, J.B., Li, Z.-X., Collins, W.J., 2019. Harmonic hierarchy of mantle and lithospheric convective cycles: Time series analysis of hafnium isotopes of zircon. Gondwana Research 75, 239-248.

Moncrieff, A.C.M., Hambrey, M.J., 1988. Late Precambrian glacially-related grooved and striated surfaces in the Tillite Group of central East Greenland. Palaeogeography, Palaeoclimatology, Palaeoecology 65, 183-200.

Morel, M.L.A., Nebel, O., Nebel-Jacobsen, Y.J., Miller, J.S., Vroon, P.Z., 2008. Hafnium isotope characterization of the GJ-1 zircon reference material by solution and laser-ablation MC-ICPMS. Chemical Geology 255, 231-235.

Murphy, J.B., Hamilton, M.A., 2000. Orogenesis and basin development: U-Pb detrital zircon age constraints on evolution of the Late Paleozoic St. Marys Basin, central mainland Nova Scotia. The Journal of Geology 108, 53-71.

Noble, S.R., Hyslop, E.K., Highton, A.J., 1996. High-precision U–Pb monazite geochronology of the c. 806 Ma Grampian Shear Zone and the implications for the evolution of the Central Highlands of Scotland. Journal of the Geological Society 153, 511-514.

Olierook, H.K.H., Agangi, A., Plavsa, D., Reddy, S.M., Clark, C., Yao, W.-H., Occhipinti, S.A., Kylander-Clark, A.R.C., 2019a. Neoproterozoic hydrothermal activity in the West Australian Craton related to Rodinia assembly or breakup? Gondwana Research 68, 1-12.

Olierook, H.K.H., Barham, M., Fitzsimons, I.C.W., Timms, N.E., Jiang, Q., Evans, N.J., McDonald, B.J., 2019b. Tectonic controls on sediment provenance evolution in rift basins: Detrital zircon U–Pb and Hf isotope analysis from the Perth Basin, Western Australia. Gondwana Research 66, 126-142.

Olierook, H.K.H., Timms, N.E., Wellmann, J.F., Corbel, S., Wilkes, P.G., 2015. A 3D structural and stratigraphic model of the Perth Basin: Implications for sub-basin evolution. Australian Journal of Earth Sciences 62, 447-467.

Patchett, P.J., Tatsumoto, M., 1981. A routine high-precision method for Lu-Hf isotope geochemistry and chronology. Contributions to Mineralogy and Petrology 75, 263-267.

Paton, C., Hellstrom, J., Paul, B., Woodhead, J., Hergt, J., 2011. Iolite: Freeware for the visualisation and processing of mass spectrometric data. Journal of Analytical Atomic Spectrometry 26, 2508-2518.

Paulsson, O., Andréasson, P.-G., 2002. Attempted break-up of Rodinia at 850 Ma: geochronological evidence from the Seve–Kalak Superterrane, Scandinavian Caledonides. Journal of the Geological Society 159, 751-761.

Petersson, A., Scherstén, A., Bingen, B., Gerdes, A., Whitehouse, M.J., 2015. Mesoproterozoic continental growth: U–Pb–Hf–O zircon record in the Idefjorden terrane, Sveconorwegian orogen. Precambrian Research 261, 75-95.

Pettersson, C.H., Pease, V., Frei, D., 2009a. U–Pb zircon provenance of metasedimentary basement of the Northwestern Terrane, Svalbard: Implications for the Grenvillian–Sveconorwegian orogeny and development of Rodinia. Precambrian Research 175, 206-220.

Pettersson, C.H., Tebenkov, A.M., Larionov, A.N., Andresen, A., Pease, V., 2009b. Timing of migmatization and granite genesis in the Northwestern Terrane of Svalbard, Norway: implications for regional correlations in the Arctic Caledonides. Journal of the Geological Society 166, 147-158.

Peucat, J.J., Ohta, Y., Gee, D.G., Bernard-Griffiths, J., 1989. U□Pb, Sr and Nd evidence for grenvillian and latest proterozoic tectonothermal activity in the spitsbergen caledonides, arctic ocean. Lithos 22, 275-285.

Prave, A.R., Fallick, A.E., Thomas, C.W., Graham, C.M., 2009. A composite C-isotope profile for the Neoproterozoic Dalradian Supergroup of Scotland and Ireland. Journal of the Geological Society 166, 845-857.

Preiss, W.V., 2000. The Adelaide Geosyncline of South Australia and its significance in Neoproterozoic continental reconstruction. Precambrian Research 100, 21-63.

Prouty, J.M., 2014. Geochronology and structural geology of the Kjerringøy Peninsula, Nordland, Norway. Auburn University, p. 199.

Rainbird, R.H., Hamilton, M.A., Young, G.M., 2001. Detrital zircon geochronology and provenance of the Torridonian, NW Scotland. Journal of the Geological Society 158, 15-27.

Rice, A.H.N., 2014. Restoration of the external Caledonides, Finnmark, north Norway. Geological Society, London, Special Publications 390, 271-299.

Rivers, T., 1997. Lithotectonic elements of the Grenville Province: review and tectonic implications. Precambrian Research 86, 117-154.

Rogers, G., Hyslop, E.K., Strachan, R.A., Paterson, B.A., Holdsworth, R.E., 1998. The structural setting and U–Pb geochronology of Knoydartian pegmatites in W Inverness-shire: evidence for Neoproterozoic tectonothermal events in the Moineof NW Scotland. Journal of the Geological Society 155, 685-696.

Rogers, G., Kinny, P.D., Strachan, R.A., Friend, C.R.L., Paterson, B.A., 2001. U–Pb geochronology of the Fort Augustus granite gneiss: constraints on the timing of Neoproterozoic and Palaeozoic tectonothermal events in the NW Highlands of Scotland. Journal of the Geological Society 158, 7-14.

Rooney, A.D., Chew, D.M., Selby, D., 2011. Re–Os geochronology of the Neoproterozoic–Cambrian Dalradian Supergroup of Scotland and Ireland: Implications for Neoproterozoic stratigraphy, glaciations and Re–Os systematics. Precambrian Research 185, 202-214.

Salters, V.J.M., Hart, S.R., 1991. The mantle sources of ocean ridges, islands and arcs: the Hf-isotope connection. Earth and Planetary Science Letters 104, 364-380.

Satkoski, A.M., Wilkinson, B.H., Hietpas, J., Samson, S.D., 2013. Likeness among detrital zircon populations—An approach to the comparison of age frequency data in time and space. Bulletin 125, 1783-1799.

Sircombe, K.N., Freeman, M.J., 1999. Provenance of detrital zircons on the Western Australia coastline—Implications for the geologic history of the Perth basin and denudation of the Yilgarn craton. Geology 27, 879-882.

Slagstad, T., Davidsen, B., Daly, J.S., 2011. Age and composition of crystalline basement rocks on the Norwegian continental margin: offshore extension and continuity of the Caledonian–Appalachian orogenic belt. Journal of the Geological Society 168, 1167-1185.

Slagstad, T., Kirkland, C.L., 2017. The use of detrital zircon data in terrane analysis: A nonunique answer to provenance and tectonostratigraphic position in the Scandinavian Caledonides. Lithosphere 9, 1002-1011.

Slagstad, T., Kulakov, E., Kirkland, C.L., Roberts, N.M.W., Ganerød, M., 2019. Breaking the Grenville–Sveconorwegian link in Rodinia reconstructions. Terra Nova 0.

Slagstad, T., Roberts, N.M.W., Kulakov, E., 2017. Linking orogenesis across a supercontinent; the Grenvillian and Sveconorwegian margins on Rodinia. Gondwana Research 44, 109-115.

Slama, J., Walderhaug, O., Fonneland, H., Kosler, J., Pedersen, R.B., 2011. Provenance of Neoproterozoic to upper Cretaceous sedimentary rocks, eastern Greenland: Implications for recognizing the sources of sediments in the Norwegian Sea. Sedimentary Geology 238, 254-267.

Smith, M.P., Higgins, A.K., Soper, N.J., Sønderholm, M., 2004a. The Neoproterozoic Rivieradal Group of Kronprins Christian Land, eastern North Greenland. Geological Survey of Denmark and Greenland Bulletin 6, 29-39.

Smith, M.P., Rasmussen, J.A., 2008. Cambrian–Silurian development of the Laurentian margin of the Iapetus Ocean in Greenland and related areas. The Greenland Caledonides: Evolution of the Northeast Margin of Laurentia. Geological Society of America, Memoirs 202, 137-167.

Smith, M.P., Rasmussen, J.A., Robertson, S., Higgins, A.K., Leslie, A.G., 2004b. Lower Palaeozoic stratigraphy of the East Greenland Caledonides. Geological Survey of Denmark and Greenland Bulletin 6, 5-28.

Smith, M.P., Robertson, S., 1999. The Nathorst Land Group (Neoproterozoic) of East Greenland–lithostratigraphy, basin geometry and tectonic history. Geology of East Greenland, 72-75.

Söderlund, U., Patchett, P.J., Vervoort, J.D., Isachsen, C.E., 2004. The 176Lu decay constant determined by Lu–Hf and U–Pb isotope systematics of Precambrian mafic intrusions. Earth and Planetary Science Letters 219, 311-324.

Sønderholm, M., Frederiksen, K.S., Smith, M.P., Tirsgaard, H., 2008. Neoproterozoic sedimentary basins with glacigenic deposits of the East Greenland Caledonides, In: Higgins, A.K., Gilotti, J.A., Smith, M.P. (Eds.), The Greenland Caledonides: Evolution of the Northeast Margin of Laurentia. Geological Society of America, p. 0.

Sønderholm, M., Tirsgaard, H., 1993. Lithostratigraphic framework of the Upper Proterozoic Eleonore Bay Supergroup of East and North-East Greenland. Grønlands geologiske undersøgelse.

Spencer, C.J., Cavosie, A.J., Raub, T.D., Rollinson, H., Jeon, H., Searle, M.P., Miller, J.A., McDonald, B.J., Evans, N.J., 2017. Evidence for melting mud in Earth's mantle from extreme oxygen isotope signatures in zircon. Geology 45, 975-978.

Spencer, C.J., Cawood, P.A., Hawkesworth, C.J., Prave, A.R., Roberts, N.M.W., Horstwood, M.S.A., Whitehouse, M.J., 2015. Generation and preservation of continental crust in the Grenville Orogeny. Geoscience Frontiers 6, 357-372.

Spencer, C.J., Kirkland, C.L., 2016. Visualizing the sedimentary response through the orogenic cycle: A multidimensional scaling approach. Lithosphere 8, 29-37.

Spencer, C.J., Kirkland, C.L., Taylor, R.J.M., 2016. Strategies towards statistically robust interpretations of in situ U–Pb zircon geochronology. Geoscience Frontiers 7, 581-589.

Stern, R.A., Bodorkos, S., Kamo, S.L., Hickman, A.H., Corfu, F., 2009. Measurement of SIMS Instrumental Mass Fractionation of Pb Isotopes During Zircon Dating. Geostandards and Geoanalytical Research 33, 145-168.

Storey, C.D., Brewer, T.S., Parrish, R.R., 2004. Late-Proterozoic tectonics in northwest Scotland: one contractional orogeny or several? Precambrian Research 134, 227-247.

Storey, M., Duncan, R.A., Swisher, C.C., 2007. Paleocene-Eocene Thermal Maximum and the Opening of the Northeast Atlantic. Science 316, 587-589.

Strachan, R.A., Nutman, A.P., Friderichsen, J.D., 1995. SHRIMP U-Pb geochronology and metamorphic history of the Smallefjord sequence, NE Greenland Caledonides. Journal of the Geological Society 152, 779-784.

Strachan, R.A., Prave, A.R., Kirkland, C.L., Storey, C.D., 2013. U–Pb detrital zircon geochronology of the Dalradian Supergroup, Shetland Islands, Scotland: implications for regional correlations and Neoproterozoic–Palaeozoic basin development. Journal of the Geological Society 170, 905-916.

Strachan, R.A., Smith, M., Harris, A.L., Fettes, D.J., Trewin, N.H., 2002. The northern Highland and Grampian terranes. The Geology of Scotland. Geological Society, London 81, 147.

Tang, M., Wang, X.-L., Shu, X.-J., Wang, D., Yang, T., Gopon, P., 2014. Hafnium isotopic heterogeneity in zircons from granitic rocks: Geochemical evaluation and modeling of "zircon effect" in crustal anatexis. Earth and Planetary Science Letters 389, 188-199.

Tanner, P.W.G., Evans, J.A., 2003. Late Precambrian U–Pb titanite age for peak regional metamorphism and deformation (Knoydartian orogeny) in the western Moine, Scotland. Journal of the Geological Society 160, 555-564.

Thrane, K., 2002. Relationships between Archaean and Palaeoproterozoic crystalline basement complexes in the southern part of the East Greenland Caledonides: an ion microprobe study. Precambrian Research 113, 19-42.

Torsvik, T.H., Mosar, J., Eide, E.A., 2001. Cretaceous–Tertiary geodynamics: a North Atlantic exercise. Geophysical Journal International 146, 850-866.

Vance, D., Strachan, R.A., Jones, K.A., 1998. Extensional versus compressional settings for metamorphism: Garnet chronometry and pressure-temperature-time histories in the Moine Supergroup, northwest Scotland. Geology 26, 927-930.

Vermeesch, P., 2004. How many grains are needed for a provenance study? Earth and Planetary Science Letters 224, 441-451.

Vermeesch, P., 2012. On the visualisation of detrital age distributions. Chemical Geology 312–313, 190-194.

Vermeesch, P., 2013. Multi-sample comparison of detrital age distributions. Chemical Geology 341, 140-146.

Vermeesch, P., Resentini, A., Garzanti, E., 2016. An R package for statistical provenance analysis. Sedimentary Geology 336, 14-25.

Vidal, G., 1976. Late Precambrian acritarchs from the Eleonore Bay Group and Tillite Group in East Greenland: a preliminary report. Grønlands Geologiske Undersøgelse:[eksp. CA Reitzel].

Vidal, G., 1979. Acritarchs from the upper Proterozoic and lower Cambrian of East Greenland: Grønlands Geologiske Undersøgelse, v. 134.

Watt, G.R., Kinny, P.D., Friderichsen, J.D., 2000. U–Pb geochronology of Neoproterozoic and Caledonian tectonothermal events in the East Greenland Caledonides. Journal of the Geological Society 157, 1031-1048.

Wessel, P., Smith, W.H.F., 1996. A global, self-consistent, hierarchical, high-resolution shoreline database. Journal of Geophysical Research: Solid Earth 101, 8741-8743.

Whipp, P.S., Jackson, C.A.L., Gawthorpe, R.L., Dreyer, T., Quinn, D., 2014. Normal fault array evolution above a reactivated rift fabric; a subsurface example from the northern Horda Platform, Norwegian North Sea. Basin Research 26, 523-549.

Wiedenbeck, M., AllÉ, P., Corfu, F., Griffin, W.L., Meier, M., Oberli, F., Quadt, A.V., Roddick, J.C., Spiegel, W., 1995. Three natural zircon standards For U-Th-Pb, Lu-Hf, trace element And REE analyses. Geostandards Newsletter 19, 1-23.

Williams, G.D., 1993. Tectonics and seismic sequence stratigraphy: an introduction. Geological Society, London, Special Publications 71, 1-13.

Williams, I.S., Claesson, S., 1987. Isotopic evidence for the Precambrian provenance and Caledonian metamorphism of high grade paragneisses from the Seve Nappes, Scandinavian Caledonides. Contributions to Mineralogy and Petrology 97, 205-217.

Woodcock, N.H., Strachan, R.A., 2009. 12 The Caledonian Orogeny: a multiple plate collision. Geological history of Britain and Ireland, 187.

Woodhead, J.D., Hergt, J.M., 2005. A Preliminary Appraisal of Seven Natural Zircon Reference Materials for In Situ Hf Isotope Determination. Geostandards and Geoanalytical Research 29, 183-195.

Zhang, W., Roberts, D., Pease, V., 2016. Provenance of sandstones from Caledonian nappes in Finnmark, Norway: Implications for Neoproterozoic–Cambrian palaeogeography. Tectonophysics 691, 198-205.

Ziemniak, G., Kośmińska, K., Schneider, D.A., Majka, J., Lorenz, H., McClelland, W.C., Wala, V.T., Manecki, M., Piepjohn, K., Strauss, J.V., Reinhardt, L., McClelland, W.C., 2019. Defining tectonic boundaries using detrital zircon signatures of Precambrian metasediments from Svalbard's Southwestern Caledonian Basement Province, Circum-Arctic Structural Events: Tectonic Evolution of the Arctic Margins and Trans-Arctic Links with Adjacent Orogens. Geological Society of America, p. 0.

Figure captions

Fig. 1: Simplified map of the North Atlantic region in an equidistant azimuthal projection, color-coded for megasequences 1 to 3 and annotated with different Meso- to Neoproterozoic regions discussed in the text. Laminar color patterns indicate that combinations of megasequence 1, 2 or 3 are present in the same area but below the resolution of the simplified map. Regional geological maps simplified for East Greenland (Henriksen and Higgins, 2008; Kalsbeek et al., 2008), Northeast Greenland (Henriksen and Higgins, 2008), Svalbard (Gasser and Andresen, 2013), Ireland (Chew et al., 2008; McAteer et al., 2010b), Scotland (Krabbendam et al., 2017; Strachan et al., 2002), Shetland (Cutts et al., 2009; Strachan et al., 2013), Southern and central Norway–Sweden (Gee et al., 2015; Gee et al., 2014) and northern Norway (Kirkland et al., 2007; Zhang et al., 2016). Coastline from Wessel and Smith (1996). Available detrital zircon data are tabulated in Supplementary Table C.

Fig. 2: Simplified geological map of the Caledonides in East Greenland modified from Henriksen and Higgins (2008) and Kalsbeek et al. (2008), emphasizing the Tonian and Caledonian granites, and Meso- to Neoproterozoic outcrops.

Fig. 3: Geological map of Wollaston Forland after mapping at 1:1 000 000 by the Geological Survey of Denmark and Greenland (GEUS) (Henriksen and Higgins, 2008), showing new sample locations. Note scale bar is approximate only.

Fig. 4: Graphical representations of the differences between nearest neighbour and inter-sample distances in MDS space via disparity analysis technique (Barham et al., 2019a). Three examples are shown, one with high overall scatter, one with low scatter but distinct subpopulations and one with low overall scatter. Nearest neighbour lines are in pale red. Inter-sample distances are in dashed grey lines but only shown for one sample.

Fig. 5: Representative cathodoluminescence (CL) images of detrital and magmatic zircon grains from samples from Wollaston Forland. Scale bar of 100 μm in bottom panel is for all zircon grains. Circles correspond to analytical spot locations. Circle colours correspond to genetic interpretation, used throughout other figures. Purple = detrital, light blue = youngest detrital grains in sample, red = inherited, green = metamorphic, yellow = igneous, grey = discordant, black = mixed core–rim domains. A compilation of all CL images may be found in Supplementary Fig. B. Dates are calculated from the most precise isotopic ratio. All dates and $\varepsilon Hf_{(t)}$ uncertainties are labelled at 2σ confidence.

Fig. 6: Tera-Wasserburg inverse concordia plots for each new sample. Square colours as used in Fig. 4.

Fig. 7: Probability density estimate (black lines) and kernel density estimation (red line) of zircon age populations. Kernel density for samples with <50 analyses used a 50 Ma bin size, whilst samples >50 analyses used the adaptive density approach (Vermeesch, 2012). Number of grains indicates the ratio of concordant to total analyses. Potential Laurentian source terranes (Cawood and Pisarevsky, 2017; Gower and Krogh, 2002; Krabbendam et al., 2017 and references therein; Rivers, 1997) include: North Atlantic/Superior Craton = 2900–2600 Ma, Nagssugtoqidian = 2090–1940 Ma, Makkovik-Ketilidian-Rhinnian (MKR) = 1820–1720 Ma, Labrador = 1690–1590 Ma, Pinwarian = 1520–1380 Ma, Elzevirian = 1300–1210 Ma, Shawinagan = 1200–1130 Ma, Grenville *sensu stricto* (s. s.) = 1095–980 Ma, Renlandian = 955–900 Ma, Caledonian (460–390 Ma). Baltican sources (Bingen and Solli, 2009; Korja et al., 2006) include: Loopian = 2900–2600 Ma, Svecofennian & Svecokarellian = 1920–1770 Ma, Transscandinavian Igneous Belt (TIB) = 1850–1760 Ma, Gothian = 1660–1520 Ma, Telemarkian = 1550–1460 Ma, Hallandian/Danopolonian = 1470–1420 Ma, Sveconorwegian = 1130–1060 Ma (Arendal phase) and 1050–980 Ma (Falkenberg phase), Caledonian = 470–400 Ma. East Greenland Sources (Johnston and Kylander-Clark, 2013; Kalsbeek et al., 1993b; Thrane, 2002) include: Archean basement = ca. 3610 (not shown), 3070–2980 Ma and 2800–2680 Ma, Paleoproterozoic basement = 2000–1900 Ma, ca. 1750 Ma, Renlandian = 970–920 Ma, Caledonian = 450–410 Ma.

Fig. 8: Hf isotopic data for (a) new samples, (b) megasequence 1, (c) megasequence 2, and (d) megasequence 3. For definition of megasequence units, see Fig. 8. CHUR = chondritic uniform reservoir. Laurentian and Baltican data from Lamminen (2011), Petersson et al. (2015), Spencer et al.

(2015) and Slagstad and Kirkland (2017). No Hf isotopic data is available from the Archean and Paleoproterozoic basement of East Greenland.

Fig. 9: Summary of stratigraphic correlations across the latest Mesoproterozoic and Neoproterozoic in the North Atlantic region. Maximum depositional ages from detrital zircon references are from Table 1). Lettered references are for all age data types, as follows. **Canadian High Arctic, allochthonous Pearya Terrane**—general stratigraphy: (Estrada et al., 2018; Malone et al., 2014), **a**: zircon U-Pb age of oldest granite in Pearya Succession I (Estrada et al., 2018); **b**: zircon U-Pb age of youngest granite in Pearya Succession I (Malone et al., 2017). **Northeast Greenland**—general stratigraphy: (Higgins et al., 2004; Smith et al., 2004a). **East Greenland**—general stratigraphy: (Sønderholm et al., 2008; Sønderholm and Tirsgaard, 1993), **c**: metamorphic rims on Krummedal Succession zircon (Strachan et al., 1995), **d**: zircon U-Pb age of oldest granitoids (Kalsbeek et al., 2000; also see Watt et al., 2000), **e**: zircon U-Pb age of youngest granitoids (Leslie and Nutman, 2003), **f**: Cryogenian acritarchs (Vidal, 1976; Vidal, 1979), **g**: late Cryogenian stromatolites (Bertrand-Sarfati and Caby, 1976). **Southwest Terrane in Svalbard**—general stratigraphy: (Dallmann et al., 2015), h: zircon U-Pb age of oldest granite (Majka et al., 2014), **i**: zircon U-Pb age of youngest granite (Gasser and Andresen, 2013), **j**: EPMA Th-U-total Pb monazite (Majka et al., 2008), **k**: zircon U-Pb age of pegmatite intrusion (Majka et al., 2014). **Northwest Terrane in Svalbard**—general stratigraphy:(Pettersson et al., 2009a), **l**: zircon U-Pb age of oldest granites (Pettersson et al., 2009b; Peucat et al., 1989), **m**: zircon U-Pb age of gabbro (Peucat et al., 1989). **Northeast Terrane in Svalbard**—general stratigraphy: (McClelland et al., 2019), **n**: youngest detrital zircon grains in (A. N. Larionov in Johansson et al., 2005; Kosteva et al.; Lorenz et al., 2012), **o**: zircon and monazite U-Pb ages of volcanics and shallow intrusives (Johansson et al., 1999), **p**: zircon and monazite U-Pb ages of augen gneiss and migmatites (Gee and Nakanishi, 1995; Johansson et al., 2004; Johansson et al., 1999; McClelland et al., 2019), **q**: possible

900–850 Ma and Cryogenian acritarchs in the lower and upper Murchisonfjorden Supergroup, respectively (Knoll, 1982). **Hebridean Foreland, NW Scotland**—general stratigraphy:(Krabbendam et al., 2017). **Moine, Naver and Sgurr Beag Nappes, Northwest Scotland**—general stratigraphy: (Cawood et al., 2015), **r**: Kinny & Strachan (unpublished) of granitic gneiss in Cawood et al. (2010), **s**: Garnet Lu-Hf age of Renlandian metamorphism (Bird et al., 2018), **t**: youngest detrital zircon U-Pb age from Emery (2005) and Cutts et al. (unpublished) in Cawood et al. (2010), **u**: zircon U-Pb age of granitoids (Friend et al., 1997; Rogers et al., 2001), **v**: zircon U-Pb age of intruding mafic sheets (Millar, 1999), **w**: U-Pb age of magmatic zircon rims on Morar Group zircon (Kirkland et al., 2008b), **x**: Sm-Nd garnet ages on growth zones within Morar Group (Vance et al., 1998), **y**: monazite U-Pb ages of intruding pegmatites (Rogers et al., 1998), **z**: monazite U-Pb ages of migmatites in the Glenfinnan Group from Cutts et al. (unpublished) in Cawood et al. (2010), **aa**: titanite U-Pb age of regional metamorphism (Tanner and Evans, 2003), **ab**: titanite U-Pb age of shearing of the Morar Group (Storey et al., 2004). **Grampian Terrane in northwest Ireland and central Scotland**—general stratigraphy: (Prave et al., 2009; Strachan et al., 2002), **ac**: Zircon U-Pb age of migmatization within sub-Grampian basement (Highton et al., 1999), **ad**: monazite U-Pb ages of pegmatites and mylonites separating sub-Grampian basement and Grampian Group (Noble et al., 1996), **ae**: Re-Os age of slate (Rooney et al., 2011). **Shetland**—general stratigraphy: (Strachan et al., 2013), **af**: Zircon U-Pb ages of metamorphic zircon growth in the Yell Sound Group (Jahn et al., 2016), **ag**: zircon U-Pb age of metamorphic zircon growth in the Westing Group (Cutts et al., 2009). **South and central Norwegian Caledonides**—general stratigraphy: (Bingen et al., 2011; Gee et al., 2015), **ah**: U-Pb age of megacrystic granite in the Tårnvika pluton (Prouty, 2014), **ai**: Zircon U-Pb age of rhyodacitic lava flow in the lower Seve Nappe Complex (Albrecht, 2000), **aj**: zircon U-Pb age of granite intrusions into the Heggmo Terrane (Agyei-Dwarko et al., 2012), **ak**: zircon U-Pb age of granite intrusions into the lower Seve Nappe Complex (Paulsson and Andréasson, 2002), **al**: plagioclase $^{40}Ar/^{39}Ar$ and K-Ar age of intruding dolerites (Claesson and Roddick, 1983). **North Norwegian Caledonides**—general

stratigraphy: (Kirkland et al., 2008a; Rice, 2014), **am**: zircon U-Pb age for granite that cuts deformed Svaerholt Succession (Kirkland et al., 2006), **an**: zircon U-Pb age for granite that cuts deformed Sørøy Succession (Kirkland et al., 2006), **ao**: zircon U-Pb age for syn-deformational leucosome (Kirkland et al., 2006), **ap**: zircon U-Pb age for overgrowths on Sørøy Succession (Kirkland et al., 2007).

Fig. 10: Kernel density estimates according to groupings and megasequences outlined in Table 1 and Fig. 8.

Fig. 11: Non-metric multi-dimensional scaling plot based on U-Pb ages of detrital zircon populations, colour-coded by megasequence (see Fig. 8). Greater distance between points relates to greater dissimilarity of detrital zircon age populations. Grey circles represent synthetic age populations, with numbers corresponding to the samples mean age in Ma, drawn from approximate age peaks within a pooled dataset of all detrital zircon data to help describe the controls of data dispersion. Each synthetic sample has an uncertainty of ± 50 Ma (1σ) and a population of $n = 300$.

Fig. 12: Relative sample difference matrix based on both U-Pb age and Hf-model age data of detrital zircon populations. Relative differences generated in Detzrcr (Kristoffersen et al., 2016), and are based on overlap of cumulative probability curves incorporating 95% confidence intervals (Andersen et al., 2016). Full overlap of confidence intervals give a value of 1, thus the differences are colour coded with grey indicating $1-\text{Overlap} \geq 0.05$, white $0 < 1-\text{Overlap} < 0.05$ and blue $1-\text{Overlap} = 0$.

Fig. 13: Zircon disparity (Barham et al., 2019a) between megasequences 1, 2 and 3, illustrating increasing disparity in terms of both nearest neighbour and inter-sample distances up stratigraphy, with a particularly large jump from megasequence 2 to 3.

Table 1: Compiled detrital zircon sample localities from the three megasequences in the North Atlantic region. See Supplementary Table C for full U-Pb and Hf isotope data compilation. Rows italicized and in grey text are samples not used for statistical comparison because these: (i) comprise too few grains (n < 20) to yield statistically-useful K–S tests, (ii) have poorly defined stratigraphic relationships, (iii) are younger than Cryogenian. *n* of t = number of concordant vs number of total analyses.

Supplementary Table A: U-Pb and Hf isotopic standard data for the new Wollaston Forland samples.

Supplementary Table B: Compendium of U–Pb and Hf isotopic data for new analyses. For interpretation of genesis: D = discordant, I = magmatic, M = metamorphic, S = detrital, Y = youngest detrital, X = inherited/xenocrystic, Z = mixed core-rim.

Supplementary Table C: Compendium of U–Pb and Hf isotopic from the Meso- to Neoproterozoic North Atlantic region. For interpretation of genesis: D = discordant, I = magmatic, M = metamorphic, S = detrital, Y = youngest detrital, X = inherited/xenocrystic, Z = mixed core-rim.

Supplementary Figure A: Cross-plot of 50 (session 1) and 38 μm (session 2) duplicate analyses, illustrating no significant difference in spot sizes.

Supplementary Figure B: Compilation of all CL images for new samples.

Region	Group	Unit	Mega-seq.	Lithology	Sample No	Longitude	Latitude	Data types	Max. depoage	± 2σ (Ma)	MSWD	*p*	*n* of *t* concordant detrital analyses	Reference
Canadian High Arctic	*Pearya Succession II*	*Unit W 2/3*	*4*	*Metasedimentary Breccia*	*SE179/01*	*-82.28508*	*83.53008*	*U-Pb*	*1063*	*21*	*1.3*	*0.27*	*5 of 68*	*Estrada et al., 2018*
Canadian High Arctic	*Pearya Succession II*	*Unit M2*	*4*	*Mica Schist*	*C11-072*	*-82.71772*	*79.42286*	*U-Pb*	*573*	*6*	*0.97*	*0.41*	*4 of 43*	*Estrada et al., 2018*
Canadian High Arctic	Pearya Succession II	Unit Y2	3	Quartzite	08-195	-81.32579	82.53126	U-Pb	1033	17	1.4	0.15	13 of 86	Malone et al., 2014
Canadian High Arctic	Pearya Succession II	Unit Y2	3	Quartzite	08-196	-81.32401	82.53141	U-Pb	1026	11	1.14	0.3	18 of 89	Malone et al., 2014
Canadian High Arctic	Pearya Succession II	Unit Y2	3	Quartzite	08-136	-81.69134	82.43282	U-Pb	921	6	1.14	0.24	49 of 94	Malone et al., 2014
Canadian High Arctic	Pearya Succession II	Unit Y2	3	Metagraywacke	08-189	-78.54708	82.24175	U-Pb	670	27	-	-	1 of 86	Malone et al., 2014
Canadian High Arctic	Pearya Succession II	Unit Y2	3	Sandstone	08-157	-81.00279	82.27631	U-Pb	635	10	-	-	1 of 89	Malone et al., 2014
Canadian High Arctic	Pearya Succession II	Unit Y2	3	Sandstone	08-177	-81.00499	82.27618	U-Pb	664	41	0.89	0.34	2 of 73	Malone et al., 2014
Canadian High Arctic	Pearya Succession II	Unit A	3	Metaconglomerate	C11-83	-82.77161	79.80050	U-Pb	970	12	0.02	1	3 of 75	Estrada et al., 2018
Canadian High Arctic	Pearya Succession II	Unit A	3	Foliated quartzite	SE 16/08	-82.83850	79.93117	U-Pb	972	15	1.08	0.36	4 of 98	Estrada et al., 2018
Canadian High Arctic	Pearya Succession II	Unit A	3	Quartzitic schist	SE 62/08 D	-82.85208	80.14078	U-Pb	921	10	0.53	0.66	4 of 75	Estrada et al., 2018
Canadian High Arctic	*Pearya Succession II*	*Unit A (fault zone)*	*3*	*Mica Schist*	*SE 61/08 C*	*-82.85208*	*80.14078*	*U-Pb*	*797*	*14*	-	-	*1 of 59*	*Estrada et al., 2018*
Canadian High Arctic	*Pearya Succession I*	*Undifferentiated*	*1*	*Mica Schist*	*SE 34+35/08*	*-82.46539*	*81.88681*	*U-Pb*	*845*	*17*	-	-	*1 of 1*	*Estrada et al., 2018*
Northeast Greenland	Moræneø Formation	Undifferentiated	3	Diamictite	CKG28	-36.02485	82.22927	U-Pb	1013	18	-	-	1 of 26	Kirkland et al., 2009
Northeast Greenland	Moræneø Formation	Undifferentiated	3	Sandstone	CKG359	-36.34440	82.22830	U-Pb	1035	23	-	-	1 of 30	Kirkland et al., 2009
Northeast Greenland	Moræneø Formation	Undifferentiated	3	Feldspathic sandstone dyke	CKG38	-31.38233	82.17070	U-Pb	1024	5	1.02	0.43	12 of 106	Kirkland et al., 2009
Northeast Greenland	Moræneø Formation	Undifferentiated	3	Feldspathic fluvial sandstone	CKG4	-36.07134	82.22716	U-Pb	1020	15	0.3	0.58	2 of 18	Kirkland et al., 2009
East Greenland	Lyell Land Group	Vibeke Sø Formation	3	Sandstone	SSFN 14	-25.13361	72.43972	U-Pb; Hf	1062	18	1.12	0.31	27 of 98	Slama et al., 2011
East Greenland	Lyell Land Group	Skjoldungebræ Formation	3	Sandstone	SSFN 2	-24.93361	72.46222	U-Pb; Hf	1043	9	1.05	0.36	82 of 115	Slama et al., 2011

East Greenland	Lyell Land Group	Vibeke Sø Formation	3	Sandstone	SSFN 9	-24.97861	72.46083	U-Pb; Hf	987	9	1.07	0.33	73 of 115	Slama et al., 2011
East Greenland	Nathorst Land Group	Sillimanite Zone	2	Metaquarzite	201728 (ICP)	-20.20857	74.30931	U-Pb	1051	30	-	-	1 of 22	Dhuime et al., 2007
East Greenland	Nathorst Land Group	Sillimanite Zone	2	Metaquarzite	201728 (SIMS)	-25.81238	72.29487	U-Pb	1008	20	-	-	2 of 10	Dhuime et al., 2007
East Greenland	Nathorst Land Group	Sillimanite Zone	2	Metaquarzite	201836 (ICP)	-25.70869	72.43199	U-Pb	1052	30	0.04	0.85	1 of 3	Dhuime et al., 2007
East Greenland	Nathorst Land Group	Migmatitic Zone	2	Metapelitic xenolith	201893 (ICP)	-25.79109	72.29510	U-Pb	1004	77	-	-	1 of 13	Dhuime et al., 2007
East Greenland	Nathorst Land Group	Migmatitic Zone	2	Metapelitic xenolith	201893 (SIMS)	-25.79109	72.29510	U-Pb	1157	45	-	-	1 of 4	Dhuime et al., 2007
East Greenland	Nathorst Land Group	Chlorite Zone	2	Orthoquarzite	201991 (ICP)	-25.45944	72.28257	U-Pb	1070	49	-	-	1 of 13	Dhuime et al., 2007
East Greenland	Nathorst Land Group	Wollaston sequence	2	Psammitic gneiss	590204	-19.32606	74.58298	U-Pb; Hf	950	23	-	-	1 of 31	This study
East Greenland	Nathorst Land Group	Wollaston sequence	2	Quartzite	590207	-19.33057	74.57573	U-Pb; Hf	925	24	0.02	0.88	2 of 135	This study
East Greenland	Nathorst Land Group	Wollaston sequence	2	Quartzite	590210	-20.08284	74.62391	U-Pb; Hf	933	49	-	-	1 of 159	This study
East Greenland	Nathorst Land Group	Wollaston sequence	2	Metapelite	590214	-19.78527	74.39987	U-Pb; Hf	1007	21	0.12	0.73	2 of 38	This study
East Greenland	Nathorst Land Group	Wollaston sequence	2	Metapsammite	590232	-20.11136	74.63862	U-Pb; Hf	1045	17	0.09	0.77	2 of 8	This study
East Greenland	Nathorst Land Group	Upper Nathorst Land Group	2	Quartz arenite	445935	-25.55969	72.44863	U-Pb	1113	41	-	-	1 of 18	Watt et al., 2000
East Greenland	Nathorst Land Group	Basal Nathorst Land Group	2	Sandstone	445979	-25.55969	72.44863	U-Pb	1078	33	-	-	1 of 33	Watt et al., 2000
East Greenland	Krummedal Succession	Smallefjord sequence	1	Migmatized kyanite-garnet schist	GGU 249933	-21.18333	75.76667	U-Pb	1111	22	-	-	1 of 3	Strachan et al., 1995
East Greenland	Krummedal Succession	Renland sequence	1	Metapsammite	GGU452619	-27.45833	70.98000	U-Pb	1039	27	0.86	0.51	6 of 38	Leslie & Nutman, 2003
East Greenland	Krummedal Succession	Renland sequence	1	Migmatitic metapsammite/semipelite	GGU452625	-27.42333	70.97833	U-Pb	1065	45	-	-	1 of 4	Leslie & Nutman, 2003
East Greenland	Krummedal Succession	Stauning Alper sequence	1	Migmatitic paragneiss	441337	-26.35071	71.96700	U-Pb	1072	28	-	-	1 of 8	Watt et al., 2000
East Greenland	Krummedal Succession	Stauning Alper sequence	1	Migmatitic paragneiss	441341	-26.35071	71.96700	U-Pb	1478	28	-	-	1 of 3	Watt et al., 2000
East Greenland	Krummedal Succession	Stauning Alper migmatite zone	1	Migmatitic paragneiss	441383	-26.35071	71.96700	U-Pb	1083	32	-	-	1 of 12	Watt et al., 2000
SW Terrane, Svalbard	*Sørkapp Land*	*Unnamed Unit 35*	*4*	*quartzite*	*HL:12-008*	*16.71347*	*76.57707*	*U-Pb*	*1116*	*47*	*0.64*	*0.64*	*5 of 39*	*Ziemniak et al., 2019*
SW Terrane,	*Sørkapp Land*	*Unnamed Unit 35*	*4*	*meta-sandstone*	*HL:12-010*	*16.56151*	*76.58404*	*U-Pb*	*1062*	*26*	*1.1*	*0.36*	*8 of 37*	*Ziemniak et*

Svalbard														*al., 2019*
SW Terrane, Svalbard	Kapp Lyell Group	Comfortlessbreen Unit	3	Tillitoid Sandstone	Sample 3	12.65000	78.55000	U-Pb	713	7	0.63	0.43	2 of 105	Gasser & Andresen 2013
SW Terrane, Svalbard	Sofiebogen Group	Undifferentiated	3	conglomerate	HL:12-019	15.25217	77.14176	U-Pb	1140	123	-	-	1 of 31	Ziemniak et al., 2019
SW Terrane, Svalbard	Deilegga Group	Undifferentiated	2	quartzite	HL:12-018	15.28075	77.14215	U-Pb	1006	69	0.58	0.56	3 of 27	Ziemniak et al., 2019
SW Terrane, Svalbard	Eimfjellet Group	Skjerstranda Fm.	2	quartzite	HL:12-012	15.18202	77.02342	U-Pb	1173	63	0.48	0.85	8 of 32	Ziemniak et al., 2019
SW Terrane, Svalbard	Eimfjellet Group	Eimfjellbreane Fm.	2	meta-sandstone	HL:12-014	15.24053	77.03163	U-Pb	1148	59	0.14	0.71	2 of 21	Ziemniak et al., 2019
SW Terrane, Svalbard	Eimfjellet Group	Gulliksenfjellet Fm.	2	green quartzite	HL:12-017	15.15838	77.06731	U-Pb	1776	32	0.86	0.52	7 of 35	Ziemniak et al., 2019
SW Terrane, Svalbard	Eimfjellet Group	Daudmannsodden Unit	2	Shale-sandstone	Sample 2	12.70000	78.54000	U-Pb	886	17	-	-	1 of 140	Gasser & Andresen 2013
SW Terrane, Svalbard	Isbjørnhamna Group.	Undifferentiated	1	quartzite	Sp21/08	15.29648	77.01011	U-Pb	1000	45	-	-	1 of 57	Ziemniak et al., 2019
SW Terrane, Svalbard	Isbjørnhamna Group	St Johnsfjorden Unit	1	Quartzite	Sample 1	12.60000	78.44000	U-Pb	1006	14	-	-	1 of 109	Gasser & Andresen 2013
NW Terrane, Svalbard	Krossfjorden Group	Signehamna Formation	1	Garnet mica schist	CP04-45	12.49460	79.00370	U-Pb, Hf	976	26	-	-	1 of 30	Petterson et al., 2009a; Spencer et al., 2015
NW Terrane, Svalbard	Krossfjorden Group	Signehamna Formation	1	Quartzite	CP04-2	12.01910	79.19960	U-Pb, Hf	985	21	-	-	1 of 39	Petterson et al., 2009a; Spencer et al., 2015
NW Terrane, Svalbard	Smerenburgfjorden Complex	Undifferentiated	1	Diatexite	CP04-27	12.13203	79.30830	U-Pb, Hf	1010	19	-	-	1 of 32	Petterson et al., 2009a; Spencer et al., 2015
NW Terrane, Svalbard	Smerenburgfjorden Complex	Undifferentiated	1	Quartzite	CP03-51	11.21120	79.77795	U-Pb, Hf	955	24	-	-	1 of 55	Petterson et al., 2009a; Spencer et al., 2015
NW Terrane, Svalbard	Smerenburgfjorden Complex	Undifferentiated	1	Quartzite xenolith	CP03-39	11.69170	79.83412	U-Pb, Hf	995	25	-	-	1 of 32	Petterson et al., 2009a; Spenc

														er et al., 2015
NW Terrane, Svalbard	Smerenburgfjorden Complex	Undifferentiated	1	Paragneiss	CP04-03	12.54393	79.00398	U-Pb	1133	37	-	-	1 of 19	Petterson et al., 2009a
Hebridean Foreland	Torridon Group	Applecross Formation	1	Sandstone	GY96-4	-5.31000	58.07000	U-Pb	1068	21	1.17	0.31	3 of 43	Rainbird et al., 2001
Hebridean Foreland	Torridon Group	Aultbea Formation	1	Sandstone	GY96-56	-5.57000	57.92000	U-Pb	1085	27	0.92	0.4	3 of 39	Rainbird et al., 2001
Hebridean Foreland	Torridon Group	Aulbea Formation	1	Sandstone	07LSC5	-5.56193	57.90869	U-Pb; Hf	1059	10	-	-	1 of 67	Lancaster et al., 2011
Hebridean Foreland	Torridon Group	Applecross Formation	1	Pebbly sandstone	07LSC6	-5.34624	58.06618	U-Pb; Hf	1065	9	0.01	0.93	2 of 50	Lancaster et al., 2011
Hebridean Foreland	Torridon Group	Applecross Formation	1	Pebbly sandstone	CS11-20	-5.83779	57.23162	U-Pb; Hf	1050	19	0.42	0.51	2 of 45	Spencer et al., 2015
Hebridean Foreland	Torridon Group	Diabaig Formation	1	Siltstone/sandstone	diab/tk2	-5.57000	57.58000	U-Pb	1092	34	-	-	1 of 5	Kinnaird et al., 2007
Hebridean Foreland	Torridon Group	Aultbea Formation	1	Sandstone	ZY320	-5.70000	57.10000	U-Pb	992	46	-	-	1 of 101	Krabbendam et al., 2017
Hebridean Foreland	Torridon Group	Applecross Formation	1	Arkosic sandstone	ZY327	-5.61060	57.41959	U-Pb	1097	13	0.8	0.57	7 of 147	Krabbendam et al., 2017
Hebridean Foreland	Sleat Group	Kinloch Formation	1?	Sandstone	ZY317	-5.86122	57.17042	U-Pb	1107	12	-	-	1 of 63	Krabbendam et al., 2017
Hebridean Foreland	Sleat Group	Kinloch Formation	1?	Sandstone	CS11-19	-5.83213	57.21587	U-Pb; Hf	1197	23	-	-	1 of 53	Spencer et al., 2015
Hebridean Foreland	Sleat Group	Kinloch Formation	1?	Sandstone	kin4	-5.58000	57.19000	U-Pb	1246	35	-	-	1 of 10	Kinnaird et al., 2007
Hebridean Foreland	Sleat Group	Beinn na Seamraig Formation	1?	Sandstone	ZY319	-5.57000	57.58000	U-Pb	1056	17	-	-	1 of 76	Krabbendam et al., 2017
Hebridean Foreland	Sleat Group	Loch na Dal Formation	1?	Sandstone	ZY315	-5.57016	57.67887	U-Pb	1102	44	-	-	1 of 155	Krabbendam et al., 2017
Hebridean Foreland	Sleat Group	Loch na Dal Formation	1?	Sandstone	07LSC2	-5.70636	57.19995	U-Pb	1072	13	-	-	1 of 9	Lancaster et al., 2011
Hebridean Foreland	Sleat Group	Loch na Dal Formation	1?	Sandstone	LD2/mt2c	-5.58000	57.19000	U-Pb	1174	80	-	-	1 of 25	Kinnaird et al., 2007
Hebridean Foreland	Sleat Group	Loch na Dal Formation	1?	Sandstone	CS11-18	-5.79628	57.16059	U-Pb; Hf	1727	12	0.34	0.56	2 of 61	Spencer et al., 2015
Hebridean Foreland	Sleat Group	Rubha Guail Formation	1?	Sandstone	09LSC1	-5.70636	57.19995	U-Pb; Hf	1589	18	-	-	1 of 32	Lancaster et al., 2011
Hebridean Foreland	Sleat Group	Rubha Guail Formation	1?	Sandstone	RG1	-5.58000	57.19000	U-Pb	1710	140	-	-	1 of 19	Kinnaird et al., 2007
Hebridean Foreland	Sleat Group	Rubha Guail Formation	1?	Sandstone	SI-RG-1	-5.58000	57.19000	U-Pb	1759	11	-	-	1 of 6	Kinnaird et al., 2007

NW Scotland	Loch Eil Group	Loch Eil Formation	2	Sandstone	CS11-13	-5.34635	56.87692	U-Pb; Hf	988	16	1.11	0.34	4 of 56	Spencer et al., 2015
NW Scotland	Loch Eil Group	Loch Eil Formation	2	Psammite	sh02-13	-5.15130	56.84460	U-Pb	969	21	0.72	0.66	8 of 67	Cawood et al., 2004
NW Scotland	Loch Eil Group	Glen Urquhart Psammite	2	Psammite	sh02-1	-4.50315	57.34178	U-Pb	918	22	0.68	0.64	6 of 68	Cawood et al., 2004
NW Scotland	Loch Eil Group (?)	Kirtomy Migmatite	2	Semi-pelitic migmatite	KM94/5	-4.14463	58.55243	U-Pb	1084	26	1.02	0.36	3 of 15	Kinny et al., 1999
NW Scotland	Loch Eil Group (?)	Naver Migmatite	2	Psammitic migmatite	S96/8	-4.25605	58.52087	U-Pb	1005	36	-	-	1 of 20	Kinny et al., 1999
NW Scotland	Glenfinnan Group	Sgurr Beag Nappe (Lochailort pelite)	2	Pelite	S00/05	-5.67000	56.88000	U-Pb	1046	24	-	-	1 of 6	Friend et al., 2003
NW Scotland	Glenfinnan Group	Glenfinnan Group (lower)	2	Quartzite	ARDN-3	-6.61759	50.38311	U-Pb; Hf	1013	16	0.05	0.82	2 of 50	Kirkland et al., 2008b; Spencer et al., 2015
NW Scotland	Glenfinnan Group (equivalent)	Ardalanish Striped and Banded unit	2	?	MG03	-6.20917	56.28905	U-Pb	948	35	0.32	0.57	2 of 43	Cawood et al., 2015
NW Scotland	Glenfinnan Group (equivalent)	Scoor Pelitic Gneiss	2	Metapelite	RS01-10	-6.17089	56.29144	U-Pb	1066	20	0.01	0.93	2 of 58	Cawood et al., 2015
NW Scotland	Morar Group	Moine Nappe	1	Psammite	S97/21	-4.50000	58.54000	U-Pb	948	52	-	-	1 of 54	Friend et al., 2003
NW Scotland	Morar Group	Upper Psammite	1	Feldspathic arenite	ARDN-2	-6.77602	50.41821	U-Pb; Hf	1004	23	-	-	1 of 61	Kirkland et al., 2008b; Spencer et al., 2015
NW Scotland	Morar Group	Lower Psammite	1	Feldspathic sandstone	ARDN-1	-6.72197	50.41318	U-Pb; Hf	1075	17	0.1	0.75	2 of 38	Kirkland et al., 2008b; Spencer et al., 2015
NW Scotland	Morar Group	Altnaharra Formation	1	Psammite	CJS 99-J5	-5.54534	57.32043	U-Pb; Hf	1160	25	-	-	1 of 140	Lancaster et al., 2011
NW Scotland	Morar Group	Basal Morar Group	1	Conglomerate	07LSC3	-5.45128	57.38089	U-Pb; Hf	1076	7	0.62	0.43	2 of 62	Lancaster et al., 2011
NW Scotland	Morar Group (equivalent)	Upper Shiaba Psammite	1	Metasandstone	MG04	-6.15726	56.28782	U-Pb	1480	19	0.82	0.35	2 of 41	Cawood et al., 2015
NW Scotland	Morar Group (equivalent)	Ladhar Bheinn Pelite	1	Metapelite	KD07-01/02	-5.62935	57.00350	U-Pb	1086	20	0.02	0.9	2 of 18	Cawood et al., 2015
NW Scotland	Morar Group (equivalent)	Lower Shiaba Psammite	1	Metasandstone	MG01	-6.13005	56.29417	U-Pb	1007	60	-	-	1 of 54	Cawood et al., 2015
NW Ireland	Argyll Group (equivalent?)	Tyrone Central Inlier	3	Psammite	JTP-210	-6.88762	54.67528	U-Pb	992	32	-	-	1 of 60	Chew et al., 2008

NW Ireland	Grampian Group	Doonamo Formation	3	Psammite	C61A	-10.02476	54.28380	U-Pb	959	17	0.65	0.69	7 of 95	McAteer et al., 2010c
NW Ireland	Grampian Group	Inishkea Division (Kinrovar Schist)	3	Schistose psammite	C63	-9.97274	54.06270	U-Pb	993	65	-	-	1 of 15	McAteer et al., 2010c
NW Ireland	Grampian Group	Inishkea Division (Kinrovar Schist)	3	Schistose psammite	C67	-10.08014	54.25500	U-Pb	968	60	-	-	1 of 9	McAteer et al., 2010c
C Scotland	Argyll Group	Ben Lawers Schist	3	Psammite/semi-pelite	SMS474	-4.29128	56.54101	U-Pb	940	35	0.78	0.5	4 of 26	Cawood et al., 2003b
C Scotland	Argyll Group	Port Askaig Tillite	3	Diamictite	GA-99-03A	-5.75943	56.24106	U-Pb	1114	34	1.14	0.33	5 of 32	Cawood et al., 2003b
C Scotland	Argyll Group	Port Askaig Tillite	3	Diamictite	IS03A	-6.10389	55.84680	U-Pb	1083	40	0.44	0.82	6 of 55	Cawood et al., 2003b
C Scotland	Appin Group	Strath Fionan Banded Semipelite	3	Semi-pelite	SMS484	-4.07765	56.68235	U-Pb	1602	87	-	-	1 of 41	Cawood et al., 2003b
C Scotland	Grampian Group	Inverlair Psammite	3	Arkosic Psammite	CJB2	-4.44659	56.96547	U-Pb	1272	30	0.67	0.61	5 of 26	Banks et al., 2007
C Scotland	Grampian Group	Strath Tummel Succession	3	Psammite	SMS509	-3.91420	56.76548	U-Pb	907	16	-	-	1 of 35	Cawood et al., 2003b
C Scotland	Grampian Group	Creag Dhubh Psammite	3	Micaceous Psammite	CJB3	-3.91570	56.21507	U-Pb	1023	53	-	-	1 of 30	Banks et al., 2007
C Scotland	Grampian Group	Loch Laggan Psammite	3	Micaceous Psammite	CJB1	-4.72454	56.88530	U-Pb	1056	69	0.22	0.64	2 of 38	Banks et al., 2007
C Scotland	Grampian Group	Glen Buck Psammite	3	Psammite	SMS516	-4.59828	57.16596	U-Pb	1430	48	0.16	0.69	2 of 65	Cawood et al., 2003b
C Scotland	Grampian Group	Garva Bridge psammite	3	Psammite	SMS521	-4.43376	57.02350	U-Pb	1043	56	1.04	0.31	2 of 64	Cawood et al., 2003b
C Scotland	Grampian Group (equivalent)	Colonsay Group (Kiloran Flags Fm.)	3	Sandstone	C14	-6.20082	56.10588	U-Pb	1019	11	0.8	0.45	3 of 29	McAteer et al., 2010a
C Scotland	Grampian Group (equivalent)	Colonsay Group (Dun Gallain Fm.)	3	Sandstone	C9.2	-6.25830	56.05803	U-Pb	1015	35	-	-	1 of 18	McAteer et al., 2010a
C Scotland	Grampian Group (equivalent)	Colonsay Group (Ornonsay Fm.)	3	Sandstone	C13	-6.26942	56.04236	U-Pb	1773	9	0.48	0.99	30 of 30	McAteer et al., 2010a
C Scotland	Grampian Group (equivalent)	Colonsay Group (Ardnave Fm.)	3	Sandstone	C29	-6.33385	55.87191	U-Pb	1306	17	-	-	1 of 22	McAteer et al., 2010a
C Scotland	Grampian Group (equivalent)	Colonsay Group (Smaull Fm.)	3	Sandstone	C22	-6.41467	55.85105	U-Pb	1112	32	-	-	1 of 22	McAteer et al., 2010a
C Scotland	Grampian Group (equivalent)	Colonsay Group (Octofad Fm.)	3	Siltstone	C37D	-6.42770	55.69856	U-Pb	1296	47	-	-	1 of 20	McAteer et al., 2010a
C Scotland	Grampian Group (equivalent)	Bowmore Sandstone Group (Blackrock Fm.)	3	Sandstone	C39	6.30471	55.78210	U-Pb	881	19	-	-	1 of 38	McAteer et al., 2010b
C Scotland	Grampian Group	Iona Group	3	Arkosic sandstone	C59	-6.40034	56.34446	U-Pb	1485	14	0.01	0.92	2 of 89	McAteer et

	(equivalent)	(upper unit)												al., 2014
C Scotland	Sub-Grampian basement	Glen Banchor Succession	2	Psammite/semi-pelite	SMS143	-4.30549	57.02215	U-Pb	900	34	-	-	1 of 36	Cawood et al., 2003
C Scotland	Sub-Grampian basement	Dava succession	2	Migmatized arkosic psammite	S99461	-3.93024	57.30255	U-Pb	-	-	-	-	-	Highton et al., 1999
Shetland	*East Mainland Succession*	*Clift Hills Group*	*4*	*Psammite*	*CHD2*	*-1.15886*	*60.19571*	*U-Pb*	*576*	*18*	-	-	*1 of 52*	*Strachan et al., 2013*
Shetland	*East Mainland Succession*	*Clift Hills Group*	*4*	*Psammite*	*CHD3*	*-1.33151*	*59.97132*	*U-Pb*	*906*	*18*	-	-	*1 of 33*	*Strachan et al., 2013*
Shetland	East Mainland Succession	Whitenes s Group	3	Psammite	WD4	-1.20841	60.22799	U-Pb	927	7	0.88	0.48	1 of 49	Strachan et al., 2013
Shetland	East Mainland Succession	Whitenes s Group	3	Psammite	WD3	-1.28362	60.19806	U-Pb	903	14	0.02	0.88	2 of 28	Strachan et al., 2013
Shetland	East Mainland Succession	Whitenes s Group	3	Psammite	WD1	-1.30501	60.22709	U-Pb	1175	25	-	-	1 of 10	Strachan et al., 2013
Shetland	East Mainland Succession	Scatsta Group	3	Quartzite	SQ2	-1.27979	60.35616	U-Pb	976	12	0.5	0.48	2 of 35	Strachan et al., 2013
Shetland	East Mainland Succession	Scatsta Group	3	Quartzite	SQ1	-1.29783	60.36847	U-Pb	962	22	-	-	1 of 31	Strachan et al., 2013
Shetland	Westing & Yell Sound Groups	Westing Group (Unst Island)	1	Metasediment	SH11	1.01000	60.73000	U-Pb	996	7	0.28	0.6	2 of 82	Cutts et al., 2009
Shetland	Westing & Yell Sound Groups	Westing Group (Unst Island)	1	Garnet-bearing metapelite	SH10	1.01000	60.72000	U-Pb	2618	24	-	-	1 of 10	Cutts et al., 2009
Shetland	Westing & Yell Sound Groups	Yell Sound Group	1	Paragneiss	SH12-14	0.54000	60.73000	U-Pb	1024	16	0.34	0.56	2 of 7	Jahn et al., 2016
Lomonosov Ridge	*Lomonosov Ridge*	*Unknown*	*1?*	*Metaarkose*	*54000 1-18*	*40.00000*	*88.00000*	*U-Pb*	*1169*	*15*	*0.48*	*0.62*	*3 of 66*	*Knudsen et al., 2018*
Lomonosov Ridge	*Lomonosov Ridge*	*Unknown*	*1?*	*Metaarkose*	*54000 1-19*	*30.00000*	*88.00000*	*U-Pb*	*1078*	*27*	-	-	*1 of 63*	*Knudsen et al., 2018*
Lomonosov Ridge	*Lomonosov Ridge*	*Unknown*	*1?*	*Metaarkose*	*54000 2-5*	*30.00000*	*88.00000*	*U-Pb*	*1046*	*11*	-	-	*1 of 63*	*Knudsen et al., 2018*
S Norway Caledonides	*North Sea*	*Unknown*	*2?*	*Metasandstone*	*25/7-1*	*2.70000*	*59.20000*	*U-Pb*	*959*	*11*	*1*	*0.41*	*5 of 42*	*Slagstad et al., 2011*
S Norway Caledonides	*Norwegian Sea*	*Unknown*	*1?*	*Metasandstone*	*6609/7-1*	*8.90000*	*66.20000*	*U-Pb*	*1041*	*26*	-	-	*1 of 24*	*Slagstad et al., 2011*
S-C Norway Caledonides	Sparagmite Sequence	Ammarnäs Complex	3	Metagraywacke	021	18.45116	65.99014	U-Pb	958	9	0.85	0.51	6 of 73	Grimmer et al., 2011
S-C Norway Caledonides	Sparagmite Sequence	Ammarnäs Complex	3	Metagraywacke	014	18.45000	65.99000	U-Pb	927	21	-	-	1 of 81	Grimmer et al., 2011

S-C Norway Caledonides	Sparagmite Sequence (Lower Allochthon)	Osen-Røa Nappe (Hedmark Group, Rendalen Fm.)	3	Arkose	104	10.92916	61.84975	U-Pb, Hf	611	15	-	-	1 of 64	Bingen et al., 2005
S-C Norway Caledonides	Sparagmite Sequence (Lower Allochthon)	Osen-Røa Nappe (Hedmark Group, Atna Fm.)	3	Subarkose	103	10.24433	61.77447	U-Pb, Hf	959	13	0.35	0.7	3 of 51	Bingen et al., 2011
S-C Norway Caledonides	Sparagmite Sequence (Lower Allochthon)	Osen-Røa Nappe (Ring Fm.)	3	Arkose	107	11.38562	61.13419	U-Pb, Hf	939	13	0.88	0.45	4 of 54	Bingen et al., 2011
S-C Norway Caledonides	Sparagmite Sequence (Lower Allochthon)	Osen-Røa Nappe (Hedmark Group, Vangås Fm.)	3	Arkose	108	11.17786	61.09751	U-Pb, Hf	867	22	-	-	1 of 49	Bingen et al., 2011
S-C Norway Caledonides	Sparagmite Sequence (Lower Allochthon)	Osen-Røa Nappe (Hedmark Group, Brøttum Fm.)	3	Greywacke	112	10.35276	61.05502	U-Pb, Hf	913	15	-	-	1 of 58	Bingen et al., 2011
S-C Norway Caledonides	Sparagmite Sequence (lower Upper Allochthon)	Upper Seve Nappe - Jämtland (Inviken area)	3	Meta-arkose	B26728	14.86878	64.60525	U-Pb, Hf	726	21	-	-	1 of 57	Kirkland et al., 2011; Spencer et al., 2015
S-C Norway Caledonides	Sparagmite Sequence (lower Upper Allochthon)	Upper Seve Nappe - Jämtland (Härbergsdalen area)	3	Meta-arkose	B26729	14.69523	64.70548	U-Pb, Hf	808	24	-	-	1 of 40	Kirkland et al., 2011; Spencer et al., 2015
S-C Norway Caledonides	Sparagmite Sequence (Middle Allochthon)	Seve Nappe Complex (Blåsjön)	3	Migmatitic paragneiss	81013	14.20000	64.95000	U-Pb	804	19	-	-	1 of 8	Williams & Claesson, 1987
S-C Norway Caledonides	Sparagmite Sequence (Middle Allochthon)	Seve Nappe Complex (Gardiken)	3?	Migmatitic paragneiss	82014	15.54000	65.50000	U-Pb	941	22	-	-	1 of 6	Williams & Claesson, 1987
S-C Norway Caledonides	Särv Succession (Middle Allochthon)	Kvitvola Nappe (Rondeslott Fm.)	2	Arkose	101	10.00266	62.00984	U-Pb, Hf	921	17	0.11	0.74	2 of 54	Bingen et al., 2011
S-C Norway Caledonides	Särv Succession (Middle Allochthon)	Valdres Nappe (Valdres Gp.)	2	Arkose	115	8.81824	61.28604	U-Pb, Hf	963	9	1.1	0.35	5 of 52	Bingen et al., 2011
S-C Norway Caledonides	Särv Succession (Middle Allochthon)	Särv Nappe (Kråkhammaren Fm.)	2	Arkose	26703	13.00999	62.60372	U-Pb, Hf	941	24	-	-	1 of 59	Bingen et al., 2011
S-C Norway Caledonides	Särv Succession (Middle Allochthon)	Särv Nappe (Funäsdalsberget)	2	Sub-arkose	76099	14.02539	63.55806	U-Pb	955	6	0.44	0.72	4 of 56	Be'eri-Shlevin et al., 2011
S-C Norway Caledonides	Särv Succession (Middle Allochthon)	Särv Nappe - Alsen	2	Fine-grained sandstone	AL08-13	14.02549	63.40822	U-Pb	911	11	0.94	0.42	4 of 94	Be'eri-Shlevin et al., 2011

S-C Norway Caledonides	Särv Succession (Middle Allochthon)	Särv Nappe - Alsen	2	Arkose	AL08-18	14.00789	63.41811	U-Pb	910	11	0.99	0.37	3 of 102	Be'eri-Shlevin et al., 2011
S-C Norway Caledonides	Särv Succession (Middle Allochthon)	Leksdal Nappe (upper part) Tømmerås	2	Semi-pelite with admixture of carbonates	DG08-3	11.49715	63.92268	U-Pb	914	4	1.1	0.35	21 of 102	Be'eri-Shlevin et al., 2011
S-C Norway Caledonides	Särv Succession (Middle Allochthon)	Leksdal Nappe (upper part) Tømmerås	2	Arkose	YBN08-13B	11.51173	63.98622	U-Pb	896	20	0.1	0.96	4 of 73	Be'eri-Shlevin et al., 2011
S-C Norway Caledonides	Särv Succession (Middle Allochthon)	Sætra Nappe - Oppdal	2	Arkosic sandstone with minor admixture of clays	AL08-42	9.57806	62.45000	U-Pb	929	23	-	-	1 of 85	Be'eri-Shlevin et al., 2011
S-C Norway Caledonides	Särv Succession (Middle Allochthon)	Sætra Nappe - Dragneset	2	Arkosic sandstone	AL08-44	6.79875	62.65272	U-Pb	881	24	-	-	1 of 99	Be'eri-Shlevin et al., 2011
S-C Norway Caledonides	Särv Succession (Middle Allochthon)	Sætra Nappe - Hellenest	2	Arkose	AL08-46	6.62056	62.61111	U-Pb	898	13	1.04	0.41	13 of 76	Be'eri-Shlevin et al., 2011
S-C Norway Caledonides	Särv Succession (Middle Allochthon)	Sætra Nappe - Lepsøya	2	Quartz-rich arkosic sandstone with minor admixture of clays	AL08-50	6.17367	62.63736	U-Pb	881	10	1.17	0.31	10 of 86	Be'eri-Shlevin et al., 2011
S-C Norway Caledonides	Särv Succession (Middle Allochthon)	Sætra Nappe - Vasslivatnet	2	Arkosic sandstone with minor admixture of clays	AL08-53	9.28139	63.22194	U-Pb	900	20	-	-	1 of 36	Be'eri-Shlevin et al., 2011
S-C Norway Caledonides	Särv Succession (Middle Allochthon)	Sætra Nappe - Almlia	2	Fine-grained feldspathic sandstone	YBN08-26	9.86935	63.33952	U-Pb	907	10	1.08	0.37	12 of 122	Be'eri-Shlevin et al., 2011
S-C Norway Caledonides	Särv Succession (Middle Allochthon)	Leksdal Nappe (lower part) Tømmerås	2?	Pelite	DG08-5	11.62184	63.87901	U-Pb	958	21	-	-	1 of 53	Be'eri-Shlevin et al., 2011
S-C Norway Caledonides	Särv Succession (Middle Allochthon)	Seve Nappe Complex (Grapesvare Nappe)	2?	Psammitic gneiss	HL10-013	15.98581	66.76042	U-Pb	991	18	-	-	1 of 45	Gee et al., 2015
S-C Norway Caledonides	Särv Succession (Middle Allochthon)	Seve Nappe Complex (Grapesvare Nappe)	2?	Psammitic gneiss	HL10-014	15.97318	66.75184	U-Pb	998	8	0.93	0.4	3 of 67	Gee et al., 2015
S-C Norway Caledonides	Särv Succession (Middle Allochthon)	Seve Nappe Complex (Lillviken Nappe)	2	Psammite	HL10-018	16.34917	66.52766	U-Pb	948	8	0.37	0.69	3 of 47	Gee et al., 2015
S-C Norway Caledonides	Särv Succession (Middle Allochthon)	Pieljekaise Nappe	2	Psammite	HL10-016	16.87855	66.35434	U-Pb	905	13	-	-	1 of 73	Gee et al., 2015
S-C Norway Caledonides	Särv Succession (Middle Allochthon)	Pieljekaise Nappe	2	Psammite	HL10-015	16.89892	66.34276	U-Pb	943	7	1.3	0.26	7 of 87	Gee et al., 2015
S-C Norway	Särv Succession (Middle	Rimobäcken Nappe	2	Metaarkose	HL10-019	16.29658	66.58489	U-Pb	958	12	-	-	1 of 58	Gee et al., 2015

Caledonides	Allochthon)													
S-C Norway Caledonides	Särv Succession (Middle Allochthon)	Rimobäcken Nappe	2	Psammite	HL10-023	16.71049	65.82226	U-Pb	984	15	-	-	1 of 74	Gee et al., 2015
S-C Norway Caledonides	Särv Succession (Middle Allochthon)	Rimobäcken Nappe	2	Metaarkose	HL10-009	17.25020	66.29917	U-Pb	940	81	-	-	1 of 86	Gee et al., 2015
S-C Norway Caledonides	Särv Succession (Middle Allochthon)	Rimobäcken Nappe	2	Metaarkose	HL10-010	17.06631	66.34751	U-Pb	943	14	1.2	0.3	7 of 87	Gee et al., 2015
S-C Norway Caledonides	Särv Succession (Middle Allochthon)	Fuda (Offerdal) Nappe	2	Schistose psammite	DG10-08	14.10556	62.91278	U-Pb	940	39	-	-	1 of 103	Gee et al., 2014
S-C Norway Caledonides	Särv Succession (Middle Allochthon)	Särv Nappe	2	Meta-sandstone	DG10-07	12.80139	62.83778	U-Pb	932	20	1.2	0.3	7 of 66	Gee et al., 2014
S-C Norway Caledonides	Särv Succession (Middle Allochthon)	Lower Seve Nappe	2	Calc-silicate psammite	AL08-54	13.21500	63.33444	U-Pb	893	13	0.16	0.69	2 of 69	Gee et al., 2014
S-C Norway Caledonides	Särv Succession (Middle Allochthon)	Lower Seve Nappe	2	Psammitic schist	AL08-11	13.09944	63.38972	U-Pb	993	8	1.2	0.26	11 of 78	Gee et al., 2014
S-C Norway Caledonides	Särv Succession (Middle Allochthon)	Lower Seve Nappe	2	Calc-silicate psammite	AL08-03	13.17444	63.40694	U-Pb	890	17	-	-	1 of 62	Gee et al., 2014
S-C Norway Caledonides	Särv Succession (Middle Allochthon)	Lower Seve Nappe	2	Calc-silicate psammite	AL08-69	13.07778	63.41694	U-Pb	862	13	0	1	2 of 61	Gee et al., 2014
S-C Norway Caledonides	Särv Succession (Middle Allochthon)	Seve Nappe correlative	2?	Psammitic schist	AL08-41	9.97806	63.71361	U-Pb	951	11	0.02	0.9	2 of 43	Gee et al., 2014
S-C Norway Caledonides	Heggmo Succession	Heggmo Terrane	1	Fine-grained schist	AA 09-8	14.82253	67.35755	U-Pb	1051	5	0.6	0.55	3 of 29	Agyei-Dwarko et al., 2012
S-C Norway Caledonides	Heggmo Succession	Heggmo Terrane	1	Orthoquarzite	AA 09-12	14.96340	67.29507	U-Pb	1096	8	1.02	0.42	8 of 84	Agyei-Dwarko et al., 2012
N Norway Caledonides	Gaissa Thrust Belt	Tanafjorden Group (Grønnes et Formation)	3	Sandstone	GRN1	30.10000	70.17000	U-Pb	934	11	1.04	0.41	27 of 127	Zhang et al., 2015
N Norway Caledonides	Gaissa Thrust Belt	Tanafjorden Group (Gamasfjellet Formation)	3	Quartzitic sandstone	GMS1	30.20000	70.14000	U-Pb	940	5	0.97	0.45	8 of 153	Zhang et al., 2015
N Norway Caledonides	Gaissa Thrust Belt	Vadsø Group (Fuglebergget Formation)	2?	Arkosic sandstone	FUG1	29.70000	70.07000	U-Pb	1097	12	0.98	0.42	5 of 136	Zhang et al., 2015
N Norway	Gaissa Thrust Belt	Vadsø Group (Veidnesbotn	2?	Sandstone	VEI1	25.10000	70.05000	U-Pb	1662	18	0.94	0.48	9 of 232	Zhang et al., 2015

Caledonides		Formation)												
N Norway Caledonides	Sørøy Succession	Havvatnet Nappe (Storelv Schist)	2	Pelite	CK031	24.60367	70.68728	U-Pb; Hf	929	26	-	-	1 of 27	Kirkland et al., 2007; Spencer et al., 2015
N Norway Caledonides	Sørøy Succession	Sørøy-Seiland Nappe (Klubben Psammite)	2	Psammite	CK240	23.12570	70.75289	U-Pb; Hf	910	15	-	-	1 of 25	Kirkland et al., 2007; Spencer et al., 2015
N Norway Caledonides	Sørøy Succession	Nappe east of Porsangerfjord	2	Psammite	CK099	26.53088	70.66882	U-Pb	951	12	0.3	0.58	2 of 43	Kirkland et al., 2007
N Norway Caledonides	Sørøy Succession	Havvatnet Nappe	2	Psammite	CK001	24.52069	70.72585	U-Pb	921	24	-	-	1 of 37	Kirkland et al., 2007
N Norway Caledonides	Sørøy Succession	Eidvågeid Paragneiss	2	Paragneiss	CK003b	24.56601	70.79572	U-Pb	962	15	0.17	0.85	3 of 13	Kirkland et al., 2007
N Norway Caledonides	Sørøy Succession	Eidvågeid Paragneiss	2	Paragneiss	CK012	23.62244	70.60118	U-Pb	960	18	-	-	1 of 1	Kirkland et al., 2007
N Norway Caledonides	Sørøy Succession	Akkajaure Nappe	2	Quartzite	CKS14	18.32478	67.48903	U-Pb	939	6	0.6	0.73	7 of 44	Kirkland et al., 2011
N Norway Caledonides	*Sørøy or Svaerholt Succession*	*Kalak Nappe (Below gneisses)*	*1?*	*Fine-grained psammite*	*CK285*	*24.75169*	*71.08388*	*U-Pb*	*1005*	*13*	*0.75*	*0.52*	*4 of 39*	*Kirkland et al., 2008b*
N Norway Caledonides	Svaerholt Succession	Kolvik Nappe (Storelv Schist)	1	Pelite	CK005a	24.85861	70.47558	U-Pb; Hf	1112	16	-	-	1 of 27	Kirkland et al., 2007; Spencer et al., 2015
N Norway Caledonides	Svaerholt Succession	Olderfjord Nappe (Klubben Psammite)	1	Psammite	CK267	25.43307	70.67036	U-Pb; Hf	1073	28	-	-	1 of 46	Kirkland et al., 2007; Spencer et al., 2015
N Norway Caledonides	Svaerholt Succession	Kolvik Nappe	1	Psammite	CK006c	23.79049	70.71879	U-Pb	1022	18	-	-	1 of 35	Kirkland et al., 2007
N Norway Caledonides	Svaerholt Succession	Kalak Nappe (Intragneiss)	1	Psammite	CK291	24.75416	71.08322	U-Pb	1029	14	0.16	0.92	4 of 71	Kirkland et al., 2008a
N Norway Caledonides	Svaerholt Succession	Kalak Nappe (Hjelmsøy)	1	Banded gneiss	CK293	24.67758	71.08253	U-Pb	1019	34	-	-	1 of 31	Kirkland et al., 2008a
N Norway	Svaerholt Succession	Kalak Nappe (Porsange	1	Psammite	CK040	24.66730	70.65317	U-Pb	1092	22	-	-	1 of 33	Kirkland et

Caledonides		rhalvøya psammite)												al., 2008a
N Norway Caledonides	Svaerholt Succession	Kalak Nappe Complex	1?	Sandstone	F-3	27.95000	70.80000	U-Pb	999	14	-	-	1 of 142	Zhang et al., 2016
N Norway Caledonides	Svaerholt Succession	Kalak Nappe Complex	1?	Sandstone	F-1	27.20000	70.85000	U-Pb	991	24	-	-	1 of 95	Zhang et al., 2016
N Norway Caledonides	Svaerholt Succession	Laksefjord Nappe Complex (Landersfjord Fm.)	1?	Sandstone	LAN1	26.90000	70.45000	U-Pb	1023	13	-	-	1 of 155	Zhang et al., 2016
N Norway Caledonides	Svaerholt Succession	Laksefjord Nappe Complex (Ifjord Fm.)	1?	Conglomerate	IFJ1	27.10000	70.44000	U-Pb	1991	32	-	-	1 of 151	Zhang et al., 2016

Highlights

- New detrital zircon U-Pb and Hf data from the Nathorst Land Group, East Greenland
- New Caledonian granite ages of 426 ± 1 Ma
- Detrital zircon U–Pb and Hf isotopic data compiled for Neoproterozoic North Atlantic
- Three megasequences identified with sharp increase in zircon disparity in megasequence 3
- Disparity related to compartmentalization of depocentres with local supply and distinct sediment routing pathways during continental breakup.

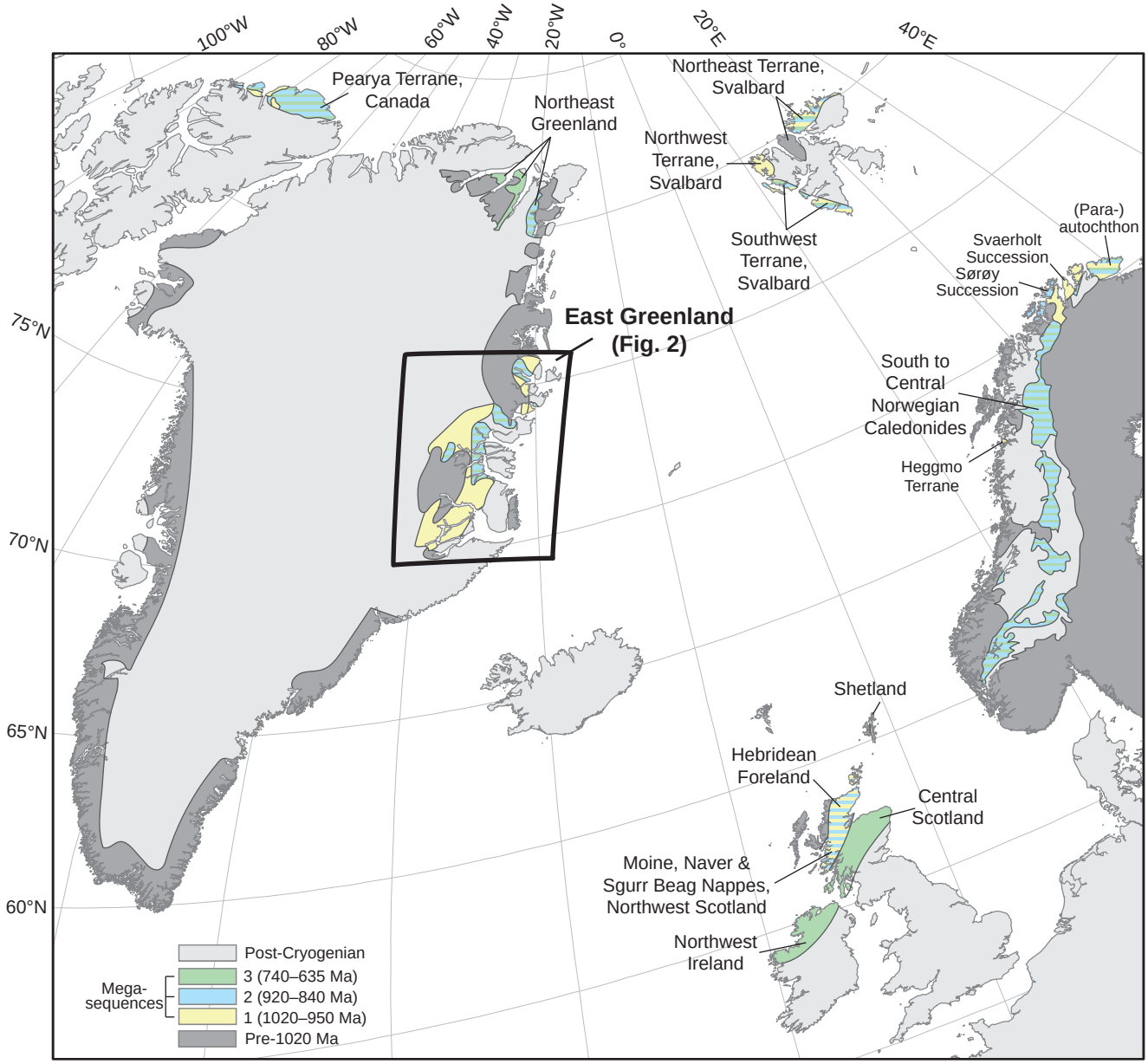

Olierook et al., Figure 1

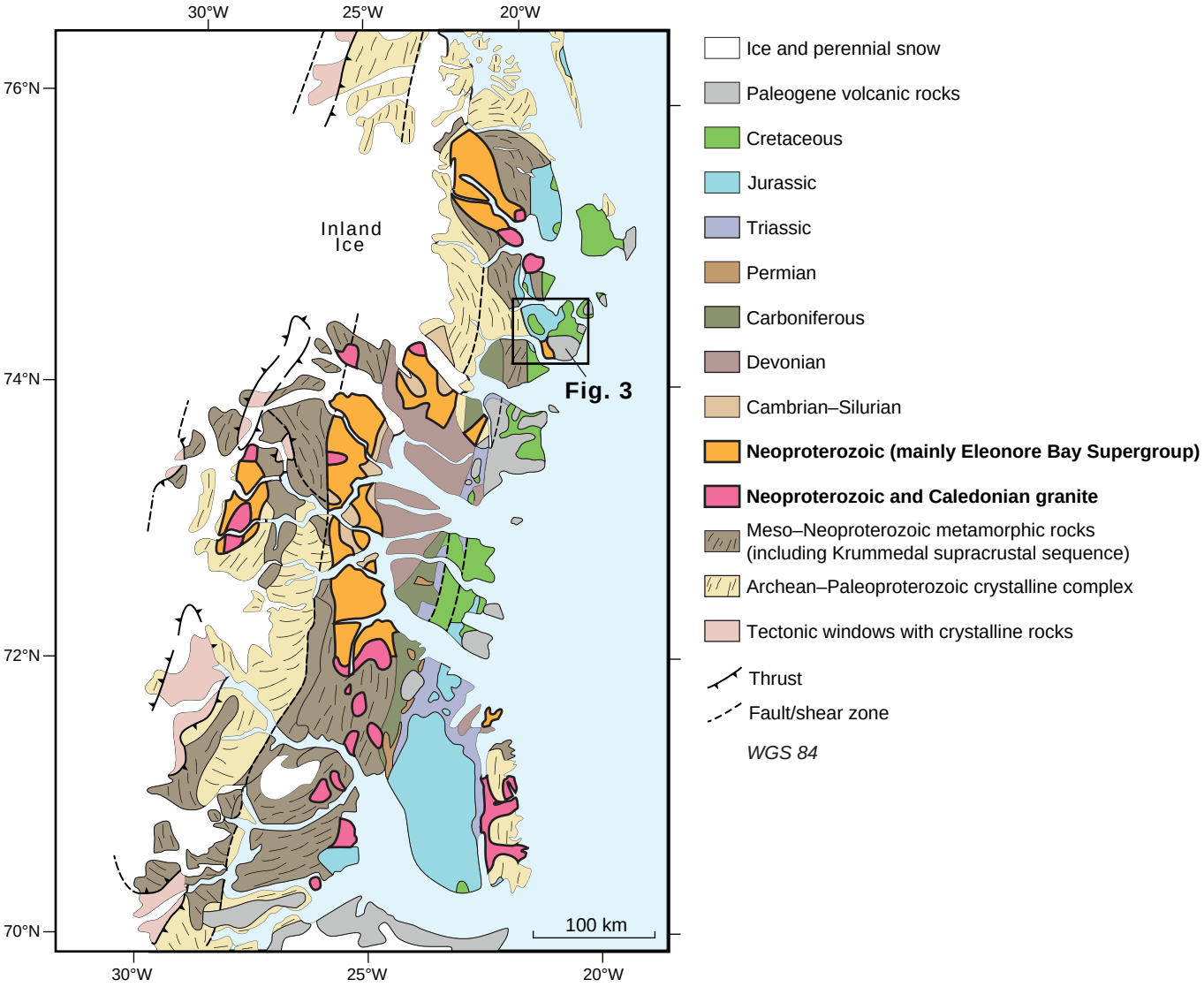

Olierook et al., Figure 2

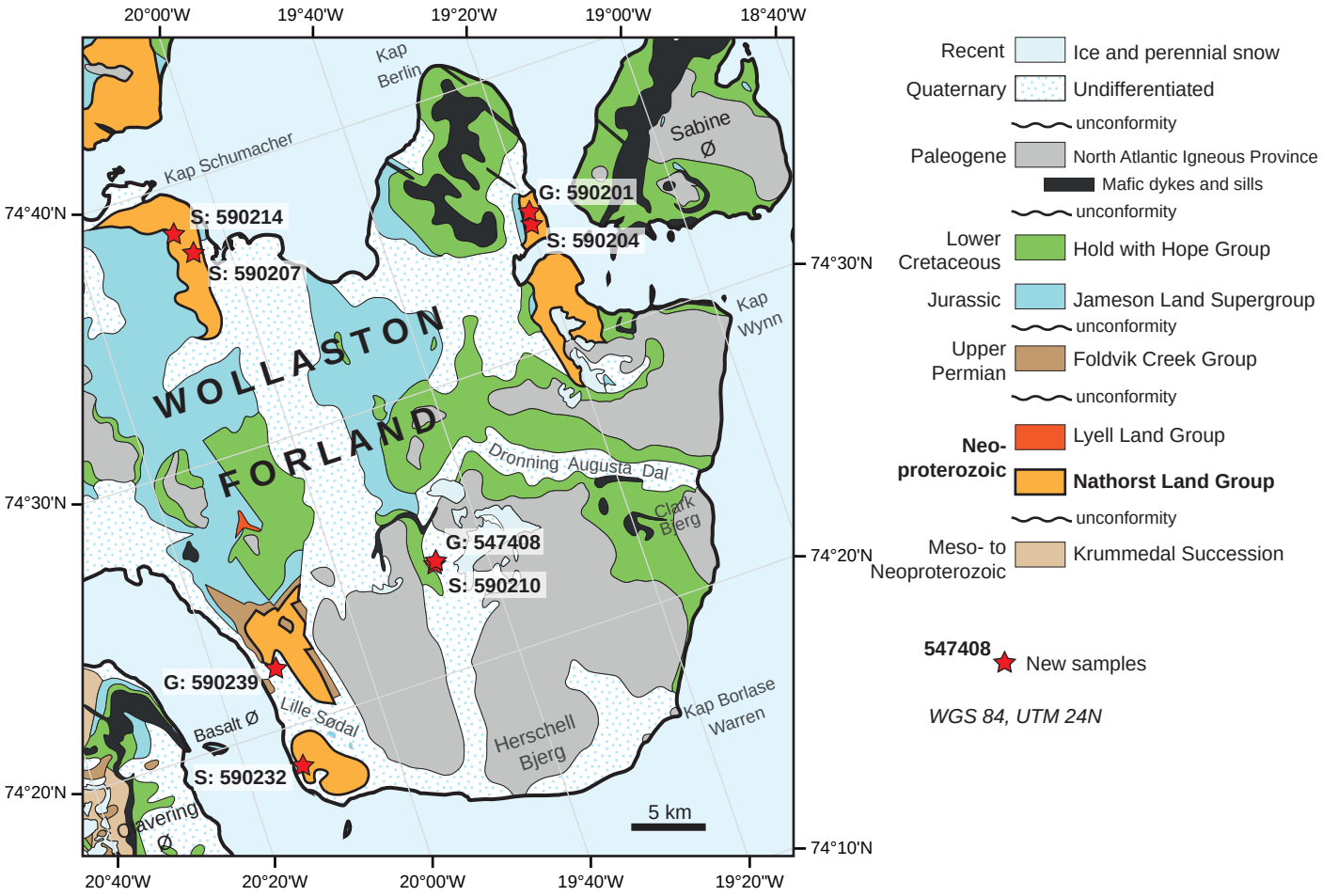

Olierook et al., Figure 3

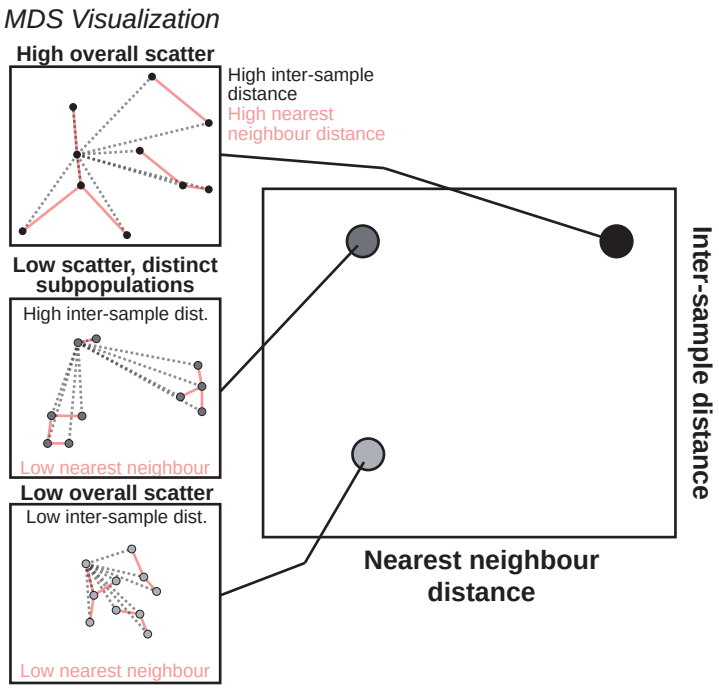

Olierook et al., Figure 4

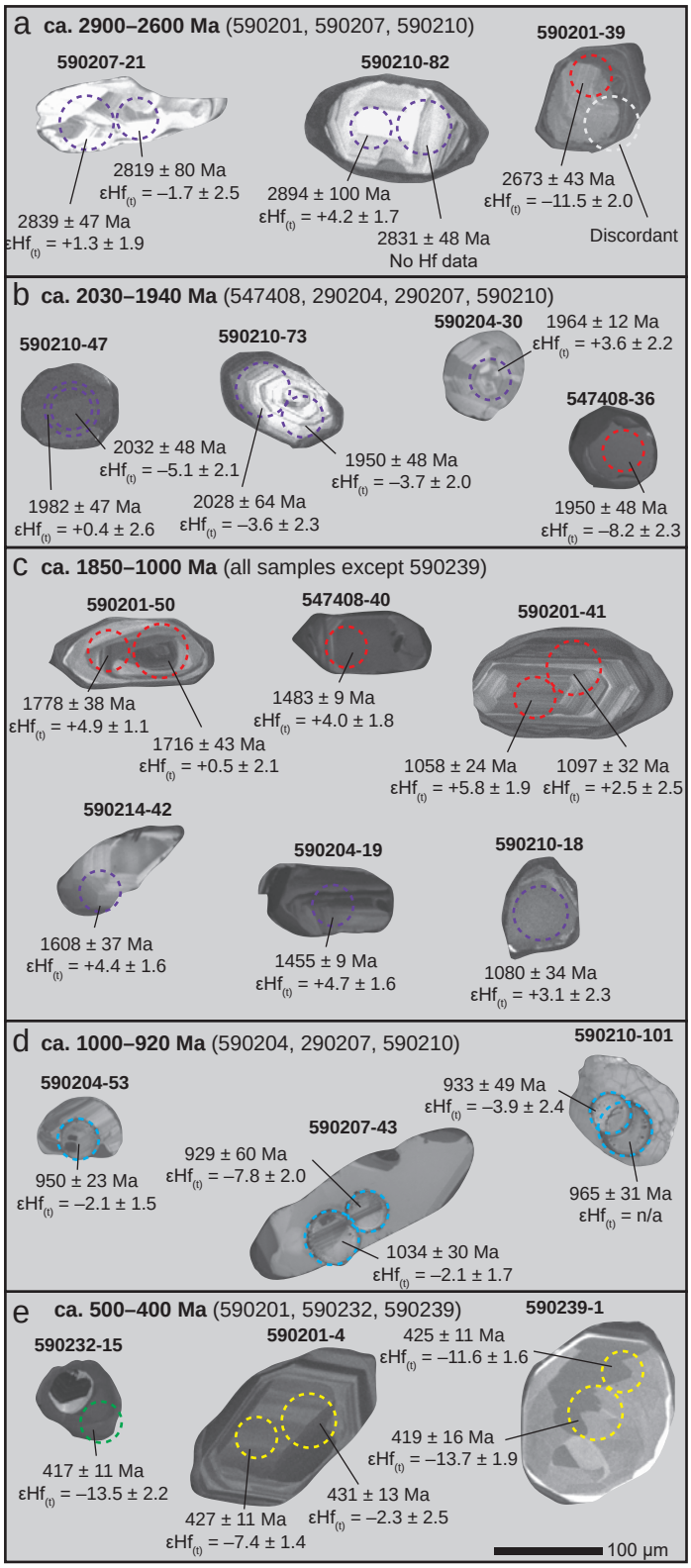

Olierook et al., Figure 5

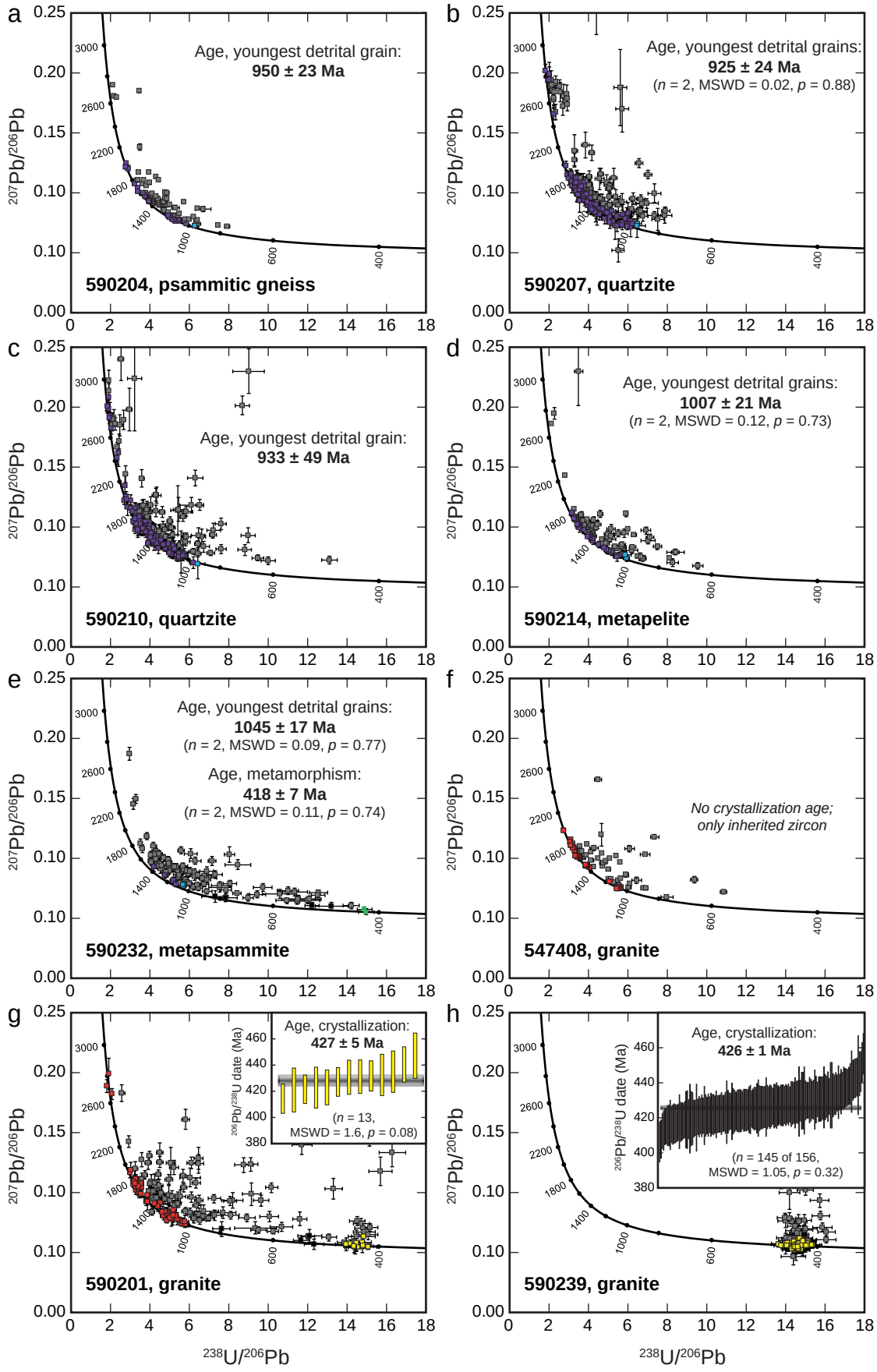

Olierook et al., Figure 6

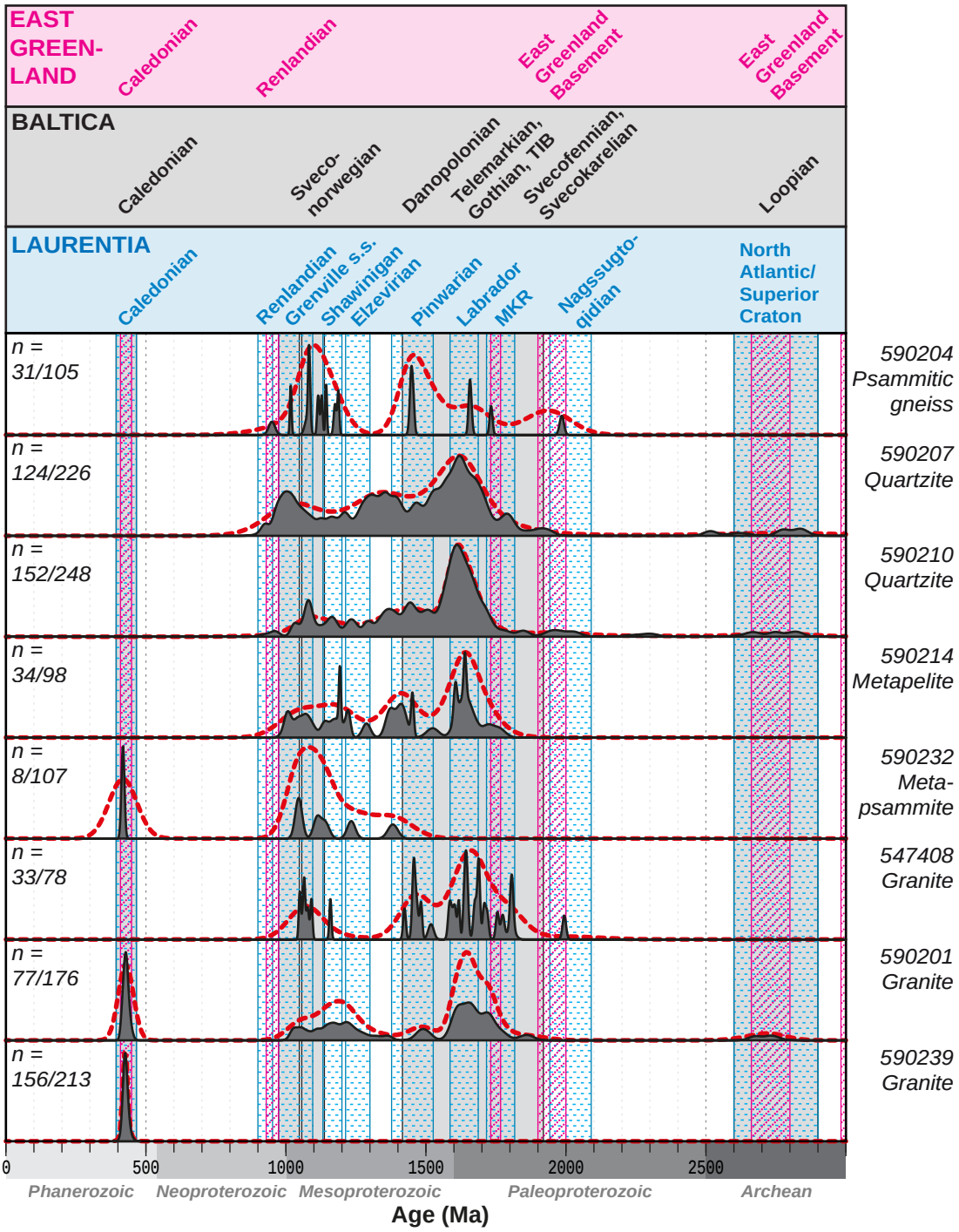

Olierook et al., Figure 7

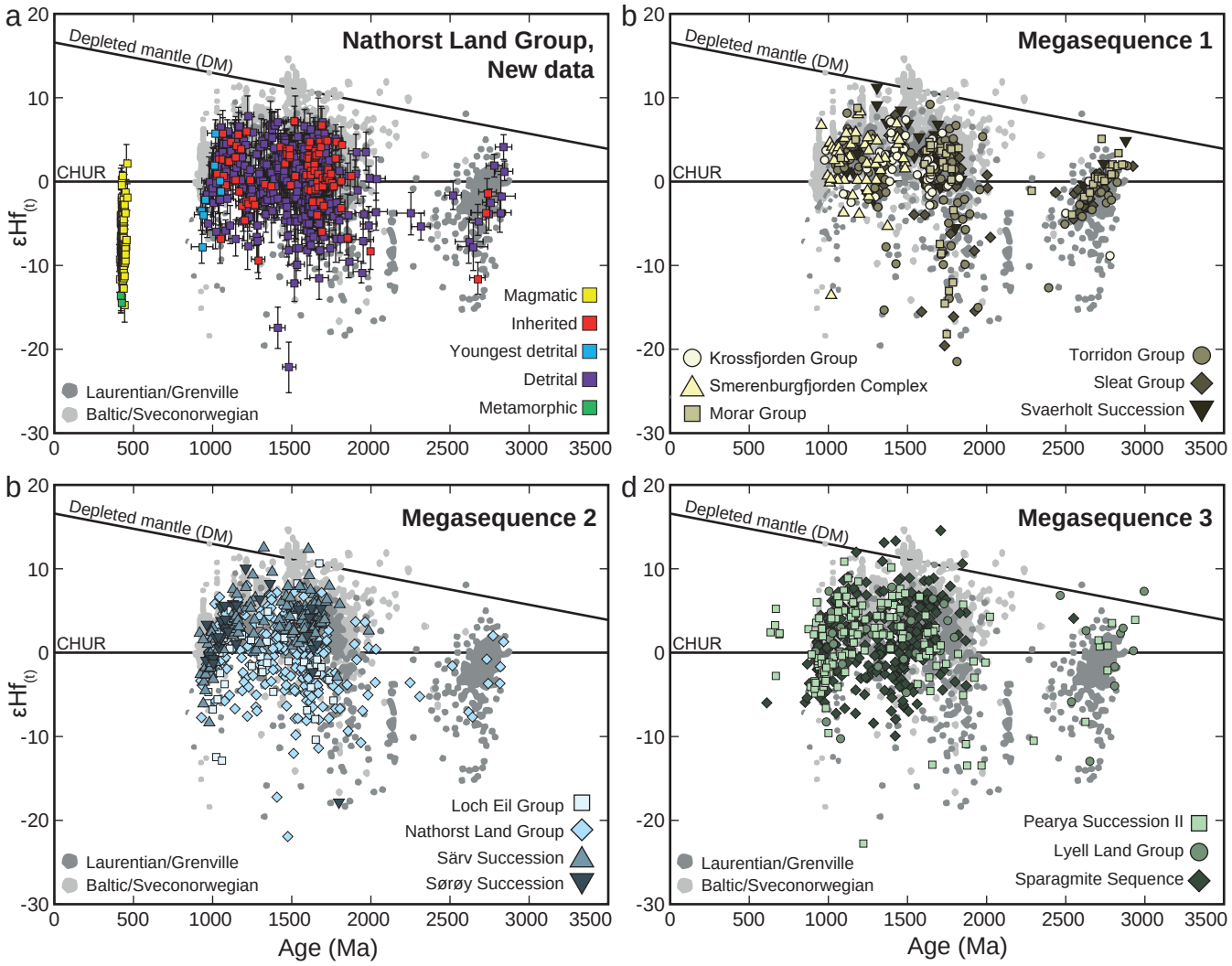

Olierook et al., Figure 8

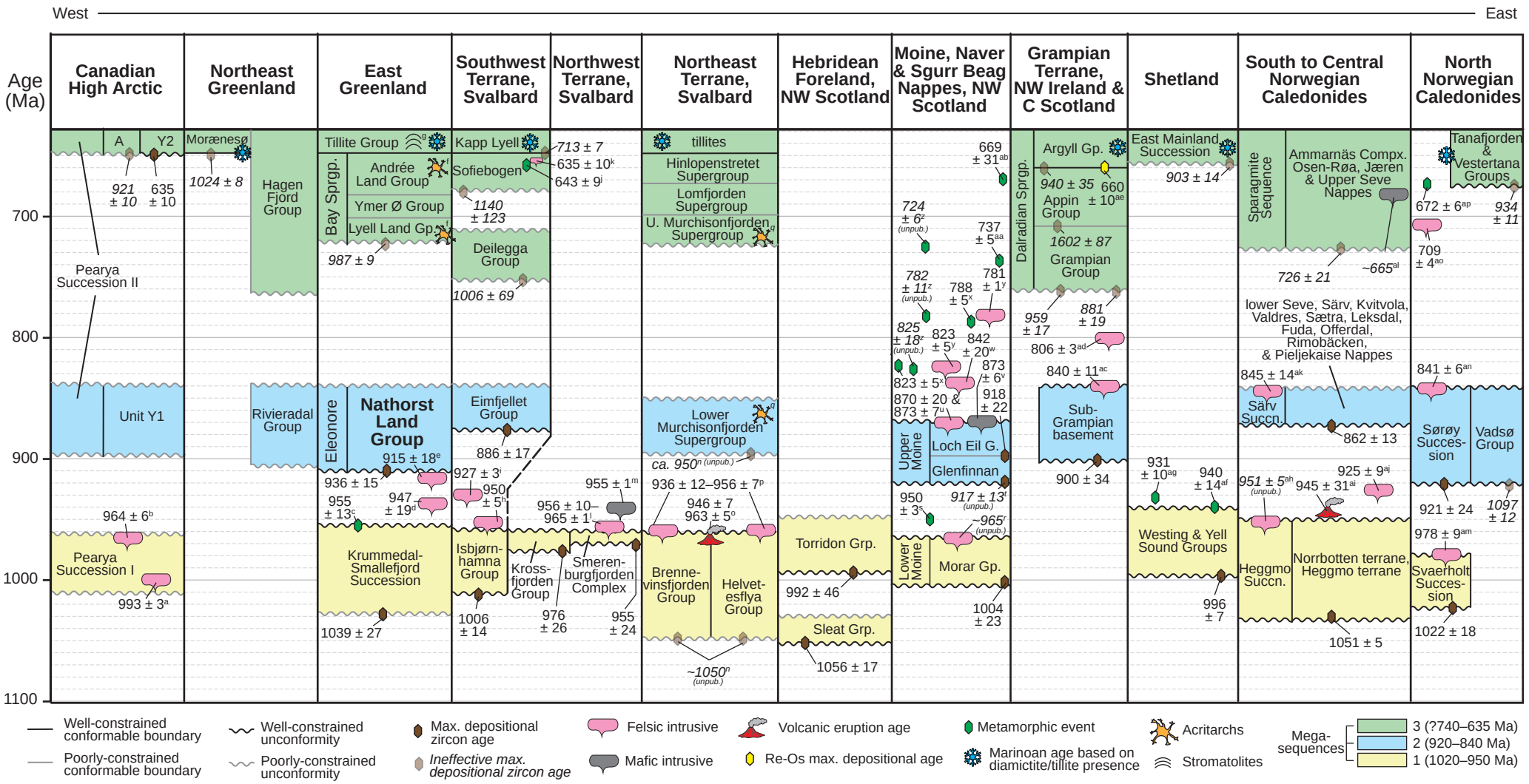

Olierook et al., Figure 9

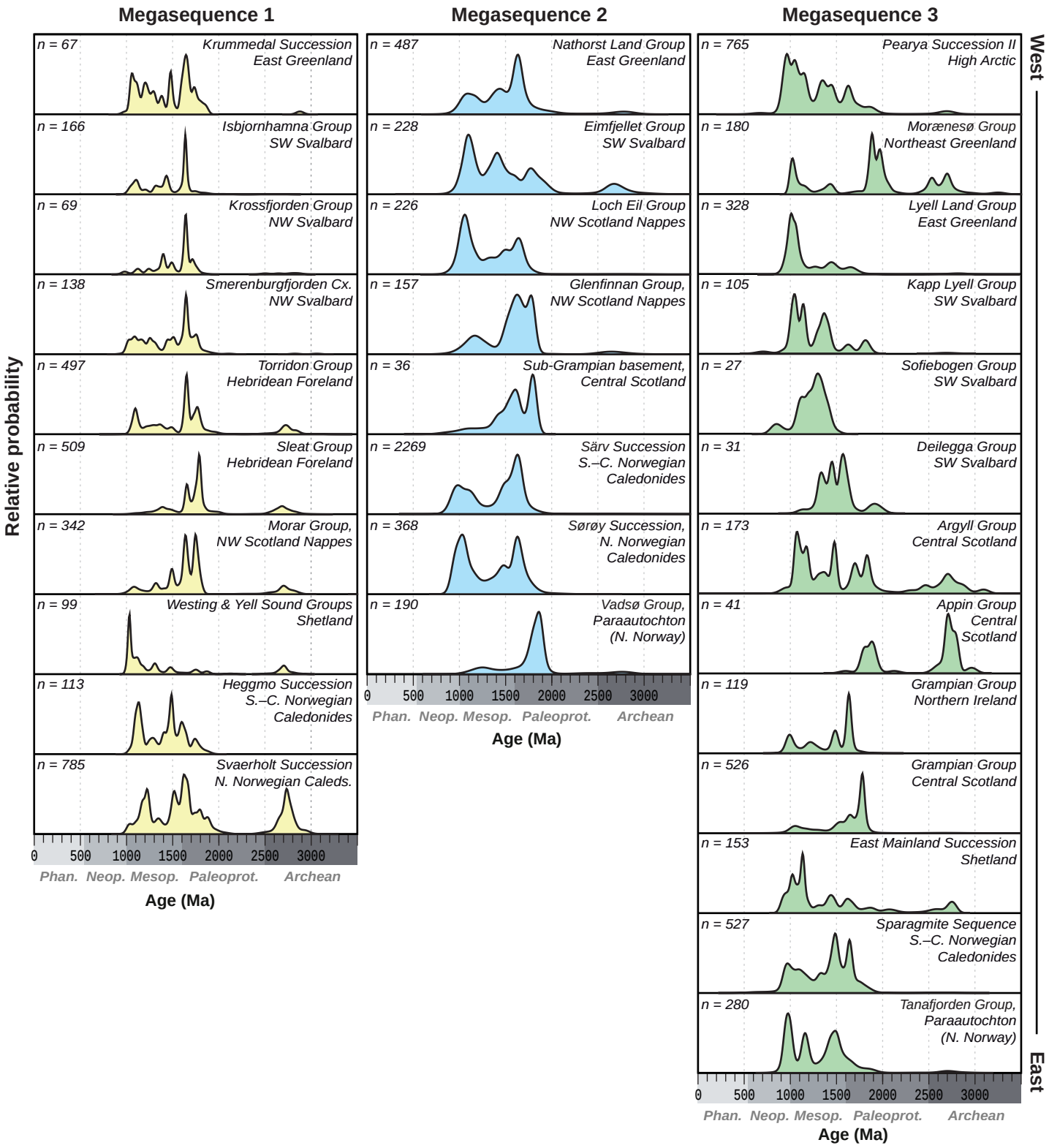

Olierook et al., Figure 10

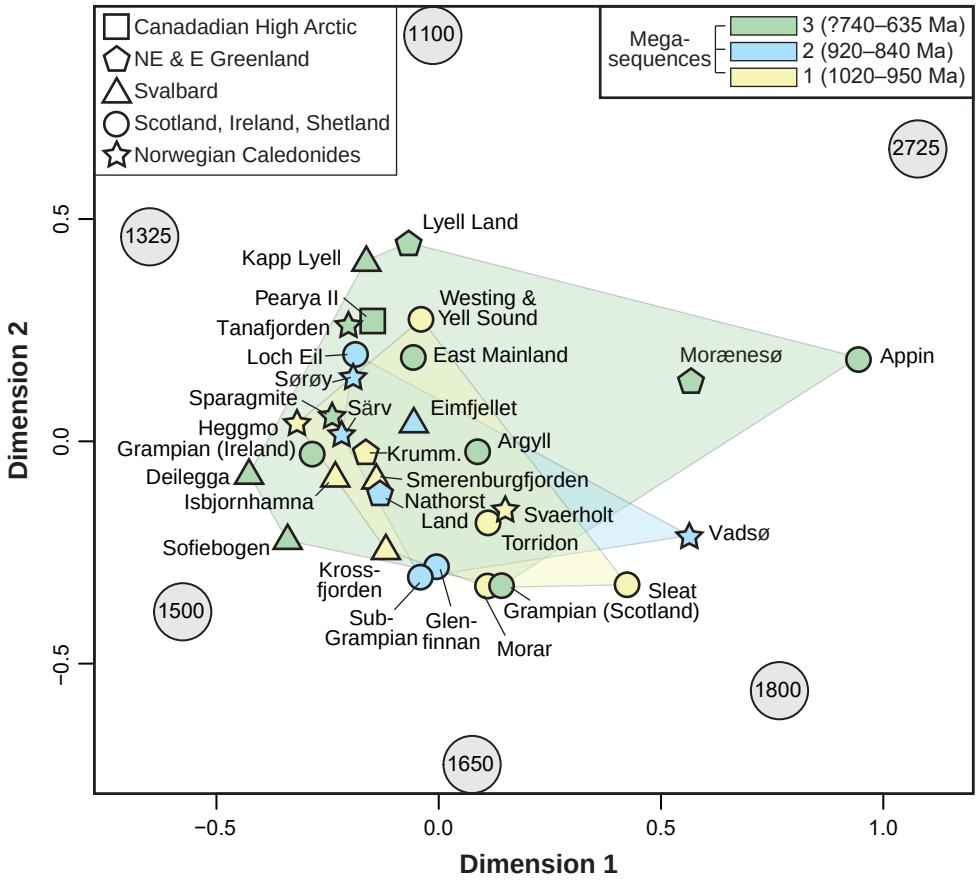

Olierook et al., Figure 11

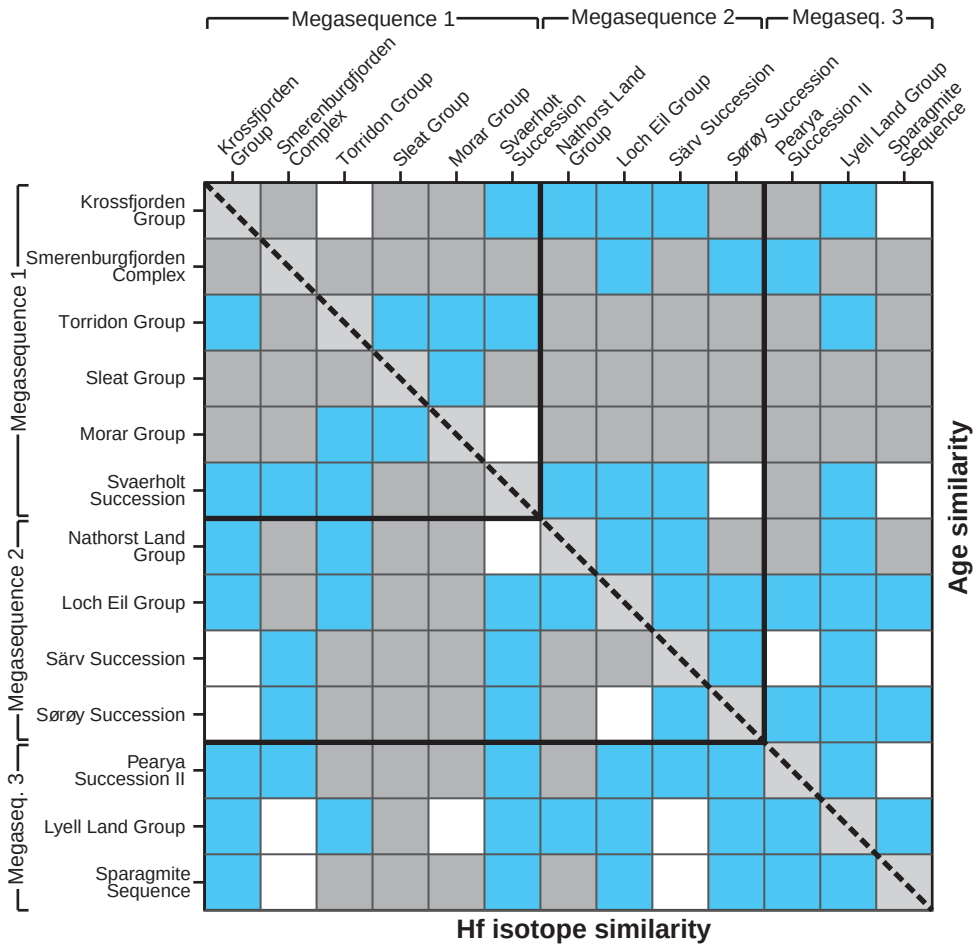

Olierook et al., Figure 12

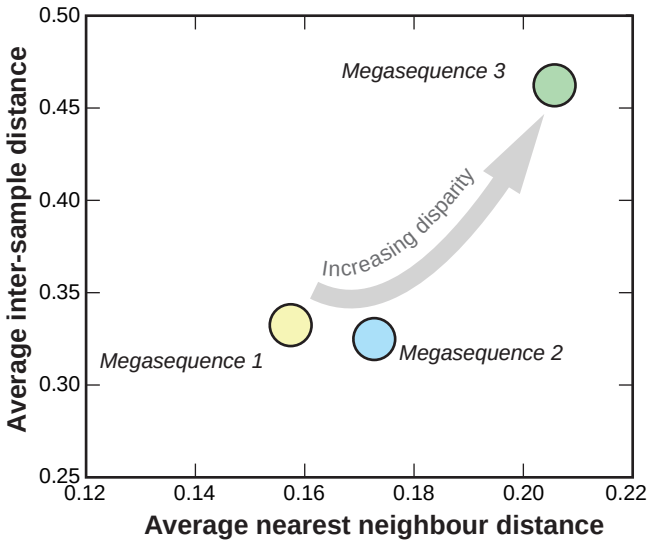

Olierook et al., Figure 13